ARCHIVES OF ACOUSTICS
23, 3, 339–352 (1998)

ASSESSMENT OF JOINT HAZARD TO THE OUTER ENVIRONMENT FROM ROAD AND INDUSTRIAL NOISE BY THE EXAMPLE OF THE KATOWICE VOIVODESHIP

J. KOMPAŁA

Central Mining Institute
Department of Technical Acoustics
(40-166 Katowice, Pl. Gwarków 1, Poland)

An analysis of available professional papers on the subject shows that, in spite of the fact that some theoretical base exist, there is no general formulation of the problem discussed in this study. This is reason for undertaking the task and making a quantitative analysis of acoustic climate for the Katowice voivodeship. This paper is a report on the first attempt in Poland to work out an acoustic map which takes into consideration all traffic and industrial sources of noise located in a large and diversified area. The purpose of this paper is create on acoustic map of Katowice voivodeship and quantitative analysis of acoustic climate which takes into consideration noise of industrial and transportation.

1. Introduction

The increasing level of social consciousness in relation to hazards of the natural environment from physical and chemical factors entails the necessity of a quantitative determination of those hazards coming from different sources, among other things also the noise sources. The instructions of the European Union, taking into account the widespread presence of noise in various domains of human activity, point to the people's right to live in silence. This implies the necessity to make an assessments of the acoustic climate not only at workplaces but also at every dwelling-places outside the working posts. In Poland, the Katowice voivodeship is one of the areas with an increasing shortage of places not endangered by excessive noise. The noise hazard in the Katowice region is a result of many unfavourable factors, the predominant ones being: an excessive urban development, concentration of obsolete industry and, as the result, a high density of population. An additional burden to the environment is the transport service that has been lackiing modernization for many years. These factors make the environmental noise, that is the noise in the places of human habitation and recreation, exceed very often the values assumed as admissible and increase further. The incoordinate land planning conducted for many tens of years has resulted in an urban aggregate which is unique in the world's scale.

Presently at the area of the Katowice voivodeship, covering ca. 6650 km^2 (2.1% of the whole area of Poland), live nearly 4 million people, which constitutes ca. 10.4% of the population of the country.

During the year 1988–1997, at the Department of Technical Acoustics of the Central Mining Institute the work on the quantitative assessment of the noise hazard in the area of the Katowice voivodeship has been conducted taking into account its main components, i.e. the road and railway traffic and industrial noise.

The initial materials for preparing an acoustic map of such an area as the Katowice voivodeship region are the following ones: a surveying map adapted for the needs of this plan (by elimination of unnecessary information) and indices of the acoustic climate assessment. In practice, different indices are used in the assessment of the environmental noise. They are extensively described in the bibliography of the subject [3, 4, 16, 17, 20]. The following ones are most often used:

1. Indices of the source noise $L_{Aeq,r}$ and $L_{Am,r}$, dB, calculated as averages of the measured sound levels A in all measuring points characterizing these objects as noise sources.

2. Indices of the degree of disturbance of the acoustic climate of the environment L_{AN} dB, calculated as the difference between the averaged level of the noise disturbing the environment and the corresponding admissible level.

3. Indices defining the percentage ratio of the length of transport routes with defined noise level to the length of all routes on which the measurements were conducted.

4. Indices defining the number of people in the analysed area endangered by noise of a level in excess to the standard value.

5. Indices defining the area of the zone under assessment endangered by the import of noise of a level in excess to the standard value.

6. Indices taking into account subjective reactions of humen to the noise influence.

2. Investigation methods

The variety of noise sources appearing in the field requires the application of manifold classification sections [6, 9, 10, 12, 13]. In relation to the shape, they are divided into:

— linear (transportation routes, ...),

— superficial (airports, depots, railway stations, large industrial plants, ...),

— punctual (small industrial plants, individual machines, ...),

— spatial (building type).

Instead, considering the environment in which the noise exists and the type of the source generating it, one can divide the noises into:

— noise coming from the means of transportation, the so-called traffic noise,

— industrial noise, and

— noise in habitable rooms, public utilities and rest and recreation areas, i.e. municipal noise.

Apart from the size, the way in which the noise is emitted into the surroundings is also of importance in assessing the impact of a specified type of noise on the environment. Its

prediction in the environment is presently based on calculation methods of the external noise determination.

However, the necessity of mathematical simplification of the assumed models introduced at every stage of the calculations leads to many mistakes; the results obtained from those operations are of lower practical importance than one could expect [4, 6, 7, 9, 10, 12, 18]. For such a complex system as the Katowice voivodeship, the creation of acoustic models proves to be difficult or simply impossible. Therefore, it has been decided to develop an assessment method based on the measurements actually performed.

The choice of the approach results also from the fact that the most accurate transformation of the existing state is ensured by a measuring method relying upon determination of the sound levels A under maintaining strictly defined and neutral methodology conditions [4, 5, 6, 7, 8, 11, 19].

The application of a suitable method depends on the way of determining an initial parameter of the acoustic field. Knowing the sound level A for any characteristic time range t_i, the basic parameter of the noise hazard assessment in the environment is determined over the time T, i.e. an equivalent sound level is given by the relationship

$$L_{A,eq} = 10 \log \frac{1}{T} \sum_{i=1}^{n} t_i 10^{0.1 L_{Ai}}, \tag{1}$$

where L_{Ai} – sound level occurring at the time t_i, dB, t_i – time of occurrence of the noise of the level L_{Ai}, min, T – time for which the equivalent level value is determined.

Under ideal conditions, the method of determining the sound level A at a certain distance from the source is based on the fundamental assumption that the noise propagates in open space without any disturbance and that the change of its level is determined solely by the distance of the observation (measurement) point from the source [7, 9, 10, 11, 12].

Under real conditions, if the sound level $L_{A,0}$ at a distance r_0 from the considered source is known, one can calculate the sound level A value at any distance r_x from the source from the relationship

$$L_{A,X}(r) = L_{A,0} - K \log \frac{r_X}{r_0} - \Delta L(d), \tag{2}$$

where $\Delta L(d)$ is the total effect of all additional factors influencing either an increase or drop of the sound level A at the observation point localized at the distance r_x from the source of noise, K is the coefficient accounting for the noise attenuation along a distance, r_0 distance of the point of reference.

From among many factors, the influence of which on the level of annoyance is the highest one, one can quote [11, 12, 13]:

— sound level A at the source,
— type of noise emitted,
— course of the spectrum of noise emitted by the source,
— type of the casing of the source or lack of thereof,
— occurrence and localization of areas liable to anti-noise protection.

In addition, several assumptions were made for carrying out tests and an noise hazard assessment for such a large area as a voivodeship:

— the testing was divided into three stages taking into account different types of sources in each case – road traffic, railway and industrial noise [14, 15],

— the area of the voivodeship was divided into squares of 5 km sides by a geodetic graticule according to the assumptions of the so-called Upper-Silesian Area Information System (GSIoT) [14, 15],

— the values of admissible levels for all types of noise were assumed to be: 55 dB for the day-time and 45 dB for the night [1, 2, 14, 15],

— the results of measurements carried out in accordance with the assumed testing procedure were collected in the database constructed on the basis of the MS ACCESS 2 PL programme.

The procedure described above enabled to calculate an index defining the percentage of the area of a defined square endangered by the noise impact of a level exceeding the admissible one. This index was determined from the relationship [4]

$$W_{KZH} = \frac{T_{KZH}}{T_{K0}}, \tag{3}$$

in which W_{KZH} – index defining, in accordance with the GSIoT, the percentage of the area of the square, endangered by the noise in excess to the standard value, T_{KZH} – area of the square endangered by the noise in excess to the standard value, T_{KO} – total area of the square.

The method described was subject to verification for the whole area of the Katowice voivodeship. On the basis of the results of measurements obtained, the values of the indices were calculated defining the percentage of the areas of individual squares – according to the assumed division graticule of the area-endangered by the noise of a level in excess to the standard value, separately for the day- and night-time. The division of the Katowice voivodeship into 300 squares the 5 km sides is in agreement with the assumptions made by the local Government of the Upper-Silesian Area Information System. Taking into account these assumptions, it was possible to utilize the results obtained for a general assessment of the hazard for the Katowice voivodeship [14, 15].

Presently, the following documents concerning the assessment of the hazard for the environment by noise are in force:

— Act of the 31-th of January, 1980 on the protection and formation of the environment,

— Order of the Cabinet of the 30-th of September, 1980 on the protection of the environment against noise and vibration.

The Order of the Cabinet on the protection of the environment against noise and vibration is an administrative act to the Act mentioned above. It wad dated at the end of 1980 and since that the moment that it coms into force has not been amended. The criterial values of the equivalent sound level A determined by in it are given separately for the day (6.00–22.00) and the night (22.00–6.00). It was assumed that during the day there are 8 most unfavourable hours, while during the night there are only 30 most unfavourable minutes.

Basing on this Order, the criterial values of the sound level A have been taken from it and assumed for the noise assessment in the area of the Katowice voivodeship. The necessity to introduce uniform values for such a diversified area was the main problem. After carrying out a number of consultations both with the representatives of the local Government (Voivodeship Office, Katowice) and the centres engaged in studying the effect of noise on health of the humans, the following co-ordinated values were assumed:

— 55 dB for the day-time,

— 45 dB for the night-time,

as the admissible ones for the whole area of the Voivodeship.

The following factors speek in advocacy of the assumed values: the way of the land development (an urban area with many centres of individual municipal units), high intensity of the road traffic, existence and size of recreation grounds (parks and chiefly allotments) situated in the periphery of towns and settlements.

3. Test results

The determination of the noise hazard condition in the Upper-Silesian urban aggregate and creation of a database of the occurring acoustic hazard had required a widespread investigation in this domain. As the result, the following picture of the hazard from individual noise components was obtained for the Upper-Silesian urban aggregate.

3.1. Road traffic noise

Measurements were made for the day-time at 1369 measuring points located along roads of different categories and of a total length of ca. 3900 km. For the night-time, the measurements were limited to 50 representative squares at the area of which 250 measuring points were localized along ca. 950 km of roads.

The following results of the performed assessment have been found that [14]:

— for day-time, about 13% of the area of the Katowice voivodeship is endangered by the influence of road traffic noise, characterized by a sound level A exceeding the assumed critical value of 55 dB,

— for night time, it has been assessed from the performed sound measurements, that ca. 20% of the area of the Katowice voivodeship is endangered by the influence of road traffic noise characterized by a values of sound level A exceeding the assumed critical value of 45 dB.

3.2. Railway noise

The total length of the railway lines in the Upper Silesia region is 2230 km (of which 29% are trunk-lines, 38% first-rank lines, 21% second-rank lines and 12% are lines of local importance). The Upper-Silesian regional railway operates over a much larger area than that of the Upper-Silesian urban aggregate analysed (the total length of railway lines of the Katowice voivodeship constitutes 62% of the total length of the Upper-Silesian

railway). The railway lines of a length of 1100 km constituting, ca. 80% of their total length in the Katowice voivodeship area, were included in the tests.

From the performed measurements and calculations of the emission and immission it follows that [15]:

— for day-time, about 11% of the area of the Katowice voivodeship is endangered by the railway noise characterized by a sound level A exceeding the assumed critical value of 55 dB,

— for night-time, about 57% of the area of the Katowice voivodeship is endangered by the influence of the railway noise characterized by values of the sound level A exceeding the assumed critical value of 45 dB.

3.3. Industrial noise

The 200 industrial plants localized in various communes and towns within the limits of the Katowice voivodeship have been subject to acoustic assessments. Their choice reflects the industrial structure in the Upper Silesia region.

From the performed measurements and calculations it follows that

— for day-time, about 1.5% of the area of the Katowice voivodeship is endangered by the influence of noise coming from the industrial activity conducted here and characterized by values of the sound level A exceeding the assumed critical value of 55 dB,

— for night-time, about 1.9% of the area of the Katowice voivodeship is endangered by the influence of industrial noise characterized by values of the sound level A exceeding the assumed critical value of 45 dB.

4. Assessment of the error in determining the equivalent sound level A at the point of reference

All the measurements carried out are related to signals which are characterized by random changes of the acoustic pressure vs. time. Each of the measurement results at a defined measuring point is encumbered by some error. This error was influenced by different factors. The total error of a single, continuous measurement of an equivalent level lasting 8 hours during the day-time or 0.5 hour during the night-time, is affected by:

— the error introduced by the equipment used in performing the measurements,

— the error introduced by the atmospheric conditions taking place during the measurements,

— the error caused by the effect of the acoustic background.

Applying the simplified methodics relying upon the shortening of the measurement time introduces an additional error which requires a separate approach (estimation) depending on the type of noise and the time assumed for carrying out the measurement.

Efforts have been made to reduce the equipment error by applying in the measurements high class meters serviced by measuring teams experienced and specialized in field tests. Also the effect of atmospheric conditions, i.e. atmospheric pressure, velocity of the

wind, temperature and humidity of the air, were minimized by controlling them and carrying out the measurements when the values of these factors were within the ranges defined in the proper standardizing documents [21, 22, 23] and the instruction manuals of the devices.

The error in determining the sound level A for individual types of noise and resulting from the remaining factors has been assessed below.

The equivalent sound level A occurring at a specified point is calculated from the relationship

$$L_{A,eq} = 10 \log \left[\frac{1}{T} \sum_{i=1}^{n} t_i 10^{0.1 L_i} \right] \tag{4}$$

or

$$L_{A,eq} = 10 \log \left[\frac{1}{T} \sum_{i=1}^{k} n_i 10^{0.1 SEL_i} \right], \tag{5}$$

where t_i – action time of the i-th source, T – time during which the equivalent level was determined, L_i – value of the sound level of the sound emitted by the i-th source in the time t_i, SEL_i – averaged exposition sound level A, eg. for the i-th category of train, n_i – number of elementary events numbered among the i-th category, and occurring within the time T.

When determining the value L_i, one should take into account the noise level existing at the considered point with a lack of activity of the investigated source (the level of the measuring background – L_T). In accordance with the above, the following relationship should be used:

$$L_i = 10 \log \left(10^{0.1 L_Z} - 10^{0.1 L_T} \right), \tag{6}$$

where L_Z – measured noise level at the measuring point, L_T – measured level of the acoustic background at the measuring point.

As $L_{A,eq}$ has been determined (following (4) or (5), at the measuring point it depends on the level of the sound emitted by the i-th source and the time of its action) the error value $\Delta L_{A,eq}$ of determining the equivalent level is calculated from the relationship:

$$\Delta L_{A,eq} = \left[\left(\frac{\delta L_{A,eq}}{\delta L_i} \right)^2 \Delta L_i^2 + \left(\frac{\delta L_{A,eq}}{\delta t_i} \right)^2 \Delta t_i^2 \right]^{1/2}, \tag{7}$$

where ΔL_i – error of determining the level value of the noise emitted by the i-th source at the measuring point, Δt_i – error of estimation of the action time, identical for each source.

Substituting (4) in (7) one obtains finally, after differentiation, the following relationship for the error of determining the value of $L_{A,eq}$:

$$\Delta L_{A,eq} = \left[\Delta L^2 + \left(\frac{\sum_{i=1}^{n} 10^{0.1 L_i}}{\sum_{i=1}^{n} t_i 10^{0.1 L_i}} 10 \log e \right)^2 \Delta t^2 \right]^{1/2}. \tag{8}$$

The calculation error of the emitted noise is determined from the formula:

$$\Delta L = \left[\left(\frac{\delta L}{\delta L_Z} \right)^2 \Delta L_Z^2 + \left(\frac{\delta L}{\delta L_T} \right)^2 \Delta L_T^2 \right]^{1/2}. \tag{9}$$

Substituting (6) in (9) one obtain after differentiation

$$\Delta L = \frac{\Delta L_Z \left(1 + 10^{-0.2\Delta K_T}\right)^{1/2}}{1 - 10^{-0.1\Delta K_T}}, \tag{10}$$

where ΔL_z – measurement error, ΔK_T – difference between the measured value and that of the measuring background (L_T) which, at the time of measurement, was at least 6 dB.

The results of calculation of the maximum error in determining the level of the equivalent sound A are presented below.

4.1. Road traffic noise

Continuous measurements (8 hours during day-time or 0.5 hour during night-time) of the sound level A at the point of reference in which there is a large difference between the investigated signal and the existing acoustic background enables to determine the equivalent level at this point with an accuracy equal to that of the instrument used in the tests [6].

The reduction of the measuring time, resolving itself, in practice, into "periodical sampling" of the investigated signal, introduces an additional error.

The methodics proposed in [6] enables to determine the values of the equivalent level with a 1.5 dB accuracy. This error was in [2] determined for a single ten minute-lasting, measurement carried out at a random time moment within 8 most unfavourable hours of the day in the surroundings of a road with a medium traffic intensity of 370 vehicles per hour. For a measurement performed in rush hours it is equal to 1.8 dB, while in the time period corresponding with the lowest traffic intensity it is 4.9 dB. Our investigations have shown the dependence of the value of this error on the traffic intensity. These errors are:

— 1.9 dB for roads with a traffic intensity above 800 vehicles per hour,
— 2.1 dB for roads with a traffic intensity between 500 and 800 vehicles per hour,
— 2.7 dB for roads with a traffic intensity between 300 and 500 vehicles per hour.

From the above it follows that the maximum error in determining the equivalent sound level A on the basis of a single ten minutes – lasting measurement during the rush hours does not exceed 3 dB during the day-time.

For the night-time, the measurement duration was 0.5 hour and was equal to the time period for which the admissible sound level A has been determined. In this connection, the error of determining the equivalent value is related only to the error of the instruments used. For further analysis a value of 1 dB has been assumed.

4.2. Railway noise

For the assessment of the maximum error in determining the equivalent sound level A for the railway traffic during both the day- and the night-time, it has been assumed

that the measurement error of the exposition level for a single measurement ΔSEL is 1 dB. The difference between the measured noise level and the acoustic background level for the measuring points localized in close surroundings of the roads was, at least, 6 dB. For such an value assumed, the error in determining the equivalent level ΔL, formula (10), is 1.4 dB. The maximum error in calculating the equivalent sound level A for eight most unfavourable day-time hours or half an hour during the night-time, and at the assumption that the accuracy of determining the number of trains is 20%, is, from formula (8), equal to 1.7 dB.

4.3. Industrial noise

In accordance with the assumed methodics, the measurements were performed at places localized outside the premises of the plant when the maximum noise emission into the environment took place. The equivalent noise level A, for eight most unfavourable day-time hours and half an hour during the night-time, was determined by performing short 10-minute measurements. On the basis of the performed tests [9, 10, 13, 25, 26, 27] it has been found that a main influence on the formation of the acoustic climate around industrial plants have the following factors: fan station, compressor stations, transformers, cooling towers, etc. The time of their operation is different. However, due to their importance in the technological processes this time is not less than 4 hours for a working shift. In connection with the above, in assessment of the maximum error in determining the value of the equivalent sound level A it has been estimated that this error, for both the day- and night-time is equal to 3 dB.

5. Estimation of the error of determining the area endangered by the influence of noise of a level in excess to the standard value

In the case of assessing the noise hazard of large areas, one utilizes the indices defining the percentage portion of the area "polluted" by the excessive noise in relation to the whole investigated area.

Generally, the scheme of determining this type of index is presented in Fig. 1 ([1]).

As it follows from the above considerations, the accuracy of calculation of the endangered area becomes important. The area in which a noise in excess to the standard value exists can always be extrapolated to determine the area of a rectangle in the case of a linear source, or that of a circle for a punctual source.

For linear sources the area is

$$P = lr, \tag{11}$$

where l – length of the road or railway line being the source of noise, r – determined range of the noise influence.

The error in the determination of the area is

$$\Delta P = \left[r^2 \Delta l^2 + l^2 \Delta r^2\right]^{1/2}, \tag{12}$$

([1]) By the term "linearized source length" appearing in the scheme the considered length of the road or railway line section or the circumference of the analysed plant is meant.

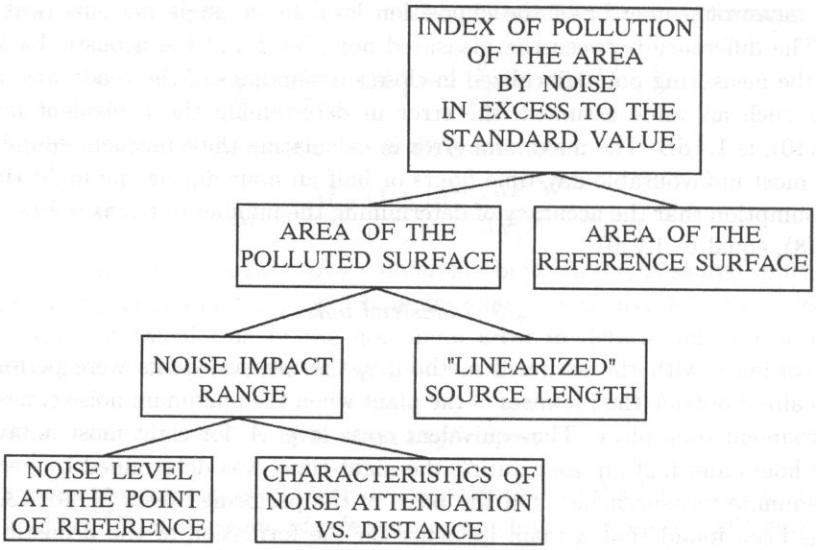

Fig. 1. Scheme of determination of the dependence of the index value of polluting an area by noise in excess to the standard value.

where Δl – error of determining the road or railway line lengths from the map base, Δr – error of calculating the range of the influence of noise.

This range is a complex function depending on the difference between the measured noise level A and the admissible value and on the character of the noise decay with distance. It is calculated from the relationship

$$r = r_0 10^{L_D/a}, \tag{13}$$

where r_0 – distance between the source and the reference point, L_D – difference between the noise level measured at the point of reference and the admissible value, a – coefficient characterizing the course of the decay with distance.

Using the relationships

$$\frac{\delta r}{\delta L} = \frac{r}{a \log e} \tag{14}$$

and

$$\frac{\delta r}{\delta a} = \frac{rl}{a^2 \log e} \tag{15}$$

and taking advantage of the fact that the range r of the noise influence depends on the difference between the measured noise level and admissible one and on the character of decay of the noise level with increasing distance from the source, the Δr value has been determined as:

$$\Delta r = \frac{r}{a \log e} \left[\Delta L^2 + \frac{L_D}{a^2} \Delta a^2 \right]^{1/2}. \tag{16}$$

Substituting (16) in (12) one obtains

$$\Delta P = \left[r^2 \Delta l^2 + \frac{r^2 l^2}{a^2 (\log e)^2} \left(\Delta L^2 + \frac{\Delta L_D^2}{a^2} \Delta a^2 \right) \right]^{1/2} . \tag{17}$$

Finally, the relative error of estimating the area polluted by the road traffic and railway noise is:

$$\frac{\Delta P}{P} = \left[\frac{\Delta l^2}{l^2} + \frac{L_D^2}{a^2 (\log e)^2} \left(\frac{\Delta L}{L_D^2} + \frac{\Delta a^2}{a^2} \right) \right]^{1/2} . \tag{18}$$

The estimation of the error in the area endangered by the excessive noise (over 55 dB) has been carried out taking as an example road sources. The following assumptions have been made:

— the value of the error, ΔL, of determining the equivalent sound level A is 3 dB,

— the error, Δl, of determining the lengths of the road sections from the map bases is 10% and is constant for each of them,

— the error, Δa, of determining the drop of the sound level A with increasing distance from the source was determined on the basis of calculations utilized in preparing Fig. 2.

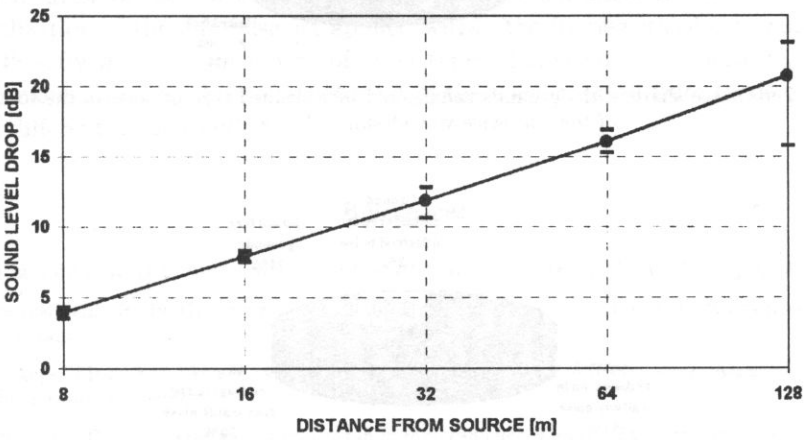

Fig. 2. Experimentally determined characteristics of the decay of the sound level A at a site for road traffic noise, with marked values of the standard deviation.

From the above assumptions, using the relationship (18) (by applying suitable procedures of transformation of the relative units (dB) into the acoustic pressure units) the maximum relative errors of determining the area endangered by excessive noise for individual reached zones have been found. These values are:

— for the distance from 4 m to 8 m from the reference point – up to 36%,
— for the distance from 8 m to 16 m from the reference point – up to 36%,
— for the distance from 16 m to 32 m from the reference point – up to 37%,
— for the distance from 32 m to 64 m from the reference point – up to 37%,
— for the distance above 64 m from the reference point – up to 37%

(for $r_{\max} = 270$, which corresponds to an equivalent noise level A at the point of reference equal to 80 dB).

The values of these errors result from the considerable simplification related to a very wide range of the measuring work conducted. Their values can be accepted, taking into account that the results obtained are intended for recognition and general administrative purposes.

6. Conclusions

As the result of the performed field testing, the complete assessment of the acoustic climate within the limits of the Katowice voivodeship resulting from the three main noise sources have been obtained. This situation is schematically presented in Figs. 3 and 4.

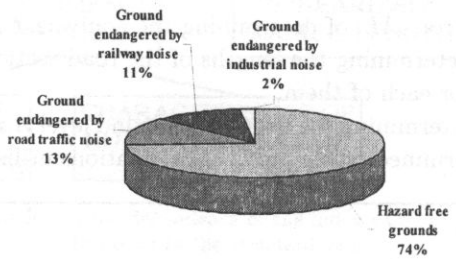

Fig. 3. Percentage share of the grounds endangered by a defined type of noise in the total area of the Katowice voivodeship. The day-time.

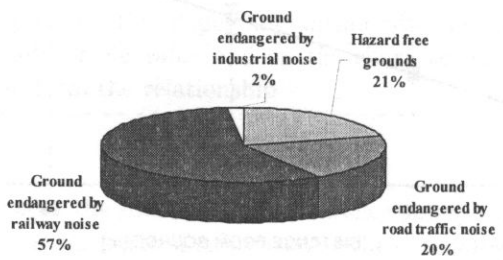

Fig. 4. Percentage share of the grounds endangered by a defined type of noise in the total area of the Katowice voivodeship. The night-time.

The presented test results enable to conclude that the hazard caused by industrial noise is much lower than to the traffic one. This is mainly caused by:

— lower values of the sound levels A of the industrial noise at the point of reference as compared to that of the traffic. The sound levels L_{eq} at the reference point were comprised within the limits:

— from 59 to 84 dB (day-time) and from 50 to 78 dB (night-time) for the road traffic noise;

— from 59 to 76 dB (day-time) and from 69 to 82 dB (night-time) for the railway noise;

— from 43 to 69 dB (day and night time) for the industrial noise;

— faster drop of the sound level A of the industrial noise with the distance;

— lower linearized sum of circumferences of the plants as compared to the length of the transportation lines.

As the result of the performed assessment, also the estimation of the hazard to people from the influence of noise of a level in excess to the standard value (55 dB) has been made. From this, it has been found that during the day-time ca. 30% of the population is endangered which constitutes ca. 1 150 000 inhabitants of the Katowice voivodeship.

In the author's opinion, a further development of the presented investigation should be:

— conduction of research work on plans of development and management of large administrative units, with particular consideration of the decision-making process, which should be advantageous from the point of view of the protection of the environment against excessive noise,

— preparation of acoustic maps of large areas,

— improvements of the methodics of carrying out measurements of various noise components,

— research work on models of noise propagation in the land with different degrees of urbanization,

— verification of the functioning models of surface and linear sources,

— utilization of the database set applied within the framework of this work as well as the GIS software for visualization of other types of environmental hazards,

— development of method of assessment of the noise emitted from roads with pavements of different quality.

References

[1] Ustawa z dnia 31.01.1980 r. o ochronie i kształtowaniu środowiska (Dz.U. Nr 3, poz. 6).

[2] Rozporządzenie Rady Ministrów z dnia 30.09.1980 r. w sprawie ochrony środowiska przed hałasem i wibracjami.

[3] Instrukcja ITB nr 308 *Metoda określania uciążliwości i zasięgu hałasów przemysłowych wraz z programem komputerowym.*

[4] Instrukcja ITB nr 310 *Metody sporządzania kompleksowych planów akustycznych miast i obszarów.*

[5] Instrukcja ITB nr 311 *Metody prognozowania hałasu emitowanego z obszarów dużych źródeł przemysłowych.*

[6] Instrukcja IOŚ *Metody pomiarów hałasu zewnętrznego w środowisku.*

[7] Instrukcja IOŚ *Obliczeniowe metody oceny klimatu akustycznego w środowisku.*

[8] R. Makarewicz, *Losowe własności poziomu równoważnego* L_{AeqT}, Materiały XXXVIII Otwartego Seminarium z Akustyki, OSA'91, Poznań 1991.

[9] A. Lipowczan, *Podstawy pomiarów hałasu*, GIG LWzH, Katowice-Warszawa 1987.

[10] Z. Engel, *Ochrona środowiska przed drganiami i hałasem*, PWN, Warszawa 1993.

[11] J.-G. Migneron, *Acoustique urbaine*, Masson, Quebec 1980.

[12] J. Sadowski, *Podstawy akustyki urbanistycznej*, ARKADY, Warszawa 1982.

[13] Cz. Puzyna, *Zwalczanie hałasu w przemyśle*, WNT, Warszawa 1974.

[14] J. Kompała, *Mapa akustyczna województwa katowickiego. Część I. Hałas drogowy*, Ekologia i Technika, 3/9 (1994).

[15] J. KOMPAŁA, *Mapa akustyczna województwa katowickiego. Część II. Hałas kolejowy*, Ekologia i Technika, 6/12 (1994).

[16] Z. KOSZARNY, *Kryteria oceny hałasu ulicznego w świetle odczuć i reakcji mieszkańców*, Mat. I Krajowego Seminarium "Oddziaływanie hałasu drogowego na środowisko", LWzH MOSZNiL, Warszawa 1994.

[17] Z. KOSZARNY, W. SZATA, P. GORYŃSKI, *Porównawcza ocena wskaźników poziomu hałasu ulicznego z uwzględnieniem oddziaływania na mieszkańców Warszawy*, Roczniki PZH, **33**, 5-6 (1982).

[18] R. KUCHARSKI, M. KRASZEWSKI, A. KURPIEWSKI, *Obliczeniowe metody oceny klimatu akustycznego w środowisku*, Wyd. Geologiczne, Warszawa 1988.

[19] R. MAKAREWICZ, *Hałas w środowisku*, Ośrodek Wydawnictw Naukowych, Poznań 1996.

[20] M. MAURIN, *Comunity noise impact indicators: a framework and examples*, Journal of Sound and Vibration, **79** (1991).

[21] ISO 1996 Acoustics – Description and measurement of enviromental noise.

[22] ISO 1996 Acoustics – Determination of occupational noise exposure and estimation of noise-induced hearing impairment.

[23] PN-81/N-01306 *Hałas. Metody pomiaru. Wymagania ogólne.*

[24] A. KURPIEWSKI, W. GAJDANOWICZ, D. GOLBA, *Sporządzenie planów akustycznych obszarów zurbanizowanych na przykładzie Jeleniej Góry*, Mat. do referatu na XXIII Zimową Szkołę Zwalczania Zagrożeń Wibroakustycznych, Wisła 1995 [niepublikowana].

[25] J. KOMPAŁA, *Próba oceny hałasu przemysłowego na terenach silnie zurbanizowanych*, Mat. XXIII Zimowej Szkoły Zwalczania Zagrożeń Wibroakustycznych, Wisła 1995.

[26] J. KOMPAŁA, *Pomiary hałasu w województwie katowickim*, Aura, 10, 1995.

[27] J. KOMPAŁA, J. ŚWIDER, A. WANDZIOCH A, *Emisja hałasu przemysłowego do środowiska na terenie województwa katowickiego*, Proceedings of the International Conferency "Noise Control'95", Warszawa 1995.

ARCHIVES OF ACOUSTICS
23, 3, 353–361 (1998)

OPTIMIZATION OF THE DURATION OF AN ECHOGRAM RESULTING FROM COMPUTER SIMULATION OF THE ACOUSTIC PROPERTIES OF A ROOM

R. GOŁĘBIEWSKI, E. HOJAN, M. WOJTCZAK and P. PĘKALA

Institute of Acoustics,
Adam Mickiewicz University
(60-769 Poznań, ul. Matejki 48/49)

The authors of this paper investigated the ways to decrease the time of calculating an echogram in the computer simulation of the distribution of the sound field in a room. The authors emphasize the existence of a limiting moment t_{st} up to which the simulation must be completed. The remaining part of the echogram may be treated as a stochastic amplitude (temporal distribution). The authors related the moment t_{st} to the reverberation time RT and the early decay time, EDT, of a room.

1. Introduction

The implementation of computer systems in acoustics allowed, among other things, a more precise prediction of acoustic properties of real rooms and room designs.

Studies based on computer simulation aim at a maximum fidelity of the representation of the actual conditions. In the case of the simulation of auditory rooms, it becomes possible to evaluate their acoustical properties already at the design stage. In simulation methods it is very easy to correct the positions of the walls, the source of sound, the observation point, etc.

Computer simulation leads to an echogram (a transient response of the room) which provides a collection of data for both objective and subjective evaluation of the acoustic properties of a room.

Basing on an echogram, a number of acoustic parameters may be determined yielding objective characteristics of a room. On the other hand, the convolution of the echogram with the function of a discretionarily selected signal allows the subjective evaluation of the quality of a sound in the simulated room.

Although computers of high processor capacity are used for this task, the time of simulation of an echogram is still too long. Therefore, scientists look for methods of decreasing the time necessary for the calculation of an echogram.

The literature of the subject often postulates that in the process of evaluating the acoustic properties of a room only the early part of the echogram is important. Basing on this postulate, it was proposed by HOJAN and PÖSSELT [2] that the simulation of the

entire echogram is not necessary. It is sufficient to simulate it up to a certain moment T_i. The relation between T_i and the duration of the entire echogram, T, is

$$T_i = \alpha T, \tag{1}$$

where $\alpha = 0.4 \div 0.5$ as results from Hojan and Pösselt's experiment. Moreover, it turned out that it is important to simulate only the very early part of the actual echogram provided that its further distribution, resulting from simulation of the entire echogram, is then replaced by a stochastic distribution of the sound amplitude decaying exponentially with time. In order to prove this hypothesis, a subjective evaluation of signals of music and speech was performed after convoluting the signals with the entire simulated echograms. The results of this procedure were compared with echograms consisting of the early parts of the actual echogram and the stochastic parts decaying exponentially. In each case, the duration of the echograms "produced artificially" (with addition of the stochastic parts) was the same as that of the entire simulated echogram, but the durations of the part of the accurate echogram and the stochastic part were varied during the experiment.

The aim of our experiments was to specify the time limit up to which an echogram should be simulated in order to obtain a subjective evaluation of a signal (convoluted with the early part of the echogram) being identical with that of this signal convoluted with the entire echogram. The evaluation was accomplished using sound signals and echograms different from those used in the experiment described by HOJAN and PÖSSELT [2].

The ultimate purpose of the experiment was to generalize the relations between the minimum time required for an accurate computer simulation of the echogram and the selected acoustic parameters of the room and, when applicable, the type of the sound signal to be evaluated after the convolution operation.

2. Computer simulation

The authors of this paper used a computer program that allowed to simulate the acoustic properties of a room. The program had been developed at the Institute of Acoustics of the Adam Mickiewicz University and implemented into a so-called cone-tracing method.

The sound energy decrease caused by the sound absorption accompanying reflections of acoustic waves from the walls was taken into account in the calculation of the echogram. The absorption of sound by the medium was disregarded because of the negligible influence of this factor on the value of the acoustic energy in the considered range of distances between the source and the sound receiver.

The directional characteristics of the human ear, a factor which produces some difference in the sound signal pressure registered by each ear, were also taken into consideration in the program.

3. Echogram

An echogram is a temporal record of the acoustic pressure at a given point in the room following a pulse stimulation of acoustic vibrations in this room. This temporal distribution of the pressure is, in fact, an impulse response of the room recorded at a specific observation point for a given specific position of the source of the sound. In view of the limited capacity of the computer memory, a histogram is used as an approximation of the echogram. The histogram is plotted by dividing the period of observation into a finite number of ranges and calculating the sum of sound intensities within each range. Thus, the histogram is a set of bars numbered from 1 to $k_{\max}$ (where $k_{\max}$ is the ordinal number of the last temporal range). The height of each bar corresponds to the value of the sum of squared acoustic pressures received at the observation point during the time indicated by the width of the bar.

The height of the i-th bar p_i^2 ($i = 1, 2, \ldots, k_{\max}$) may be expressed by the equation

$$p_i^2 = \sum_t p^2(t), \tag{2}$$

where $t \in \langle t_i, t_{i+1} \rangle$, and

$$t_k = (k-1)\frac{T_{\max}}{k_{\max}}, \tag{3}$$

where k – ordinal number of the bar, $T_{\max}$ – duration of the histogram, $k_{\max}$ – total number of bars in the histogram.

In the calculation of the histogram, the above-mentioned energy decrease due to reflections of acoustic waves from the walls of the room is taken into account. Hence, the values of the squared pressure corresponding to individual cones "emitted" by the source are multiplied by the factor

$$\prod_{i=1}^{N}(1-\alpha_i), \tag{4}$$

where N – number of reflections of the observed cone from the walls of the room, α_i – absorption coefficient of the i-th wall.

4. Parameters calculated on the basis of an echogram

An echogram provides the basis for the calculation of a number of parameters which allows an objective acoustic evaluation of the room. The criterion in the selection of objective parameters was their correlation with subjective evaluations of selected sound attributes, while the heed was paid particularly to the aim of this paper, i.e. to the specification of the limiting value t_{st}.

All parameters were calculated assuming both the monaural and binaural perception of sound. The calculated parameters are as follows:

- the reverberation time RT, basing on the histogram transformed into the Schroeder's curve,

- the early decay time EDT, basing on the histogram transformed into the Schroeder's curve,
- the sound pressure level L_p,
- the temporal centre of the echogram t_s,
- the articulation (Deutlichkeit) D,
- the clarity C.

Schroeder's curve, which is the basis for calculation of all the parameters mentioned above is defined by the following equation

$$R_{db}(k') = 10\mathrm{Lg}\frac{\sum_{k=k'}^{k_{\max}} p_{lk}p_{pk}}{\sum_{k=1}^{k_{\max}} p_{lk}p_{pk}} \quad [\mathrm{dB}], \tag{5}$$

where p_{lk}, p_{pk} – total values of the RMS for the left and the right ear in the k-th range, respectively, $k_{\max}$ – ordinal number of the last temporal range, k – ordinal number of the temporal range (k, $k' = 1, 2, \ldots, k_{\max}$).

4.1. Reverberation time

In the range of $t \in (0, T_{\max})$, the function $R(t)$ is a continuous and non-growing function which allows the calculation of the reverberation time from the equation

$$RT = 3|t_{-5} - t_{-25}|, \tag{6}$$

where t_{-5} denotes the time corresponding to the value of $-5\,\mathrm{dB}$ on the Schroeder's curve, t_{-25} denotes the time corresponding to the value of $-25\,\mathrm{dB}$ on the Schroeder's curve.

A discretization of equation (6) produces

$$RT_d = 3|k_{-5} - k_{-25}|, \tag{7}$$

where k_{-5} denotes the ordinal number of the temporal range corresponding to the value of $-5\,\mathrm{dB}$ on Schroeder's curve, k_{-25} denotes the ordinal number of the temporal range corresponding to the value of $-25\,\mathrm{dB}$ on Schroeder's curve.

4.2. Early decay time

The EDT is calculated on the basis of the reverberation curve (5) using the relation

$$EDT = 6k_{-10}\,, \tag{8}$$

where k_{-10} is the ordinal number of the temporal range corresponding to the value of $-10\,\mathrm{dB}$ on the Schroeder's curve.

Since no consistent correspondence was found between the time limits t_{st} and other acoustic parameters of the room, except RT and EDT, they are not defined in this paper.

5. Convolution function

A subjective evaluation of signals in the simulated room was possible by applying a convolution function defined as follows:

$$f(t) = \int_{-\infty}^{\infty} f_1(\tau) f_2(t-\tau)\, d\tau\,, \tag{9}$$

where $f_1(\tau)$ – impulse response of the room, i.e., in this case, the echogram resulting from simulation, $f_2(t-\tau)$ – signal of music or speech to be submitted to the subjective evaluation in the simulated room.

In order to eliminate the influence of any other rooms on the signal to be evaluated in the simulated one, it was recorded under anechoic conditions using a digital tape recorder. Subsequently, the signal was put into the computer via an analog-digital converter, at a sampling frequency eliminating the so-called "aliasing" effect, and the convolution operation of the recorded signals with entire or "produced artificially" echograms was then carried out. The output signal, after its analog-digital conversion, was recorded again using a digital tape recorder and then reproduced via headphones in order to present it to the listener for the subjective evaluation.

6. Test signals

The two echograms used in the experiment were obtained by means of a computer simaulation of the interior of a church under two different acoustic conditions. The signals were speech (a sentence in Polish), guitar music and violoncello-and-violin music. All signals were recorded in an anechoic chamber. The duration of each signal did not exceed 10 s.

Echogram 1, of duration of 600 ms, was convolved with the signal of speech and the signal of guitar music. Echogram 2, of duration of 1000 ms, was convolved with the signal of speech (the same as in the case of echogram 1) and the signal of violoncello-and-violin music.

After convolution with the echograms, the signals were recorded using a digital tape recorder and submitted to subjective evaluation by means of earphone listening applying constant stimuli method.

The process of "artificial production" of the echograms comprised the removal of their final parts (of various duration) and the addition of a stochastically distributed amplitude decaying exponentially with time. While producing such compounded echograms, the problem arose how to relate the last bar of the echogram (after the removal of its final part) to the first one of the stochastic part. In the present work it was assumed that the amplitude of the last bar of the actual echogram was identical with that of the first one of the stochastic part; following the latter, the value of the sound amplitude decayed exponentially with time.

Table 1. Initial parameters for computer simulation.

		Echogram 1	Echogram 2
1.	Number of rays	12.000	10.000
2.	Duration of the echogram	600 ms	1000 ms
3.	Maximum order of the ray	8	12

7. Experiment

The experiment was divided into several stages. The first one was the preparation of echograms, i.e. the removal of their final parts and the addition of the stochastic part; the duration of the removed part was each time increased by 20 ms. The stochastic part was generated anew after each removal.

The duration of the echogram with the stochastic part added was identical to that of the actual echogram. All such echograms were subsequently convolved with a selected signal.

The next stage was the preparation of pilot experiments in order to assess preliminarily the limiting moment t_{st} of the computer simulation of the echogram. These experiments were conducted in a downgoing series with signals grouped in pairs. Each pair consisted of a signal convolved with an entire echogram (the standard signal) and a signal convolved with an echogram with a part removed (the test signal). The sequence of signals in a pair was random. Each subsequent pair of signals differed from the previous one by the duration of the removed part of the echogram in the test signal. The duration of the removed part was increased each time by 20 ms. The intervals between the signals in a pair did not exceed 1 s, and those between pairs did not exceed 5 s.

The pilot experiments were conducted with the participation of 6 listeners. The same listeners participated in the main experiments in which the constant stimuli method was applied as well. The listeners aged from 21 to 29 and had no musical education. At most two listening session were caried out within a day (with an hour's intermission). The prepared listening tests were recorded by means of a digital tape recorder and reproduced via earphones.

A listening test using the constant stimuli method included 3 to 5 series (depending on the duration of the signal and the number of pairs in a series). From 12 up to 14 pairs of signals were presented to the subject in each series. The number of pairs in a series depended on the accuracy margin of the assumed time values t_{st} in the individual listeners responses. Hence, in order to fill the "transition range" around the assumed temporal limit, more pairs of signals had to be presented. As in the pilot experiments, the sequence of signals in a pair was random.

Each series contained the same pairs of signals arranged randomly within each series. The sequence of series at each listening session was also random. One listening session lasted at most 20 minutes.

After the listening session, the number of affirmative responses of each listener was counted. The results were presented in the form of a psychometric curve of a single

listener. Subsequently, the numbers of affirmative responses of all listeners were avaraged; they are presented in the form of a psychometric curve (see Fig. 1).

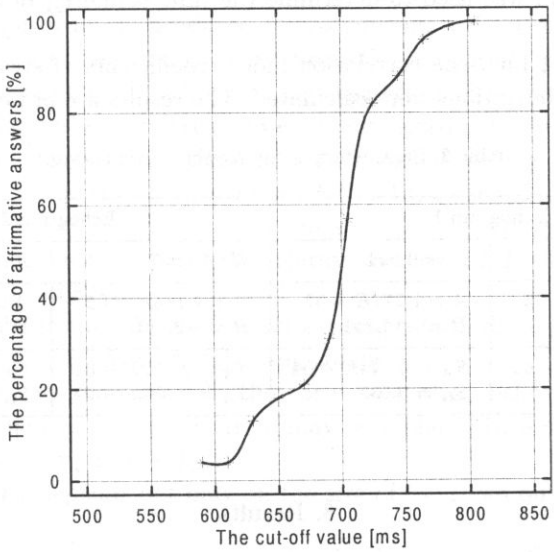

Fig. 1. Psychometric curve of the results for all the listeners (signal of speech, echogram 2).

Using a table of conversions of the values of the psychometric curve p to values projected along the straight line with ordinates z, the results were presented in the form of a straight line from which the values of the time limit t_{st} were read (see Fig. 2).

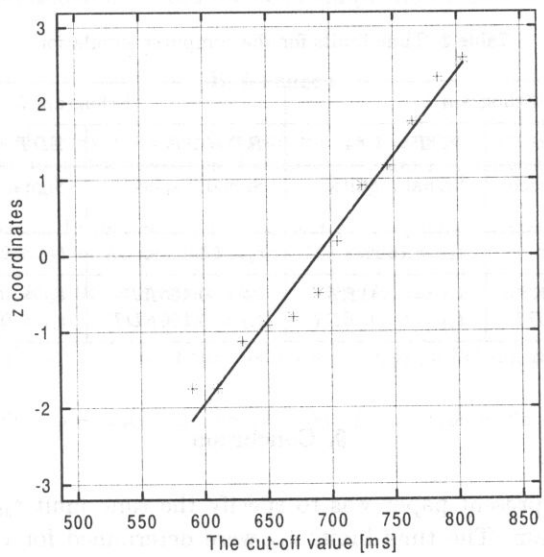

Fig. 2. The straight line resulting from the conversion of p values to z values, for all the listeners (signal of speech, echogram 2).

The value of t_{st} corresponds to the abscissa of the point on the line whose ordinate is equal to zero.

A similar method was used to determine the time values t_{st} of all signals and both the echograms.

For each straight line, the correlation index, coefficients of straight lines A and B and their standard deviations were calculated. The results are presented in Table 2.

Table 2. Parameters of the psychometric curves.

Echogram 1		Echogram 2	
$K = 0.983$	$K = 0.994$	$K = 0.997$	$K = 0.982$
$A = 2.138E - 02$ $B = -14.747$	$A = 1.777E - 02$ $B = -14.851$	$A = 1.115E - 02$ $B = -2.701$	$A = 1.011E - 02$ $B = -3.733$
$S_A = 1.321E - 03$ $S_B = 0.912$	$S_A = 6.344E - 04$ $S_B = 0.537$	$S_A = 2.932E - 04$ $S_B = 7.604E - 02$	$S_A = 5.6E - 04$ $S_B = 0.223$

8. Results

In Table 3, the values of t_{st} obtained in the experiments for two echograms are presented. The values are also related to the reverberation time RT and the early decay time EDT of the simulated room for either echogram and for two types of signals convolved with either echogram.

Our data did not support the extant relationship between the time value t_{st} and other acoustic parameters of the room, mentioned previously (Sec. 4 of this paper).

Table 3. Time limits for the computer simulation.

Echogram 1		Echogram 2	
$RT = 0.79$ s	$EDT = 1.84$ s	$RT = 1.17$ s	$EDT = 1.78$ s
Signal : speech	Signal : guitar	Signal : speech	Signal : violin and violoncello
$t_{st} = 320$ ms	$t_{st} = 165$ ms	$t_{st} = 360$ ms	$t_{st} = 230$ ms
$t_{st} = 0.279RT$ $t_{st} = 0.18EDT$	$t_{st} = 0.141RT$ $t_{st} = 0.092EDT$	$t_{st} = 0.465RT$ $t_{st} = 0.196EDT$	$t_{st} = 0.291RT$ $t_{st} = 0.125EDT$

9. Conclusion

The aim of the present paper was to specify the time limit t_{st} of computer simulation of an echogram. The time limits t_{st} were determined for two echograms characterizing a simulated church under various acoustic conditions and with the same shape of the church. The signals used in the experiment were speech, guitar music and

violoncello-and-violin music. The determined time values t_{st} are shown in Table 3. The subjective evaluation of the signals of speech produced time values t_{st} larger than those in the case of music signals. It was due presumably to a certain amount of reverberation inherent in the sound of music produced by instruments with a resonance box. There were no significant objective differences between the magnitude spectra of the signal convoluted with "compounded" echogram and that convoluted with the entire simulated echogram, although such differences were easily heard in the subjective evaluation.

Table 3 contains values of the time limit t_{st} obtained during the experiment and shows their relation to the reverberation time RT and the early decay time EDT of the simulated room. As shown in Table 3, the values of t_{st} are scattered between $0.141\,RT$ and $0.465\,RT$, whereas, in the case of the relation to their EDT, the scatter is smaller: from $0.092\,EDT$ to $0.196\,EDT$.

Comparison of the results obtained in our experiments to those presented in a paper by HOJAN and PÖSSELT [2] leads to following conlusions:

1. It is necessary to simulate only the early part of an echogram limited by the time moment t_{st}. The rest of the echogram may be replaced by a stochastic amplitude distribution of a duration of $(T_i - t_{st})$,

2. The value of t_{st} depends not only on the size of the room but also on the type of the signal,

3. The t_{st} values are always smaller for signals of music than for those of speech,

4. The time limit values t_{st} may be related to the reverberation time RT and the early decay time EDT. Any change of the experimental conditions (such as, e.g., a change of total absorption in a room) alters the relation between t_{st} and RT. Therefore, the parameter EDT seems to be more useful as an objective measure of reverberation in the computer simulation of a room.

All the statements above are valid for both simple and complex rooms.

References

[1] A.C. GADE, *Acoustical survey of eleven European Halls – a basis for discussion of hall in Denmark*, Raport No. 44 (1989) from The Acoustical Laboratory Technical University of Denmark, Building 352, DK 2800 Lyngby.

[2] E. HOJAN, CH. PÖSSELT, *Prediction of the early part of echograms indispensable in computer simulation in rooms*, Archives of Acoustic, **16**, 2, 295–303 (1991).

[3] P. LEHMAN, *Über die Ermittlung Raumakustischer Subjektiven Beurteilungen der Hörsamkeit D83*, Berlin 1976.

[4] R.S. WOODWORTH, H. SCHLOSBERG, *Experimental psychology* [in Polish], 2nd ed, PWN, Warszawa 1975.

[5] R. GOŁĘBIEWSKI, *The optimization of the duration of an echogram* [in Polish], Master Thesis, Poznań 1993.

ARCHIVES OF ACOUSTICS
23, 3, 363–378 (1998)

DETECTION AND DISCRIMINATION OF MODULATION TYPE AT LOW MODULATION RATES

A.P. SĘK

Institute of Acoustics,
Adam Mickiewicz University
(60-769 Poznań, ul. Matejki 48/49)

For a sinusoidal carrier at a frequency of 1 kHz, amplitude (AM) or frequency (FM) modulated by a sinusoidal modulator at a rate of $f_{\mathrm{mod}} = 2$, 5 or 10 Hz, psychometric functions for the detection and the discrimination of modulation type were measured as a function of an appropriate modulation index (i.e. m or β). Stimuli were presented in quiet or with a band of noise chosen to mask the low- or high-frequency side of the excitation pattern produced by a modulated signal. In AM case d' markedly depended on the presence of a noise that masked the high-frequency part of the excitation pattern. For FM signals, on the other hand, when modulation rate was equal to 2 Hz bands of noise did not influence d' values. Probability of identification of modulation type (AM or FM) was the highest for the smallest modulation rate and it was nearly equal to the probability of modulation detection. Presence of any of these two bands of noise did not effect the modulation identification. The results suggest that there are two mechanisms underlying the detection and the discrimination of modulation type. One of them is based entirely on the changes in the excitation pattern level and operates for a whole range of carrier frequencies and modulation rates (place mechanism). However, for a low modulation rate there is another mechanism responsible for the detection of frequency changes only. This mechanism provides additional information about frequency changes and brings about markedly higher delectability d' for the detection and discrimination of frequency changes. This mechanism is not based on the ability of the auditory system to compare a phase of the excitation pattern changes at different frequency areas. It seems that information about frequency changes at a low rate may be effectively coded in a time distribution of neural spikes.

1. Introduction

Investigations concerned with amplitude and frequency changes at very low modulation rates (i.e. less than 20 Hz) have provided a great variety of data about the auditory system and have been extensively discussed in the psychoacoustical literature, [1–3, 8, 11, 12, 16–19, 21, 26–28, 30, 32]. There are two basic hypotheses that have been advanced about the perception of amplitude and frequency changes in an acoustic signal. One of them, called the ZWICKER–MAIWALD model [11, 12, 30, 32] postulates that a single mechanism is responsible for the perception of changes in amplitude and frequency. The other one, presented by CONINX [2, 3] and FETH [5], assumes the existence of two independent mechanisms, one for amplitude changes and one for frequency changes.

The Zwicker–Maiwald model is essentially a place model based on the concept of the psychoacoustical excitation pattern. The excitation pattern evoked by a sound can be defined as the output of the auditory filters as a function of centre frequency, in response to that sound [13, 15]. A maximum of the excitation pattern evoked by a sinusoidal signal is observed at a characteristic frequency which corresponds to the frequency of exciting sinusoid. This excitation pattern is a lot steeper on the low-frequency side and decays gradually on the high-frequency side.

In a more recent version of this model [16, 18] a non-linear compression that takes place on the basilar membrane is included [23, 24], as well as some of the phenomena occurring in the auditory nerve [22]. An increase in amplitude of a signal gives rise to an increase in the maximum of the excitation pattern but also brings about a spread of the excitation pattern in frequency domain; more auditory filters are active.

When the auditory system is excited by AM signal then the excitation pattern changes in the same way as the amplitude of the stimulating signal; this is illustrated in the upper left panel of Fig. 1. To make the excitation pattern changes clearly visible two curves illustrate the excitation patterns for extreme values of AM signal and for AM index equal to 20% that corresponds to difference in level $\Delta L = 4.5\,\mathrm{dB}$. It is worth noting that a bigger change in excitation level occurs on the high-frequency side of the excitation pattern. This happens because the excitation level on the high-frequency side of the pattern grows non-linearly with changes in level. The left lower panel of Fig. 1 presents a difference of the excitation patterns evoked by AM signal for extreme values of its amplitude for modulation depth of $m = 0.04$ ($\Delta L = 0.7\,\mathrm{dB}$) which is close to the average threshold for modulation rate from the range of $f_{\mathrm{mod}} = 2 - 50\,\mathrm{Hz}$. Note that the difference on both sides of the maximum is in the phase and bigger on the high-frequency side.

The excitation pattern produced by the FM signal has a constant maximum but it moves along a frequency axis as the signal frequency changes. The excitation patterns evoked by the FM signal at extreme values of its frequency are presented in the upper right panel of Fig. 1. To make the excitation pattern changes clearly visible deviation was equal to 100 Hz. For FM signals a bigger change in excitation level usually occurs on the low-frequency side of the pattern, where the slope is steepest. This is also shown in the lower right panel of Fig. 1. It shows the difference in the excitation patterns produced by FM signal at extreme frequencies for deviation of 4 Hz. This value is close to the average threshold for modulation rate from the range of $f_{\mathrm{mod}} = 2 - 50\,\mathrm{Hz}$.

In the simplest version Zwicker–Maiwald's model assumes that changes in either amplitude or frequency are detected by monitoring the single point on the excitation pattern that changes most. This is equivalent to monitoring a single auditory filter. The detection of changes in amplitude or frequency occurs when the change in the excitation pattern exceeds a criterion amount, which was empirically established to be approximately 1 dB. The model also assumes that amplitude and frequency changes cannot be distinguished at the detection threshold.

Some more recent models assume that information about amplitude and frequency changes can be combined over a certain region of the excitation pattern. This is equivalent to monitoring several auditory filters simultaneously [6, 14].

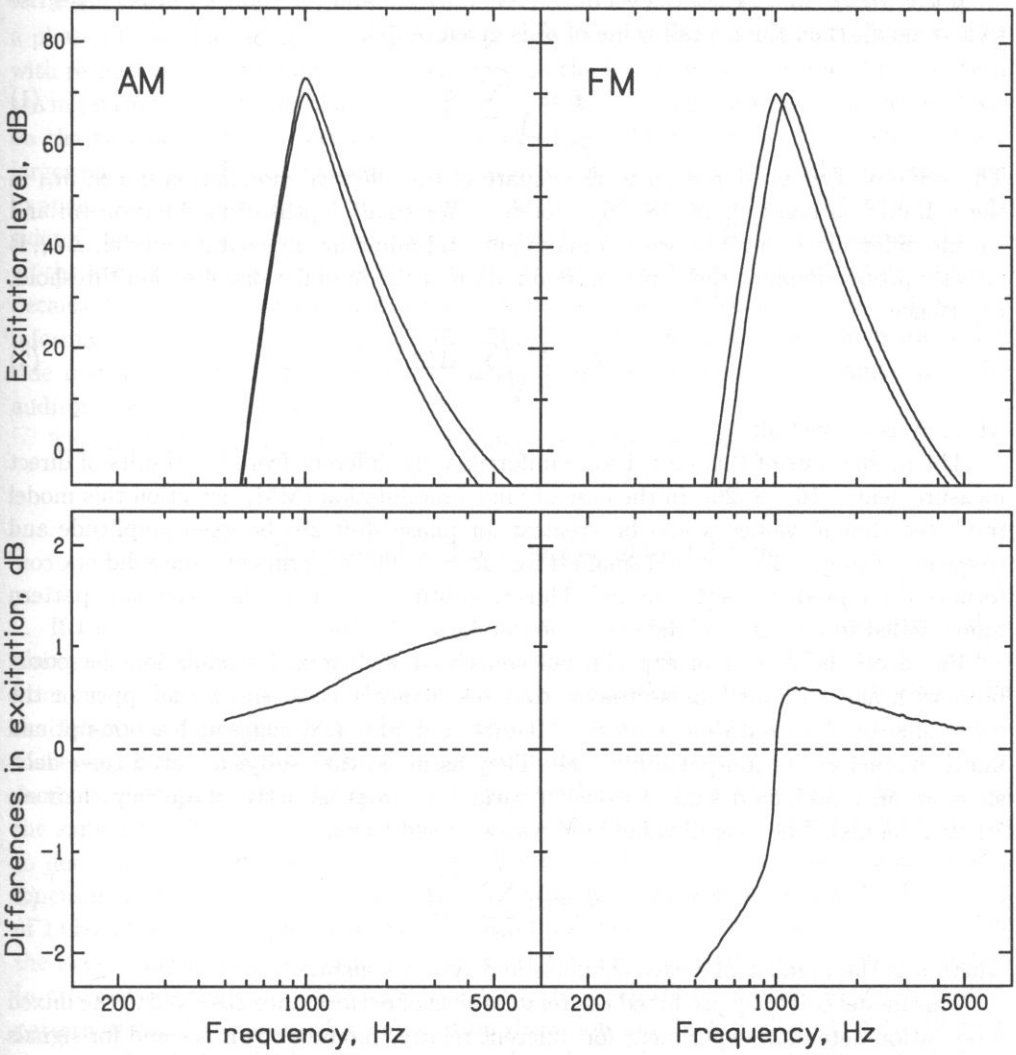

Fig. 1. Upper row shows the excitation patterns produced by amplitude (left panel) and frequency (right panel) modulated tones for extreme values of amplitude and frequency respectively, for suprathreshold values of appropriate modulation indices. Lower row shows the differences in excitation patterns produced by amplitude (left panel) and frequency (right panel) modulated tones for extreme values of amplitude and frequency respectively, for nearthreshold values of appropriate modulation indices.

For example, the model proposed by FLORENTINE and BUUS [6] assumes that information from the entire excitation pattern, i.e. from each excited critical band or active auditory filter, is combined in an *optimal* way (so-called optimal multi-channel model, [16]), from the point of view of the signal detection theory (so-called integration model) [7].

If the change in excitation level in the i-th critical band (or auditory filter) gives rise to a value d'_i, then the overall value of d' is given by [7]:

$$d' = \sqrt{\sum_i d'^2_i}. \tag{1}$$

The value of d'_i is proportional to the square of the effective modulation index, m_i, in the i-th critical band [9, 16, 18, 26]. Moreover, for small depths of modulation (m and β), the difference in level between a maximum and minimum in excitation level, ΔL_i, is directly proportional to the depth of modulation at the modulation detection threshold, m_i. Hence,

$$d' = K\sqrt{\sum_i \Delta L_i^4}, \tag{2}$$

where K is a constant.

The predictions of this model were unfortunately different from the results of direct measurements, [16, 18, 26]. In the case of mixed modulation (MM) detection this model predicted that d' values would be greatest for phase shift $\Delta\phi$ between amplitude and frequency changes $\Delta\phi = \pi$, and smallest for $\Delta\phi = 0$. The experimental data did not conform to these predictions [16, 18, 26]. Thus the optimal multi-channel excitation-pattern model failed to account for the experimental data.

Based on the results of experiments concerned with mixed modulation detection, both with and without bands of noise that selectively masked either the upper or the lower side of the excitation pattern, MOORE and SĘK [18] suggested a non-optimal multi-channel excitation-pattern model. They assumed that subjects based their decisions on an unweighted sum of decision variables across all active frequency channels (critical bands). The overall value of d' was assumed to be:

$$d' = K\sum_{i=1}^{n} \frac{\Delta L_i^2}{\sqrt{n}}, \tag{3}$$

where n is the number of active channels and K is a constant.

This model correctly predicted the relative level of performance observed in the mixed modulation detection experiment for different relative modulator phases and for signals presented in quiet or with noise bands. Correlation of the predictions and measured d' values reached about 90% [18, 27]. Based on this model it is possible to interpret a monotonic increase in difference limens for AM and FM signals [20, 29].

The non-optimal multi-channel excitation-pattern model also predicts that the discrimination of modulation type (or modulation identification) is impossible at the detection threshold of modulation. The ability of subjects to identify the modulation type, i.e. AM or FM was studied by DEMANY and SEMAL [4] for very low modulation rates. They showed that the identification performance was almost equal to the detection performance when the modulation rate was less than 5 Hz which cannot be explained by the non-optimal multi-channel. Thus is there any additional mechanism that enhances sensitivity of the auditory system to very low changes in physical parameters of an acoustic signal?

Identification of modulation type would be possible if the subject was able to compare a phase of the changes in the excitation pattern on the low- and high-frequency sides with respect to the maximum. If the changes on the lower and upper side of the pattern are in phase this indicates that AM is present. If these changes are in an opposite phase on the two sides of the pattern this indicates that FM is present. If the changes are larger on the high-frequency side of the pattern, this indicates that AM is present (this happens because of expansive non-linear growth of excitation level on the high-frequency side of the patterns with increase in signal level; see Fig. 1). If the changes are larger on the low-frequency side of the pattern this indicates that FM is present (this happens because the excitation pattern is usually steeper on the low-frequency side). Thus the information about the phase of excitation level changes on the low- and high-frequency side may be a source of an additional information about the signal changes and the auditory system may effectively use it.

The main purpose of this paper is verification of this hypothesis.

2. Experiment 1. The detection of modulation

If the detection (or identification) of modulation depended on comparison of displacements of different regions of basilar membrane then the limiting of information from one of the active areas of the membrane (using masking band of noise) should make the detection of modulation much more difficult and consequently increase in threshold. Moreover, if the detection of modulation for all modulation rates was based exclusively on the excitation pattern changes, then using masking band of noise should bring about the same effect for all modulation rates. The main purpose of the first experiment was to determine the detectability d' for amplitude and frequency modulated signals as a function of m or β respectively. It was carried out for a sinusoidal carrier at a frequency of 1 kHz presented in quiet and with bands of noise designed to mask selectively either the low- or high-frequency side of the excitation pattern evoked by a modulated signal. In other words the aim of the experiment was to establish which side of the excitation pattern is more important for modulation detection and how it changes with modulation rate for AM and FM. The results gathered in this experiment were also a starting point for the next experiment concerned with the modulation type discrimination (see Sec. 3).

2.1. Method

Psychometric functions for the detection of amplitude and frequency modulated signals were determined in two separate experiments using a two-alternative forced-choice (2AFC) method. On each trial two successive signals were presented. One of them was modulated (AM or FM) and the other one was a pure tone. The order of the signals was random and subject's task was to indicate which of two signal in a pair was modulated. Each signal had an overall duration of 1000 ms including raised-cosine rise/fall times of

50 ms. The long duration was chosen so that several cycles would occur in each stimulus. The time interval between two successive signals was 500 ms.

A run consisted of 55 trials. Five different modulation depths, i.e. m or β for AM and FM respectively, were used in each run, and they were used in random order. The highest value of an appropriate modulation index was chosen to be easily detectable, giving typically 90–95% correct responses, and the smallest one was chosen to be difficult to detect, typically giving 55–60% correct responses. These values were established in several pilot runs individually for each subject. Twenty blocks of trials were run for each modulation rate and modulation type (AM and FM), so any point on each psychometric function is based on at least 200 judgements.

In separate experimental sessions, using the above described method, psychometric functions for detection AM and FM signals presented with bands of noise chosen to mask either the lower or the upper part of the excitation pattern were measured.

The carrier was a sinusoid with a frequency of $f_c = 1$ kHz, and level 70 dB SPL. Modulation rate was equal $f_{\text{mod}} = 2$, 5 and 10 Hz. Bands of noise had essentially rectangular spectral envelopes and cut-off frequencies: $f_l = 500$ Hz, $f_u = 800$ Hz – low-band noise and $f_l = 1250$ Hz, $f_u = 2000$ Hz – high-band noise. Spectrum level was equal to 49 and 45 dB (re. 20 μPa) for low- and high-band noise respectively. The parameters of these bands were chosen to give a crossing point of the excitation patterns [15] produced by the carrier signal and by each band of noise, 10 dB below maximum of the excitation pattern evoked by the carrier. Moreover, the maxima of the excitation patterns produced by bands of noise were approximately equal.

These parameters of the bands of noise allowed a little effect of low-band noise on the high-frequency side of the excitation pattern and *vice versa*. Noise used in this study was not so-called frozen noise but it was calculated individually for each stimulus by means of Inverse Fourier Transform. Bands of noise were not presented continuously as in MOORE and SĘK's [18] experiments but were gated synchronously with stimuli. Signals were generated via 16-bit digital-to-analogue converter (Tucker and Davis Technology) at a sampling rate of 50 kHz and presented monaurally by means of Sennheiser 414 headphones in a sound attenuating chamber. Three normal hearing subjects were used.

2.2. Results and discussion

As results of the experiment, probabilities of correct answers for each of 5 values of appropriate modulation indices (m or β) were obtained. These probabilities were transformed into detectability d' [7, 10]. Functions describing dependencies of d' on m or β, i.e. $d'(m)$ and $d'(\beta)$ were similar for all subjects and in general they could be approximated by linear functions of the modulation index square:

$$d'_{\text{AM}} = K_{\text{AM}} m^2 , \tag{4}$$

$$d'_{\text{FM}} = K_{\text{FM}} \beta^2 , \tag{5}$$

where K_{AM} and K_{FM} are constants expressing slopes of the best-fitting lines. Correlation coefficients of collected data were relatively high and no smaller than 0.92.

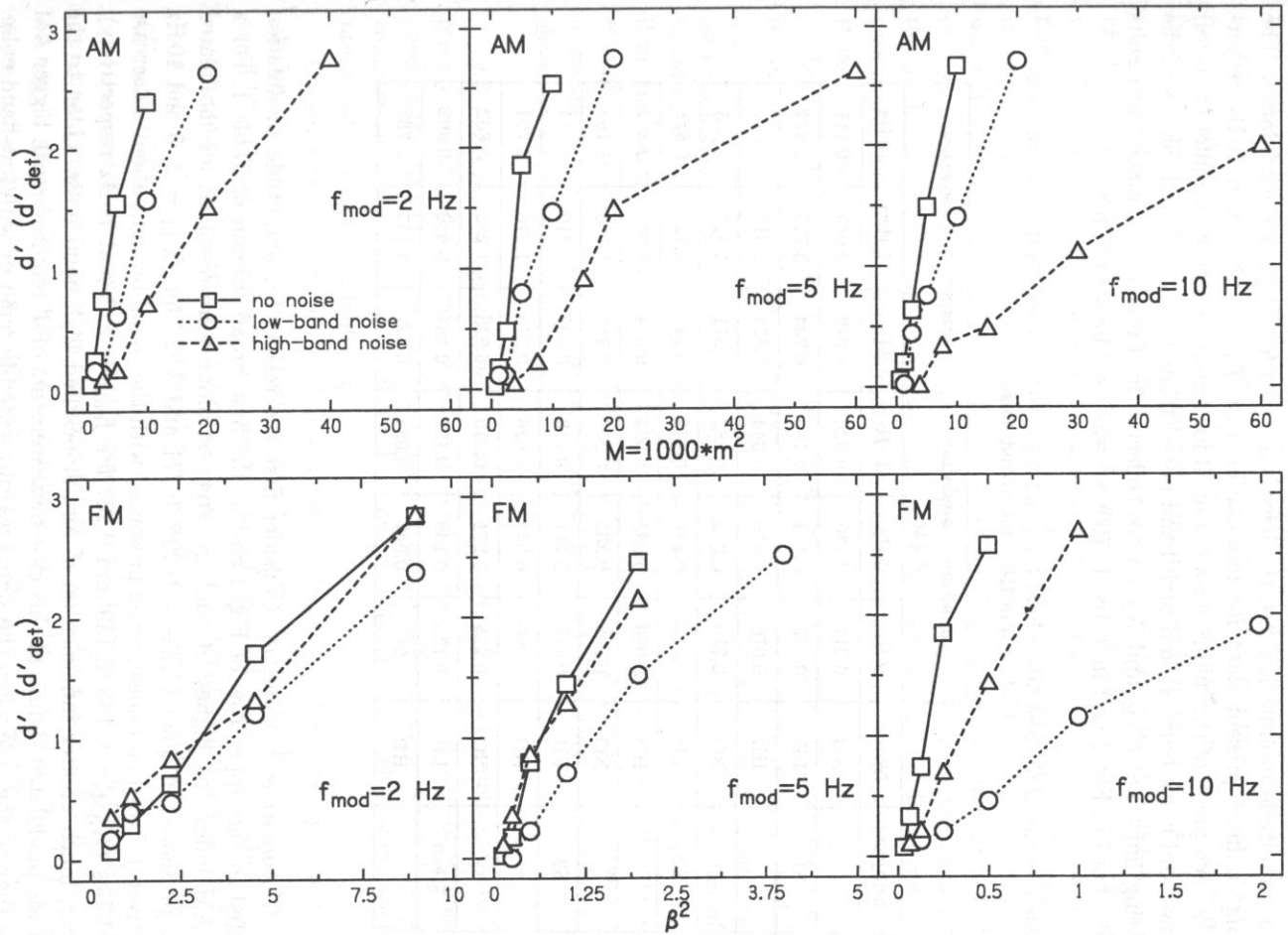

Fig. 2. Psychometric function for the detection of AM (upper row) and FM (lower row). The following columns show data for modulation rates $f_{\mathrm{mod}} = 2$, 5 and 10 Hz for different ways of signal presentation: in quiet (squares), with low-band noise (circles) and with high-band noise (triangles).

The data averaged across the subjects are presented in Fig. 2. The upper row shows data for amplitude modulation and the lower one data for frequency modulation. The following columns present data for modulation rate $f_{\text{mod}} = 2$, 5 and 10 Hz respectively. In each panel of this figure data obtained for signals presented in quiet (squares) with low-band noise (circles) and high-band noise (triangles) are plotted. Slopes of the best-fitting lines, i.e. K_{AM} and K_{FM} were collected in Table 1. (To make the results readable, both in Fig. 2 and in Table 1, $1000m^2$ was used instead of m^2).

Table 1. Slopes of the best-fitting lines K_{AM} and K_{FM}: NO – no noise, LB – low-band noise and HB – high-band noise.

		Amplitude modulation K_{AM}			Frequency modulation K_{FM}		
Subject	Noise	2 Hz	5 Hz	10 Hz	2 Hz	5 Hz	10 Hz
	NO	0.212	0.230	0.320	0.279	0.949	6.141
S1	LB	0.159	0.164	0.156	0.234	0.725	1.074
	HB	0.070	0.049	0.044	0.376	1.317	3.077
	NO	0.259	0.279	0.282	0.371	1.327	5.503
S2	LB	0.132	0.141	0.142	0.248	0.720	0.828
	HB	0.080	0.053	0.033	0.324	0.939	2.419
	NO	0.295	0.303	0.209	0.325	1.568	5.162
S3	LB	0.115	0.111	0.113	0.309	0.510	1.074
	HB	0.060	0.040	0.026	0.274	1.216	2.704
	NO	0.225	0.271	0.270	0.325	1.281	5.602
Mean	LB	0.135	0.139	0.137	0.264	0.652	0.992
	HB	0.070	0.047	0.034	0.327	1.157	2.733

2.2.1. Amplitude modulation. Consider first the results for amplitude modulation presented in the upper row of Fig. 2 and in the first broad column of Table 1. For a given AM index the highest d' and the steepest slope were obtained for modulated signals presented in quiet ($K_{\text{AM}} = 0.225$, 0.271 and 0.227 for $f_{\text{mod}} = 2$, 5 and 10 Hz respectively). Low-band noise, when presented with the signal brought about a decrease in d' slopes ($K_{\text{AM}} = 0.135$, 0.139 and 0.137 for $f_{\text{mod}} = 2$, 5 and 10 Hz respectively). However, much greater influence on d' and slopes had high-band noise added to the amplitude modulated signal. In this case measurements of d' required much bigger AM indices than in the case when the signal was presented in quiet or with low-band noise. Slopes are also shallower in this case: $K_{\text{AM}} = 0.070$, 0.047 and 0.034 for $f_{\text{mod}} = 2$, 5 and 10 Hz respectively. It should be noted that low-band noise had the same effect on d' values for all modulation rates used. High-band noise, however, had a bigger effect for higher modulation rates.

Slopes of the best-fitting lines ([1]) for AM, as collected in Table 1, were subjected to a within-subjects analysis of variance (ANOVA) with factors: way of presentation (in quiet, with low-band noise and with high-band noise) and modulation rate (f_{mod} = 2, 5 and 10 Hz). The main effect of the way of presentation was a highly significant factor ($F(2,4) = 142.1$, $p < 0.0001$) reflecting marked increase in threshold, observed especially for high-band noise. The main effect of the modulation rate was not significant ($F(2,4) = 0.1$, $p = 0.91$); d's and slopes obtained for all modulation rates (for a given way of presentation) did not change markedly with modulation rate. This confirms earlier findings that the threshold for detecting of AM does not depend on modulation rate for low modulation rates. The interaction of the modulation rate and the way of presentation was not significant ($F(4,8) = 0.55$, $p = 0.702$) which means that masking of the low- or high-frequency side of the excitation pattern has approximately the same effect on the modulation detection. (However this is not quite true for high-band noise; in this case coefficients K_{AM} were different across modulation rates, see the upper row of Fig. 2 (triangles) and Table 1).

Based on these results it may be stated that the detection of amplitude modulation is similar for all modulation rates used, which is consistent with Zwicker's model. Much higher d's obtained when the AM signal was presented with the high-band noise are also consistent with this model. Zwicker's model assumes that the detection of AM is based on changes observed on the high-frequency side of the excitation pattern. Thus, if the information from this part of the excitation pattern were limited in some way (for example by masking, as in this study) then the detection of modulation would be much more difficult and growth in the threshold would also be observed. This effect is clearly shown by the presented data.

2.2.2. Frequency modulation. The lower row in Fig. 2 presents data gathered for frequency modulated sinusoid, presented in quiet and with low- and high-band noise, averaged across subjects. Note that the range of x axis is different in each panel. This makes comparison of the data more difficult but, on the other hand, it also allows them to be presented in a more readable way.

Consider the results for modulation rate of $f_{\mathrm{mod}} = 10$ Hz. The detection of modulation is easier (higher d's) when signals are presented in quiet ($K_{\mathrm{FM}} = 5.6$). When the FM signal is presented at a background of the high-band noise, that masks the high-frequency side of the excitation pattern, then a given d' requires a bigger FM index by a factor of 2. Thus the slope of the best-fitting line is shallower by a factor of 2 ($K_{\mathrm{FM}} = 2.733$).

Low-band noise, however, that masked the low-frequency side of the excitation pattern had a much greater effect. In order to get d's from the range of 1–2 it was necessary to use β_s greater by a factor of 3, compared to a situation when the FM signal was presented in quiet. Quite a different situation can by observed for a modulation rate of $f_{\mathrm{mod}} = 2$ Hz. The presentation of FM stimuli in quiet or with low-band noise that

([1]) Since the data for different modulation rates were gathered for markedly different ranges of an appropriate modulation index, raw data could not be subjected to this analysis. Such analysis would require many so-called "missing values" that could markedly influence the final results of the analysis.

masks the low-frequency side of the excitation pattern or with high-band noise that masks the upper side of the excitation pattern gives similar slopes of the best-fitting lines describing d' as a function of FM index. The detection of frequency modulation in this case did not depend on presence of masking bands of noise, but took place for bigger values of β than for $f_{\text{mod}} = 10\,\text{Hz}$. For modulation rate of 5 Hz a sort of "half way through" situation, between these for $f_{\text{mod}} = 2\,\text{Hz}$ and $f_{\text{mod}} = 10\,\text{Hz}$, is observed (see Fig. 3).

The highest d's were obtained for FM tone presented in quiet ($K_{\text{FM}} = 1.281$). High-band noise that masks the high-frequency side of the excitation pattern did not affect the results. However, the low-band noise markedly influenced the slope ($K_{\text{FM}} = 1.157$). Thus decreasing in modulation rate required much bigger FM indices to reach the detection threshold.

Slopes of the best-fitting lines for FM, presented in the second broad column of Table 1 were subjected to within-subjects analysis of variance (ANOVA) with factors: way of presentation (in quiet, with low-band noise and with high-band noise) and modulation rate ($f_{\text{mod}} = 2$, 5 and 10 Hz). The main effect of the modulation rate was highly significant ($F(2,4) = 210.30, p < 0.0001$) which confirms earlier findings that if the threshold is expressed in units of β then it decreases with increase in the modulation rate [25, 31]. The main effect of the way of presentation was also statistically significant ($F(2,4) = 301.72$, $p < 0.0001$). It emphasised the effect of masking, particularly for $f_{\text{mod}} = 10\,\text{Hz}$. However, the most important result of this analysis is that the interaction of the modulation rate and the way of presentation was also highly significant ($F(4,8) = 79.44$, $p < 0.0001$). This interaction means that the masking effect was markedly different across modulation rates.

The results for FM stimuli are consistent with Zwicker's model but only for a modulation rate of 10 Hz. Only for this modulation rate the effect of the low-band noise was observed. As Zwicker's model suggests, the detection of frequency modulation is based on the low-frequency part of the excitation pattern. Thus if the information from this part of the excitation pattern is limited in some way (for example by masking, as in this study) the detection of FM would be much more difficult and the threshold much bigger. However, this was observed for modulation rate of $f_{\text{mod}} = 10\,\text{Hz}$ only. If Zwicker's model had been correct for the whole range of modulation rate, then the same influence of the low-band noise should have been observed for modulation rate of $f_{\text{mod}} = 2\,\text{Hz}$. Such an influence was not observed in this study.

2.2.3. Interim summary. In summary of this part of the results it can be stated that the effect of the high-band noise that masked the high-frequency side of the excitation pattern on d's was bigger for amplitude modulated signals. The effect of this band as well as the effect of the low-band noise was approximately the same across all modulation rates used. The detection of frequency modulation at a modulation rate of $f_{\text{mod}} = 2\,\text{Hz}$ did not depend on presence of any band of noise. However, an increase in the modulation rate brought about that the effect of the noise was bigger, particularly for the low-band noise that masked the low-frequency side of the excitation pattern.

3. Experiment 2. Effect of modulation rate on the discrimination of modulation type

As mentioned earlier, one of the possible ways of modulation type discrimination may be a comparison of magnitudes and phases of excitation level changes on the low- and high-frequency sides: changes on the two sides in phase suggest that amplitude modulation as a stimulating signal is present; if the changes are not in phase then this may suggest that the FM signal is present. If the auditory system indeed makes such a comparison of two sides of the excitation pattern then a selective masking of any of these two sides, that limits the amount of the information available from masked part of the excitation pattern should bring about noticeable decrease in probability of modulation type discrimination.

Thus in the next experiment the discrimination of modulation type (AM from FM) was analysed. This was done for AM and FM signals presented in quiet and with bands of noise that selectively masked the low- or high-frequency side of the excitation pattern.

3.1. Method

An ability of discrimination of modulation type (AM from FM) was analysed for a sinusoidal carrier signal at a frequency of 1 kHz with level of 70 dB SPL, amplitude or frequency modulated by a sinusoid at a frequency of 2, 5, and 10 Hz. The same masking bands of noise were used as in Experiment 1 (see Sec. 2.1). A two-alternative forced-choice (2AFC) method was used. Two successive signals in a random order were presented on each trial. One of them was amplitude modulated, whereas the other one was frequency modulated. The subject's task was to indicate an order of the signals in each trial, i.e. AM was first then FM, or *vice versa*.

Values of appropriate modulation indices i.e. m and β for AM and FM respectively within each trial were chosen to produce equally detectable amount of each type of modulation. Six different values of d' were chosen namely: $d' = 0.66$, 1.16, 1.66, 2.16, 2.66 and 3.16. For these d's six pairs of $(m_{d'}, \beta_{d'})$, i.e. $\{(m_{0.66}, \beta_{0.66}), (m_{1.16}, \beta_{1.16}), \ldots, (m_{3.16}, \beta_{3.16})\}$ were calculated based on equations (4) and (5) (see Sec. 2.2). Pairs of $(m_{d'}, \beta_{d'})$ were determined separately for each subject (based on individual data for each subject) and for modulation presented in quiet and with bands of noise.

A single experimental run consisted of 65 trials that were presented in random order. In the first five trials modulation indices m and β were the biggest i.e. $m = m_{3.16}$ and $\beta = \beta_{3.16}$. Twenty blocks of trials were run for each way of signal presentation and for each subject. This gave at least 200 judgements for each point on the psychometric function. Signals were presented in the same way as in Experiment 1. The same normal hearing subjects took part in this experiment.

3.2. Result and discussion

Probabilities of correct response, as raw experimental data for all pairs of $(m_{d'}, \beta_{d'})$ were transformed into d' domain and presented in Fig. 3 as a function of detectability d' for detection of AM or FM. Since d's obtained for three subjects were similar,

Fig. 3 presents mean data. Top, middle and bottom panels show data for modulation rates f_{mod} = 2, 5 and 10 Hz respectively. Each panel shows the results for different ways of signal presentation: in quiet (squares), with low-band noise (circles) and with high-band noise (triangles). Solid lines with no data points show hypothetical situations where data would fall if probability of modulation detection were equal to probability of modulation type discrimination ($d'_{det} = d'_{dis}$).

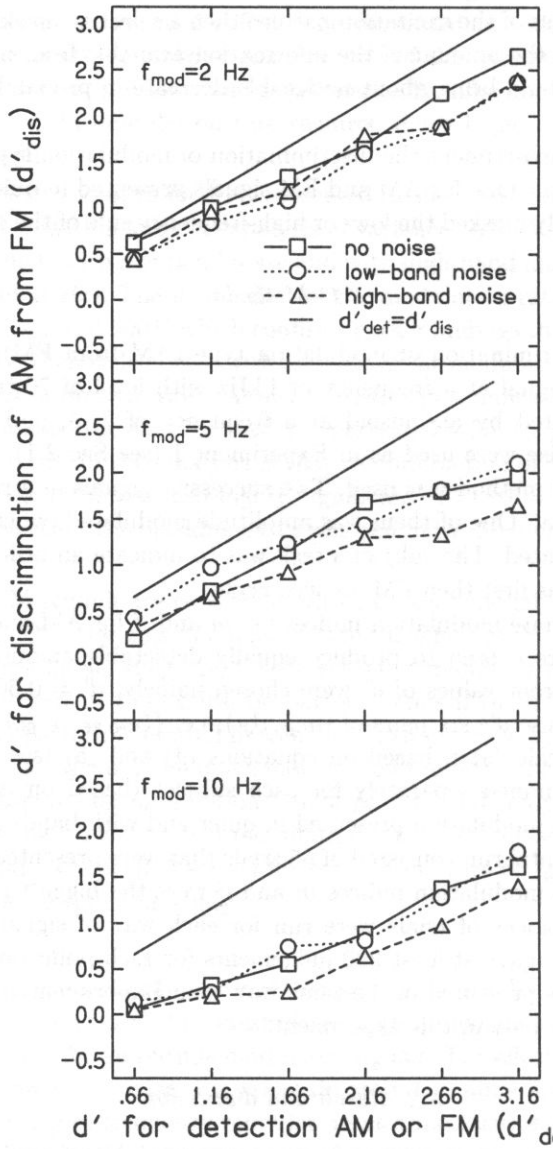

Fig. 3. Psychometric function for the discrimination of modulation type AM or FM as a function of d' for detection of AM or FM. Each panel shows data for one modulation rate and for three ways of signal presentation: in quiet (squares), with low-band noise (circles) and with high-band noise (triangles).

In general it can be stated that an increase in detectability d' for detection AM or FM brings about an increase in detectability d' for the discrimination of modulation type. For $f_{\text{mod}} = 2\,\text{Hz}$ (top panel of Fig. 3) the discrimination (or identification) of modulation type is nearly as good as the detection of modulation. This finding is consistent with that of DEMANY and SEMAL [4]. Thus, for this modulation rate the discrimination of modulation type is quite possible at the detection threshold of modulation. For slightly higher d's for detection of AM or FM the discrimination of modulation type (AM from FM) worsens. It is worth to add, that the way of modulation presentation (i.e. in quiet or with bands of noise) did not influence obtained data: these obtained for signals presented in quiet are very close to those when the signals were presented with low- or high-band noise. This means that the presence of masker, that selectively masked either the low- or high-frequency side of the excitation pattern did not impair the discrimination of modulation type. The middle panel of Fig. 3 shows data for modulation rate of $f_{\text{mod}} = 5\,\text{Hz}$. d's presented in there are, in general, smaller than those for $f_{\text{mod}} = 2\,\text{Hz}$. They increase more slowly as d' for detection of AM or FM increases. This means that the discrimination of modulation type (identification) in this case is more difficult. The way of stimuli presentation does not seem to be important. A pattern of the data obtained for $f_{\text{mod}} = 10\,\text{Hz}$ (bottom panel of Fig. 3) is similar to those for $f_{\text{mod}} = 2\,\text{Hz}$ and 5 Hz. An increase in d' for discrimination is smaller than in the two first cases. No effect of the way of signal presentation was also observed. Thus, for a near-threshold modulation indices an increase in modulation rate makes the discrimination of modulation type progressively more difficult: the discrimination of AM from FM seems to be easy for $f_{\text{mod}} = 2\,\text{Hz}$, more difficult for $f_{\text{mod}} = 5\,\text{Hz}$ and almost impossible for $f_{\text{mod}} = 10\,\text{Hz}$.

The results were subjected to analysis of variance (ANOVA) with the following factors: modulation rate ($f_{\text{mod}} = 2$, 5 and 10 Hz), way of signal presentation (in quiet and with bands of noise) and detectability d' for detection of AM or FM (6 values). As expected, the main effect of the detectability d' for detection of AM or FM was highly significant ($F(2,4) = 210.34$, $p < 0.001$); it is clear that an increase in appropriate modulation indices largely improves performance. The main effect of the modulation rate was also highly significant ($F(2,4) = 15.90$, $p = 0.012$). That means, that the discrimination of modulation type depends on modulation rate. The main effect of the way of signal presentation was not significant ($F(2,4) = 2.61$, $p = 0.188$). The interaction of the modulation rate and the detectability for detection of AM or FM was also significant which indicates that an increase in d' for detection of AM or FM brought about a different increase in d' for discrimination for different modulation rates.

The results of this experiment suggest that when trying to identify modulation type the auditory system does not use information connected with an envelope of the phase of the excitation pattern changes in different frequency regions. However, two factors that affected the results should be borne in mind. First, the modulation depths used (for a given d' for detection of AM or FM) were markedly greater where noise bands were presented than when they were not presented. Secondly bands of noise were not completely effective in masking one side of the excitation pattern only: a small area adjacent to the maximum of the excitation pattern always remained unmasked.

While trying to identify modulation type the auditory system does not use the phase of the excitation pattern changes on the low- and high-frequency side of the pattern. If this information had been used then the discrimination of modulation type would have worsened when AM or FM signals were presented with bands of noise. Subjects can perform the discrimination task even when noise band masks either the low- or high-frequency side of the excitation pattern and d's for discrimination are nearly as good as d's for detection of AM or FM for the lowest modulation rates.

4. Concluding remarks

The results of the presented investigations suggest that the discrimination of modulation type at the modulation detection threshold is possible for the lowest modulation rates; this finding is not consistent with Zwicker's model. They also suggest that while trying to identify modulation type the auditory system does not use information connected with the excitation pattern changes on the low- and high-frequency side of the pattern. Information about relative phases of the excitation pattern changes is not crucial for the discrimination of modulation type. Changes in the excitation pattern seem likely to be more important for amplitude modulation because low- and high-band of noise impaired AM detection to a larger extent. Thus, if the information contained in changes in the excitation pattern do not play the most important role then an additional mechanism (or mechanisms) must exist in the auditory system that enables fine discrimination of modulation type at the detection threshold for AM and FM. This mechanism does not have to be connected with both types of modulation and it may be connected with either amplitude or frequency changes only. Since the detection of frequency modulation depends less on masking bands of noise it seems that this mechanism may be connected with frequency changes only. However, this mechanism operates more effectively for very low modulation rates. It enhances a sensitivity of the auditory system to frequency changes. This mechanism may be based on information available in phase locking. It seems likely that the auditory system is capable of analysing the time intervals between neural spikes, for relatively long time samples of the signal. If this is the case, the accuracy and efficiency of this analysis would depend on the absolute number of the impulses characterised by a constant time interval between them. The number of spikes is roughly proportional to the duration of the signal, if the signal level is constant. Increasing the duration of the signal with the constant frequency introduces more equal time intervals between spikes. This provides more precise information about the frequency of the signal and, as a consequence, better performance in frequency modulation detection. A strong argument supporting this point of view are the results of experiments, when the task was to detect a difference between two successive sinusoidal tones: these threshold are largely lower that those for modulation detection [28].

In summary it may be stated that there are two mechanisms for the detection of amplitude and frequency changes of a signal at low rates. One of them is a mechanism based entirely on changes in excitation level, proposed by Zwicker. This mechanism operates for amplitude and frequency changes for all range of carrier frequencies and modula-

tion rates, being most effective for modulation rates higher than 5 Hz. However, for very low modulation frequencies, less than 5 Hz, an additional mechanism enhances the auditory system's sensitivity to frequency changes. The mechanism provides additional information about frequency changes and brings about markedly higher detectability for the detection and discrimination of the frequency changes. The mechanism is probably based on the analysis of the phase-locking to samples of the signal.

The concept of the two independent mechanisms for detection amplitude and frequency changes has already been presented by FETH [5] and CONINX [2, 3]. However, they assumed that differences in the detection of amplitude and frequency changes occur over the whole range of modulation rates. The model suggested in this paper assumes that detection of changes in amplitude or frequency of a signal is based primarily on the changes in excitation level over the active region of the excitation pattern. However, for very low modulation rates, when the changes in the signal's parameters are very slow, the information conveyed by inter-spike intervals is used to evaluate the frequency of the signal.

References

[1] J.T. ALLANSON and A.F. NEWELL, *Subjective responses to tones modulated simultaneously in both amplitude and frequency*, J. Sound. Vib., **3**, 135–146 (1966).

[2] F. CONINX, *The detection of combined differences in frequency and intensity*, Acustica, **39**, 137–150 (1978).

[3] F. CONINX, *The perception of combined frequency and amplitude modulation with clearly audible modulation depths*, Acustica, **39**, 151–154 (1978).

[4] L. DEMANY and C. SEMAL, *On the detection of amplitude modulation and frequency modulation at low modulation frequencies*, Acustica, **61**, 243–255 (1986).

[5] L.L. FETH, *Combinations of amplitude and frequency differences in auditory discrimination*, Acustica, **26**, 67–77 (1972).

[6] M. FLORENTINE and S. BUUS, *An excitation-pattern model for intensity discrimination*, J. Acoust. Soc. Am., **70**, 1646–1654 (1981).

[7] D.M. GREEN and J.A. SWETS, *Signal detection theory and psychophysics*, Krieger, New York 1974.

[8] W.M. HARTMANN and G.M. HNATH, *Detection of mixed modulation*, Acustica, **50**, 297–312 (1982).

[9] W.M. HARTMANN and M.A. KLEIN, *Theory of modulation detection for low modulation frequencies*, J. Acoust. Soc. Am., **67**, 935–946 (1980).

[10] N.A. MACMILLAN and C.D. CREELMAN, *Detection theory: A User's guide*, Cambridge University Press, Cambridge, England 1991.

[11] D. MAIWALD, *Die Berechnung von Modulationsschwellen mit Hilfe eines Funktionsschemas (calculation of differential thresholds by means of a functional model)*, Acustica, **18**, 193–207 (1967).

[12] D. MAIWALD, *Ein Funktionsschema des Gehörs zur Beschreibung der Erkennbarkeit kleiner Frequenz- und Amplitudenänderungen*, Acustica, **18**, 81–92 (1967).

[13] B.C.J. MOORE and B.R. GLASBERG, *Formulae describing frequency selectivity as a function of frequency and level and their use in calculating excitation patterns*, Hear. Res., **28**, 209–225 (1987).

[14] B.C.J. MOORE and B.R. GLASBERG, *Mechanisms underlying the frequency discrimination of pulsed tones and the detection of frequency modulation*, J. Acoust. Soc. Am., **86**, 1722–1732 (1989).

[15] B.C.J. MOORE and B.R. GLASBERG, *Suggested formuale for calculating auditory-filter bandwidth and excitation patterns*, J. Acoust. Soc. Am., **74**, 750–753 (1983).

[16] B.C.J. MOORE and A. SĘK, *Detection of combined frequency and amplitude modulation*, J. Acoust. Soc. Am., **92**, 3119–3131 (1992).

[17] B.C.J. MOORE and A. SĘK, *Discrimination of modulation type (AM or FM) with and without background noise*, J. Acoust. Soc. Am., **96**, 726–732 (1994).

[18] B.C.J. MOORE and A. SĘK, *Effects of carrier frequency and background noise on the detection of mixed modulation*, J. Acoust. Soc. Am., **96**, 741–751 (1994).

[19] B.C.J. MOORE and A. SĘK, *Effects of carrier frequency, modulation rate and modulation waveform on the detection of modulation and the discrimination of modulation type (AM vs FM)*, J. Acoust. Soc. Am., **97**, 2468–2478 (1995).

[20] E. OZIMEK and A. SĘK, *AM and FM difference limens and their reference to amplitude-frequency changes of a sound in a room*, Acta Acustica, **82**, 114–122 (1996).

[21] E. OZIMEK and A. SĘK, *Perception of amplitude and frequency modulated signals (mixed modulation)*, J. Acoust. Soc. Am., **82**, 1598–1603 (1987).

[22] J.O. PICKLES, *An introduction to the physiology of hearing*, 2nd Ed., Academic Press, London 1988.

[23] M.A. RUGGERO and N.C. RICH, *Application of a commercially-manufactured doppler-shift laser velocimeter to the measurement of basilar-membrane motion*, Hear. Res., **51**, 215–230 (1991).

[24] M.A. RUGGERO and N.C. RICH, *Furosemide alters organ of Corti mechanics: Evidence for feedback of outer hair cells upon the basilar membrane*, J. Neurosci., **11**, 1057–1067 (1991).

[25] A. SĘK, *Critical modulation frequency and critical band based on random amplitude and frequency changes*, Archives of Acoustics, **19**, 59–74 (1994).

[26] A. SĘK and B.C.J. MOORE, *Detection of mixed modulation using correlated and uncorrelated noise modulators*, J. Acoust. Soc. Am., **95**, 3511–3518 (1994).

[27] A. SĘK and B.C.J. MOORE, *The detection of modulation at low modulation rates*, [In:] Auditory Perception: Some Principles and Applications, U. JORASZ, Adam Mickiewicz University Press, Poznań 1996.

[28] A. SĘK and B.C.J. MOORE, *Frequency discrimination as a function of frequency, measured in several ways*, J. Acoust. Soc. Am., **97**, 2479–2486 (1995).

[29] A. SĘK and E. OZIMEK, *AM and FM difference limens*, Archives of Acoustics, **19**, 37–58 (1994).

[30] E. ZWICKER, *Die elementaren Grundlagen zur Bestimmung der Informationskapazität des Gehörs*, Acustica, **6**, 356–381 (1956).

[31] E. ZWICKER, *Die Grenzen der Hörbarkeit der Amplitudenmodulation und der Frequenzmodulation eines Tones*, Acustica, **2**, 125–133 (1952).

[32] E. ZWICKER, *Temporal effects in simultaneous masking and loudness*, J. Acoust. Soc. Am., **38**, 132–141 (1965).

ARCHIVES OF ACOUSTICS
23, 3, 379–390 (1998)

PERCEPTION OF MIXED MODULATION FOR SINGLE COMPONENTS IN HARMONIC COMPLEX FOR HIGH MODULATING FREQUENCIES

M.J. KIN and A.B. DOBRUCKI

Institute of Telecommunications and Acoustics
Wrocław University of Technology
(50-370 Wrocław, Wybrzeże Wyspiańskiego 27)

Results and problems of perception of mixed modulation in a harmonic multitone are discussed. The experimental research was done for higher modulating frequencies (70 and 200 Hz) and a 5-harmonics complex with fundamental frequency of 256 Hz. The results indicated that for a modulating frequency of 70 Hz, the perception of frequency modulation in the presence of the threshold values of the amplitude modulation is different from the perception of amplitude modulation in the presence of the threshold values of the frequency modulation. This means clearly that there are two mechanisms of the perception for these kinds of modulation.

1. Introduction

Problems of perception of simultaneous amplitude and frequency modulation have been widely discussed [3, 4, 6, 14, 15]. For low modulating frequencies, the perception is based on the changes in pitch and loudness and the auditory system follows the temporal structure of the sound. For higher modulating frequencies, when the spectrum covers a wider frequency range, the perception of AM, FM and MM is based mostly on the spectrum of the modulated sound, i.e. on the low and high sidebands produced by modulation process, and it could be said that, in this case, the auditory system analyses the spectral structure of the sound. This means that we perceive a steady "rough" sound or two tones of different pitches depending on the frequency of modulation and the carrier. VOGEL [21, 22] presented a model, derived partially from the TERHARDT'S model [19], in which the partial roughness is evaluated within each critical band on the basis of the fluctuation in excitation. FASTL [5] suggested that for AM-modulated broad-band noise the differences in the level are evaluated using the masking period patterns produced by AM broad-band noise differing in the modulation frequency, degree of modulation, and level. ZWICKER [25] compared the sensations produced by the AM and FM octave-band noise. The result indicated a correlation between the sensations produced by these two kinds of noise which suggests that the roughness for both AM and FM is perceived by the same mechanism. In other ZWICKER'S works [23, 24, 26] it was found that the just-noticeable modulation index for AM and the just-noticeable

frequency deviation for the FM tones, changed in the same manner of change as the function of the modulating frequency when other parameters were constant. This means that the threshold of roughness behaves similarly for AM and FM tones. TERHARDT [18, 20] compared the roughness of AM tones with that produced by FM tones at a constant modulation index and concluded that the mechanism producing this effect was similar for the two kinds of modulation.

ZWICKER [27] and MAIWALD [12, 13] proposed a functional scheme in which the frequency and intensity differences are assumed to be detected by one single mechanism rather than by two independent mechanisms. CONINX [3, 4] found an independent detection of the pitch and loudness differences on the basis of his experiment in which the detection of combined differences in frequency and intensity was investigated. HARTMANN and HNATH [7] determined the influence of each component of the AM, FM and MM signal spectrum on the modulation threshold values. Most important is the relation between the MM threshold and the ratio of the frequency and amplitude modulation indices for coincident and opposed phases between the amplitude and frequency modulating signals. OZIMEK and SĘK'S research [15] shows that there exists a fairly complex perception mechanism for MM signals which depends on the kind and frequency of the modulating signal. For the modulating frequency in the "spectral" region, there are probably two independent mechanisms that may operate either separately or in combination; the component whose frequency is lower than the carrier frequency of the signal determines the perception of simultaneous amplitude and frequency changes.

From the musical point of view, two aspects of the changes in the spectra should be taken into consideration: firstly, when two sidebands have frequencies in harmonic order with the carrier frequency and they assemble in some kind of a harmonic multitone; secondly, when those sidebands are not in harmonicity that causes some kind of dissonance. The second aspect was widely discussed by BREGMAN [2] on the basis of perceptual grouping. According to this theory, listeners could "remove" some nonharmonic partials from the consonance complex creating a sound image based on two separate perceptual streams: one with the products of modulation, and another one – the harmonic signal with the carrier.

The main aim of this paper is to find how the human ear can percept a mixed modulation in the roughness and "spectral" regions for the single components at the presence of other partials of the harmonic complex. Another interesting problem was the interaction between these two kinds of modulation.

2. Stimuli and procedure

When a pure tone with amplitude A and frequency f_c:

$$x(t) = A \cos 2\pi f_c t, \tag{1}$$

is processed by frequency and amplitude modulation using another pure tone with amplitude M and frequency F_m:

$$y(t) = M \cos 2\pi F_m t, \tag{2}$$

the result is given by the following formula:

$$X(t) = A(1 + m\cos 2\pi F_m t)\cos(2\pi f_c t + \beta \sin 2\pi F_m t), \tag{3}$$

where: $m = M/A$ – AM modulation index, $\beta = \Delta f / F_m$ – FM modulation index, and Δf – frequency deviation.

Formula (3) expresses the spectral structure of the mixed-modulated tone containing three components:

— a carrier of frequency f_c and amplitude $A \cdot J_0(\beta)$,

— a low sideband of frequency $f_c - F_m$ and amplitude $A\left|J_1(\beta)\cdot\left(1-\frac{m}{\beta}\right)\right|$,

— a high sideband of frequency $f_c + F_m$ and amplitude $A\left|J_1(\beta)\cdot\left(1+\frac{m}{\beta}\right)\right|$,

(for $\beta \ll 1$ only), where $J_0(\beta)$ and $J_1(\beta)$ are the Bessel functions of zero and first order of the argument β, respectively.

When only one of the partials is modulated, the spectrum contains other harmonics with their own amplitudes, modulated harmonic and two sidebands which result from the modulation process.

Test signals were generated by an IBM PC computer with a 16-bit sound board at a sampling rate of 16 000 points per second. The phases of each of the generated components and the modulation signal were equal to zero. Both the duration of the signal and the pause between two stimuli was 1 s. The stimulus presentation, timing and response recording were controlled by the computer. In the first interval, subjects listened to the AM or FM modulated single components of the investigated complex at the threshold values of m or β obtained in the experiment, presented partially previously [9]. The second interval always contained the same modulated partial with constant threshold values of m or β and a co-existing FM or AM modulation, respectively. This sequence was used because it could help the listeners to decide whether the sounds in those two intervals were the same or different and listeners did not have to care which one contained AM, FM, and MM-modulated partials. During this experiment, the AM and FM modulating signals were in-phase, i.e. the maximum in amplitude coincided with the maximum in frequency. An adaptive PEST method [16, 17] with the "yes – no" subjects' task was used. The modulation index values were decreased after two correct responses and increased by an apprioprate step after one incorrect response. Initially, the step size was 6 dB, but it was reduced to 0.5 dB after the first four reversals. A response feedback was not provided. The threshold value of the AM index, in the presence of threshold values β of the FM presented alone, was denoted m_β, and similarly, the threshold value of the FM index in the presence of threshold values m of the AM presented alone, was denoted by β_M. The values of m_β and β_M were defined as an average reversal level occuring during 10 trials starting with the fourth reversal. Ten threshold estimates were obtained for each observer under every condition.

In the experiment, the complex consisting of 5 components of 256 Hz as the fundamental frequency was presented via an Audiostatic ES 100 electrostatic loudspeaker and a Pioneer A 400 X amplifier with the level according to the isophone of 60 phones. Five male subjects with normal, good hearing participated in the experiment. All of them

were experienced in psychoacoustic tests and were paid for their service. The subjects' task was to answer the question: is the sound in the second interval the same as in the first one or not?

3. Results

The results of the experiment are presented in Figs. 1 and 2. They show the threshold values of m_β and β_M obtained for a mixed modulation in comparison with the values of m and β obtained under the same listening conditions but for the modulation of amplitude or frequency only. The standard deviations for these results did not exceed 10% of the obtained values. It can be seen that the MM thresholds are different from those

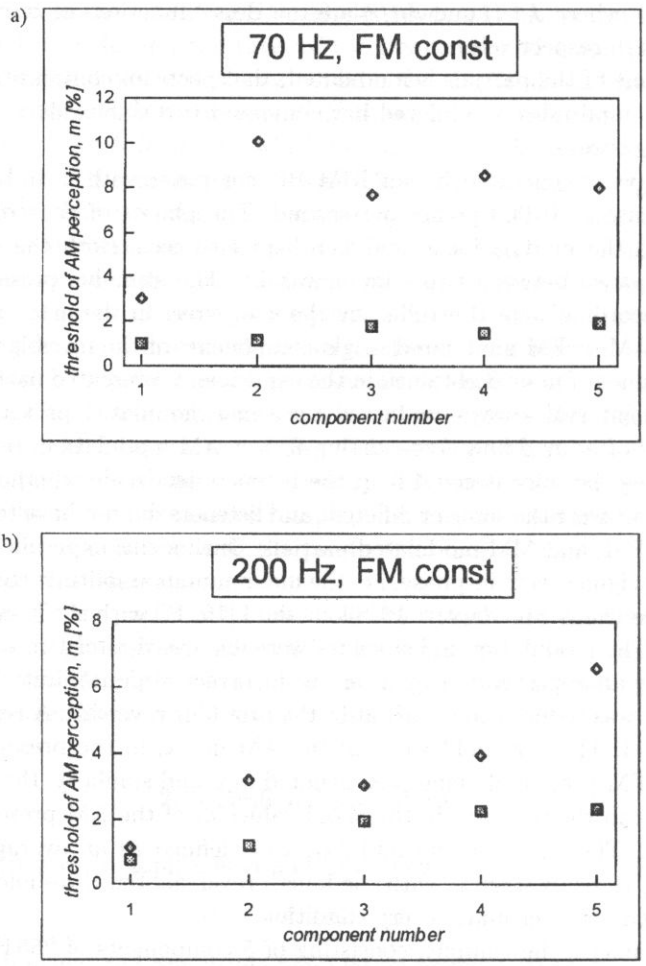

Fig. 1. Threshold values of the perception of amplitude modulation for the modulating frequencies: a) 70 Hz, and b) 200 Hz. ■ – amplitude modulation exposed separately, ♦ – amplitude modulation exposed with FM at its threshold values.

of AM and FM. The amplitude modulation in the presence of the threshold values of the FM perception has higher threshold values than the amplitude modulation without simultaneous fast changes in the frequency (Fig. 1). This takes place for both the modulating frequencies, i.e. for 70 and 200 Hz. The perception of the frequency modulation in the presence of the threshold values of the AM perception depends on the modulating frequency (Fig. 2). For modulating frequency of 200 Hz, the situation is similar to the AM perception in the presence of the FM threshold (Fig. 1), while for modulating frequency of 70 Hz the situation is completely different, i.e. the thresholds of the perception of frequency changes in the presence of the threshold values of AM are higher than in the case when only FM exists. Another interesting fact, which has been found in this experiment, is that for the 70 Hz-amplitude modulation in the presence of frequency

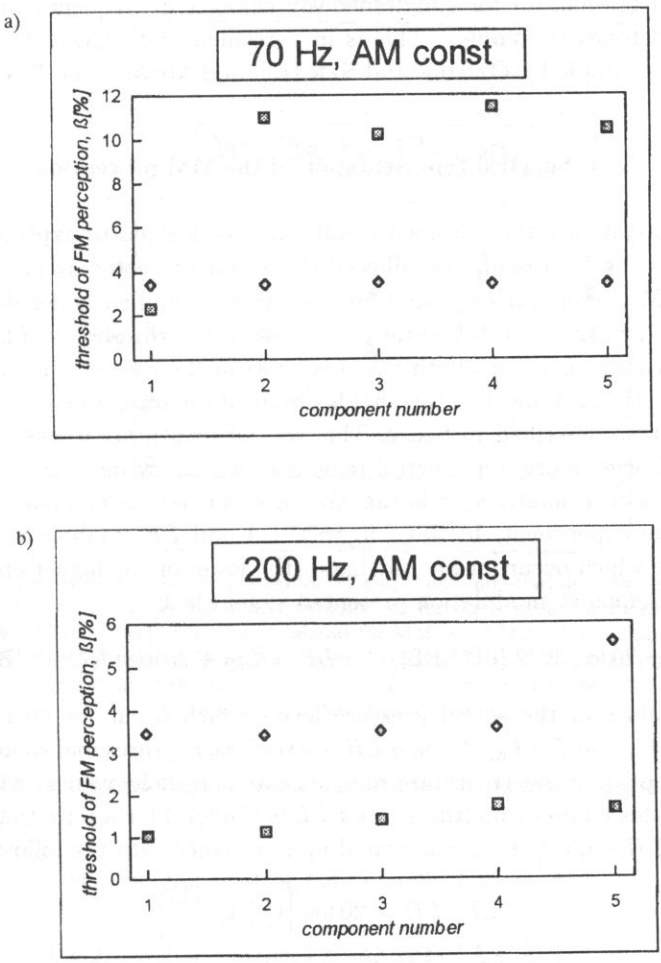

Fig. 2. Threshold values of the perception of frequency modulation for the modulating frequencies: a) 70 Hz, and b) 200 Hz. ■ – frequency modulation exposed separately, ♦ – frequency modulation exposed with AM at its threshold values.

modulation the threshold values of m are approximately the same for the partials 2 to 5, while for the fundamental component the threshold of AM is three times lower. For a modulating frequency of 200 Hz, the threshold values of m increase for higher components however this increase is greater than for the case when only the AM perception was measured.

For the 70 Hz-frequency modulation in the presence of an amplitude modulation, the perceived values of β are smaller than the thresholds of perception when only FM occured. These values are equal for all the investigated partials. For the modulating frequency of 200 Hz, the threshold values of the FM perception are higher for a mixed modulation in comparison to these when only FM exists alone.

The above mentioned facts suggest that for modulating frequencies equal to 70 and 200 Hz, an interaction between the modulations of amplitude and frequency exists, and the perceptual mechanism for simultaneously changes in frequency and amplitude of the modulated tones is complex. This is in agreement with CONINX suggestion [3, 4] confirmed, for example by OZIMEK and SĘK [15], and MOORE and SĘK [14].

4. Spectral representation of the MM perception

In order to compare the obtained results, it was decided to express them as levels of sound. This way of presentation allowed the authors to compare all the results referring to the MM perception suggested previously but obtained under different listening conditions [3, 7, 8, 12, 14, 15]. Figures 3 and 4 show the thresholds of hearing for tones that frequency corresponds to both the sidebands in the case of a multitone. They are compared with the AM and FM thresholds obtained separately and the MM thresholds for the conditions described in Sec. 2. This way of presentation was used because for roughness and, even more, for spectral regions of frequency modulation the human ear behaves as a spectral analyzer; it is therefore a useful way of comparing all the results obtained in the experiment. In those figures, LA and LF symbolize the levels of the sound pressure which occur for one sideband (the lower or the higher one) as a result of amplitude or frequency modulation presented alone; thus:

$$LA = L_{60} + 20\log M/2 \text{ [dB SPL]}, \qquad LF = L_{60} + 20\log|J_1(\beta)| \text{ [dB SPL]}. \tag{4}$$

L_{60} are the values of the sound pressure levels which occur for 60 isophone for the frequency $f_c - F_m$ and $f_c + F_m$. LL and LH are the hearing threshold values resulting only from masking phenomena (these are not absolute threshold values) which "normally" could exist in this complex multitone, and LL is the level for a pure tone at frequencies $f_c - F_m$, and LH – for $f_c + F_m$ calculated in accordance with the following formula [1].

$$LL,\ LH = 20\log\left[\left(\sum A_i^{\alpha}\right)^{1/\alpha}\right], \tag{5}$$

where A_i is the amplitude of the masked threshold produced by i-th component of a 5-harmonic complex and $\alpha = 0.8$ is a typical value for the frequency domain when more than one masker is present at the same time [10, 11].

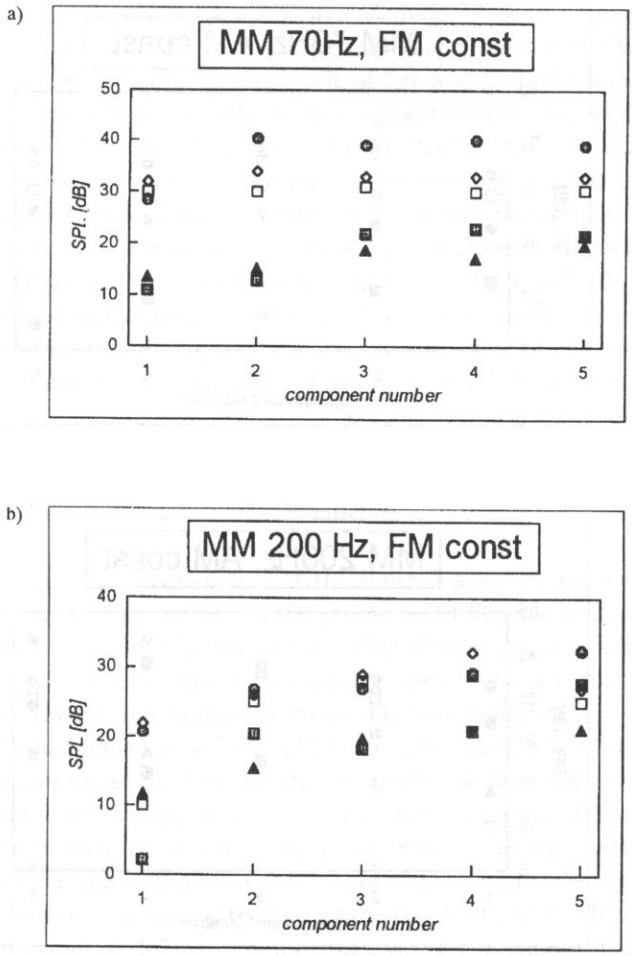

Fig. 3. Spectral representation of the perception of amplitude modulation in the presence of the threshold values of frequency modulation and without FM for the modulating frequencies: a) 70 Hz, and b) 200 Hz. ■ – LML – level of the low sideband for MM, • – LMH – level of the high sideband for MM, ▲ – LA – level of sidebands for AM exposed separately, □ – LL – masking threshold for the frequency corresponding to the low sideband, ◊ – LH – masking threshold for the frequency corresponding to the high sideband.

The levels of the low and high sidebands produced by mixed modulation were calculated as follows:

$$\begin{aligned} LML &= L_{60} + 20\log\left(A \cdot \left|J_1(\beta) \cdot \left(1 - \frac{m}{\beta}\right)\right|\right), \\ LML &= L_{60} + 20\log\left(A \cdot \left|J_1(\beta) \cdot \left(1 + \frac{m}{\beta}\right)\right|\right). \end{aligned} \tag{6}$$

It can be seen that the perception of mixed modulation changes in a different manner for the two cases, i.e. when m = const or when β = const. In the case when both

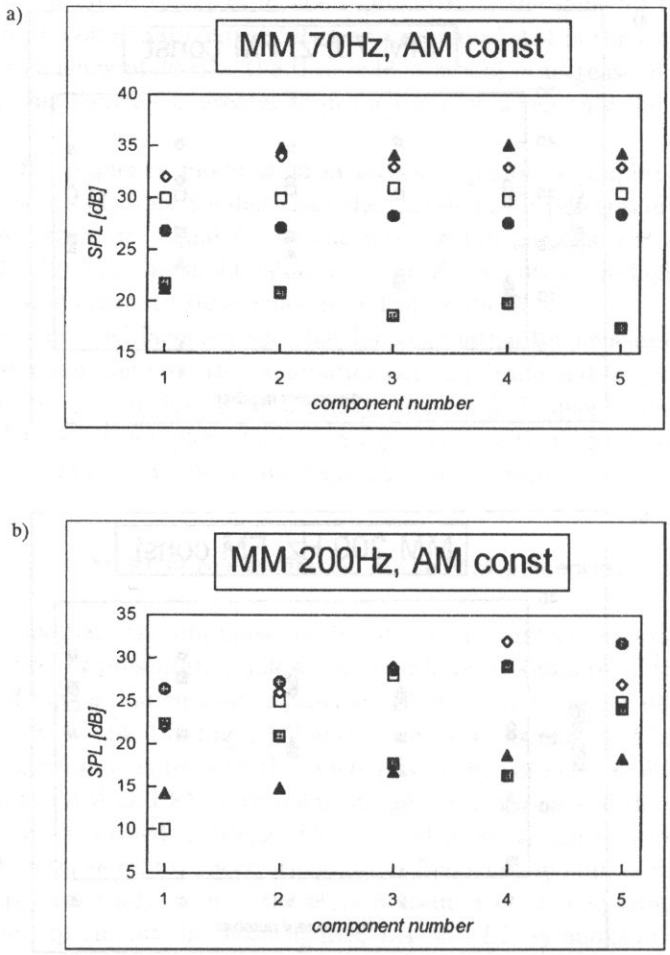

Fig. 4. Spectral representation of the perception of frequency modulation in the presence of the threshold values of amplitude modulation and without AM for the modulating frequencies: a) 70 Hz and b) 200 Hz. ■ – LML – level of the low sideband for MM, • – LMH – level of the high sideband for MM, ▲ – LF – level of sidebands for FM exposed separately, □ – LL – masking threshold for the frequency corresponding to the low sideband, ◊ – LH – masking threshold for the frequency corresponding to the high sideband.

kinds of modulation (AM and FM) are applied to a single component in the harmonic complex and frequency modulation is presented at the threshold levels (Fig. 3), the levels of the low sideband, resulting from mixed modulation, are lower than the thresholds of hearing at the corresponding frequencies when all the 5-component complex is on. Previous results [3, 5, 7, 15] indicated rather the opposite – the perception of AM, FM and MM is based on the lower sideband and the higher one is masked by the carrier. However, those results were obtained in experiments without masking and under different hearing conditions different from those in our experiment. Our results show that this kind of perception is based rather on the higher sidebands the levels of which

exceed the thresholds of hearing (for a 70-Hz modulator) or are equal to them (for a 200 Hz modulation). For a 70 Hz modulating frequency, when the AM is presented at the threshold of perception (Fig. 4), the levels of low and high sidebands are below the threshold of hearing for all partials which can suggest that in this case the summation of partially roughnesses takes place as proposed by TERHARDT [20] and VOGEL [21, 22]. For the modulating frequency of 200 Hz, the low sideband is higher than the corresponding hearing threshold (resulting from masking) only for the fundamental harmonic, and equal for the 5-th one, but for the basic partial this low sideband does not play any role because its level is lower than the absolute hearing threshold. This leads to the conclusion that the low sideband resulting from mixed modulation does not play an important role in the MM perception; this perception is based mostly on the high sideband caused by the modulation process or on both the sidebands as a result of summation of partial roughnesses.

5. Discussion

For the the modulating frequency of 70 Hz, there is a significant decrease in the AM threshold for the 2-nd to 5-th partials in the presence of FM presented at the threshold of detection. This may be caused by two factors. One of them is the masking phenomenon according to which some components appearing in the middle of a multitone are masked stronger than the lowest and highest partials [11] and therefore it is necessary to use a higher level of sidebands caused by AM to produce an audible "roughness effect". Moreover, in all cases the sound level for the low sidebands does not exceed the threshold of hearing calculated according to equation (5), which can suggest that the "roughness effect" is based not only on the low sidebands existing in the spectrum. The main argument supporting this effect may be a short-time amplitude spectrum evaluated with a time window corresponding to the critical-band filters [20]. In the case like this, two subthreshold values of different components, which can cause separate roughnesses, should be added in one critical band to make an audible sensation. This fact is confirmed for all partials in the experiment, if it can be assumed that both the lower and higher sidebands are in one critical band. Secondly, in this case there is no specific pitch which could help the listeners to recognize the MM process as a dissonance effect and for all the partials a disturbing specific sound appears consisting of two additional components in the spectrum which are nonharmonic to the other ones. Despite the levels of the sidebands, we can still say that a partial roughness summation mechanism may exist when the 70 Hz sinusoid is used as an amplitude modulator. The third aspect, which should be noticed here, is that the change of the excitation place appearing for the 70 Hz-modulation may play an important role in the MM-perception, especially when the modulating signal contains only a clear sinusoid.

For the higher modulating frequency (200 Hz), the perceptual grouping mechanism [2] plays the main role in the AM perception in the presence of FM for all the modulated harmonics. For all partials, the threshold values of the modulation index increase for the higher partials. For the first four harmonics, the level of the low sideband is lower

than the hearing threshold which suggests that a summation mechanism of subthreshold values may exist even for partials from different critical bands except for the 5-th partial where the low sideband is higher than the hearing threshold for its frequency. For high sidebands, the levels are equal to the hearing threshold values obtained on the basis of the masking phenomena.

For a modulating frequency of 70 Hz, and the FM perception in the presence of AM presented with the threshold of perception, the levels of both the sidebands do not exceed the hearing threshold values; this is the main difference between the AM and FM perceptions found in this experiment. This means that when the frequency deviation is smaller than the critical bandwidth, the human ear can also perceive temporal changes in the sound level of the processed partials. Finally, it can be concluded that the perception of "roughness" is based on both the sound spectra with sidebands produced by the modulation process and on fast changes in the frequency of the modulated component. However, a boundary which would clearly separate these two mechanisms has not been defined precisely for MM-modulated tones.

For a modulating frequency of 200 Hz, the spectral model of hearing plays the decisive role in the FM perception in the case of AM presented simultaneously. In the case of modulated partials of the investigated harmonic complex, all the rules applying to the masking phenomena have been confirmed by the obtained results, however, for higher components the high sideband produced by mixed modulation plays the most important role in the MM perception. Another phenomenon that can help listeners in the MM detection is the perceptual grouping mechanism. According to this, for some of the modulated partials MM can be perceived as an additional pitch occuring in multitones which is usually out of tune of the fundamental frequency of the complex; this causes two independent perceptual streams [2]. The summation of the next (or previous) partial and the higher (or lower) sideband, respectively, takes place in one critical band, which suggests that a specific pitch for that partial could be changed and, from the musical point of view, this could be considered as a simple way to detect these simultaneous fast changes in the amplitude and frequency of the modulated partials.

6. Conclusions

The results of this experiment have confirmed all the rules applying to the masking process in the investigated multitones. On the basis of the sound spectra of investigated complexes, it should be noticed that the higher sidebands are more important for MM-perception than the lower ones. However, it can be said that two underthreshold values of the lower and higher sideband levels may be added in some cases, even if the products of the modulation process are spread widely in the frequency domain. Another important rule refers to the summation of excitation: in most cases, for 70 Hz-modulation, such a summation does exist allowing listeners to detect fast changes in the amplitudes and frequencies of a single components in the harmonic complex.

This work was supported by the Polish Committee of Scientific Research, grant no. 7 T07 B 034 08.

References

[1] J.G. BEERENDS and J.A. STEMERDINK, *A perceptual audio quality measure based on a psychoacoustic sound representation*, J. Audio Eng. Soc., **40**, pp. 963–978 (1992).

[2] A.S. BREGMAN, *Auditory Scene Analysis – The Perceptual Organization of Sound*, MIT Press, Cambridge, Mass 1990.

[3] F. CONINX, *The Detection of Combined Differences in Frequency and Intensity*, Acustica, **39**, pp. 137–150 (1978).

[4] F. CONINX, *The Perception of Combined Frequency and Amplitude Modulations with Clearly Audible Modulation Depths*, Acustica, **39**, pp. 151–154 (1978).

[5] H. FASTL, *Roughness and temporal masking patterns of sinusoidally amplitude modulated broadband noise*, [In:] Psychophysics and psychology of hearing, E.F. EVANS and J.P. WILSON [Eds.], Academic Press, London 1977.

[6] L.L. FETH, *Combinations of amplitude and frequency differences in auditory discrimination*, Acustica, **26**, pp. 67–77 (1972).

[7] W.M. HARTMANN and G.M. HNATH, *Detection of mixed modulation*, Acustica, **50**, pp. 297–312 (1982).

[8] S. KEMP, *Roughness of frequency-modulated tones*, Acustica, **50**, pp. 126–133 (1982).

[9] M.J. KIN and A.B. DOBRUCKI, *Roughness effect as a result of amplitude or frequency modulation of single components in harmonic complex*, Proc. of 102nd AES Convention, Munich, Germany, preprint 4481 (L2) (1997).

[10] R.A. LUFTI, *Additivity of simultaneous masking*, J. Acoust. Soc. Am., **73**, pp. 262–267 (1983).

[11] R.A. LUFTI, *A power-law transformation predicting masking by sounds with complex spectra*, J. Acoust. Soc. Am., **77**, pp. 2128–2136 (1985).

[12] D. MAIWALD, *Ein Funktionsschema des Gehörs zur Beschreibung der Erkennbarkeit klein Frequenz und Amplitudenänderungen*, Acustica, **18**, pp. 81–92 (1967).

[13] D. MAIWALD, *Die Berechnung von Modulationsschwelten mit Hilfe eines Funktionsschemas*, Acustica, **18**, pp. 193–207 (1967).

[14] B.C.J. MOORE and A. SĘK, *Detection of combined frequency and amplitude modulation*, J. Acoust. Soc. Am., **92**, pp. 3119–3130 (1992).

[15] E. OZIMEK and A. SĘK, *Perception of amplitude and frequency modulated signals (mixed modulation)*, J. Acoust. Soc. Am., **87**, pp. 1598–1603 (1987).

[16] M.M. TAYLOR, *PEST: Efficient estimates on probability functions*, J. Acoust. Soc. Am., **41**, pp. 1224–1235 (1967).

[17] M.M. TAYLOR, *PEST reduces bias in forced choice psychophysics*, J. Acoust. Soc. Am., **74**, pp. 375–387 (1983).

[18] E. TERHARDT, *Über akustische Rauhigkeit und Schwankungsstrke*, Acustica, **20**, p. 215 (1968).

[19] E. TERHARDT, *Schallfluctuation und Rauhigkeitsempfinden: Akustik und Schwingungstechnik* VDI-Verlag, Düsseldorf 1971.

[20] E. TERHARDT, *On the perception of periodic sound fluctuation (Roughness)*, Acustica, **30**, pp. 201–213 (1974).

[21] A. VOGEL, *Roughness and its relation to the time-pattern of psychoacoustical excitation*, [In:] Facts and Models in Hearing, E. ZWICKER and E. TERHARDT [Eds.], Springer, Berlin – Heidelberg – New York 1974.

[22] A. VOGEL, *Ein gemeinsames Funktionsschema zur Beschreibung der Lautheit und der Rauhigkeit*, Biol. Cybernetics, **18**, pp. 31–37 (1975).

[23] E. ZWICKER, *Die Grenzen der Hrbarkeit der Amplitudenmodulation und der Frequenzmodulation eines Tones*, Acustica, **2**, pp. 125–133 (1952).

[24] E. ZWICKER, *Die elementaren Grundlagen zur Bestimmung der Informationskapazität des Gehörs*, Acustica, **6**, pp. 356–381 (1956).

[25] E. ZWICKER, *Direct comparisons between the sensation produced by frequency modulation and amplitude modulation*, J. Acoust. Soc. Am., **34**, pp. 1425–1430 (1962).

[26] E. ZWICKER and R. FELDTKELLER, *Das Ohr als Nachrichtenempfanger*, Hirzel Verlag, Stuttgart 1967.

[27] E. ZWICKER, *Masking and psychological excitation as consequences os the ear's frequency analysis* [In:] Frequency analysis and periodicity detection in hearing, Driebergen Symposium 1969, R. PLOMP and G. SMOORENBURG [Eds.], Sythof, Leiden 1970.

ARCHIVES OF ACOUSTICS
23, 3, 391–401 (1998)

CYLINDRICAL WAVE DIFFRACTION BY AN ABSORBING STRIP

S. ASGHAR and TASAWAR HAYAT

Department of Mathematics,
Quaid-i-Azam University
(Islamabad, Pakistan)

A solution for the problem of diffraction of a cylindrical sound wave near an absorbing strip introducing the Kutta–Joukowski condition is obtained. The two faces of the strip have impedance boundary conditions. The problem which is solved is a mathematical model for a noise barrier whose surface is treated with acoustically absorbing materials. It is found that the field produced by the Kutta–Joukowski condition will be substantially in excess of that in its absence when the source is near the edge.

1. Introduction

Much interest has been shown in recent years to the problem of noise reduction. Unwanted noise from motorways, railways and airports can be shielded by a barrier which intercepts the line of sight from the noise source to a receiver. To design and performance of noise barriers, particularly, for the reduction of traffic noise, has received considerable attention [1]. An effective way of reducing the noise is to use absorbing linings. Absorbing linings have also been used on noise barriers to improve their efficiency. The rationale for such a noise barrier design is given in RAWLINS [2].

In 1970, it was shown by FFOWCS–WILLIAMS and HALL [3] that the aerodynamic sound scattered by a sharp edge is proportional in intensity to the fifth power of the flow velocity and inversely to the cube of the distance of the source from the edge. Thus, the edge is likely to be the dominant sound source, especially when the source is very close to the edge. Their findings were however based upon the assumption of a potential flow near the sharp edge with velocity becoming infinite there. Instead of that if one wishes to prescribe that the velocity is finite, there are two possible points of view. One way is to abandon lighthill's theory and use linearized Navier–Stoke's equation with a source term as employed by ALBLAS [4]. Before discussing the second option, it is better to introduce the Kutta–Joukowski condition.

JONES [5] adopted this approach and introduced the wake condition to examine to effect of the Kutta–Joukowski condition at the edge of the half-plane. He calculated the field scattered from a line source and observed that for the moving medium the

imposition of the Kutta–Joukowski condition does not have much influence on the scattered field away from the diffracting plane. Near the wake this condition produces a much stronger field than elsewhere even when the source is not near the edge. Thus the wave acts as a convenient transmission channel for carrying intense sound away from the source. This problem was further extended to the point source excitation by BALASUBRAMANYAM [6].

Keeping in view the importance of the Kutta–Joukowski condition, diffraction of a cylindrical acoustic wave by an absorbing strip is considered in this paper. It is found that the field produced by this condition (Kutta–Joukowski) will be substantially larger than the field produced in its absence when the source is near the edge. The results for rigid and soft strips can be obtained as special cases of this problem by taking the absorbing parameter $\beta = 0$ and $\beta = \infty$, respectively.

2. Formulation of the problem

We shall consider small amplitude sound waves diffracted by a strip. An absorbing strip is assumed to occupy $y = 0$, $-l \leq x \leq 0$ as shown in the Fig. 1. The strip is assumed to be of negligible thickness and satisfying absorbent boundary conditions [7]

$$p - u_n z = 0, \tag{2.1}$$

on both sides of its surface. Here p is the acoustic pressure of the surface, u_n is the normal component of the perturbation velocity at a point on the surface of the strip and z is the acoustic impedance of the surface. We shall restrict our consideration to a harmonic time dependence, with the time factor $e^{-i\omega t}$ (ω is low angular frequency) being suppressed throughout.

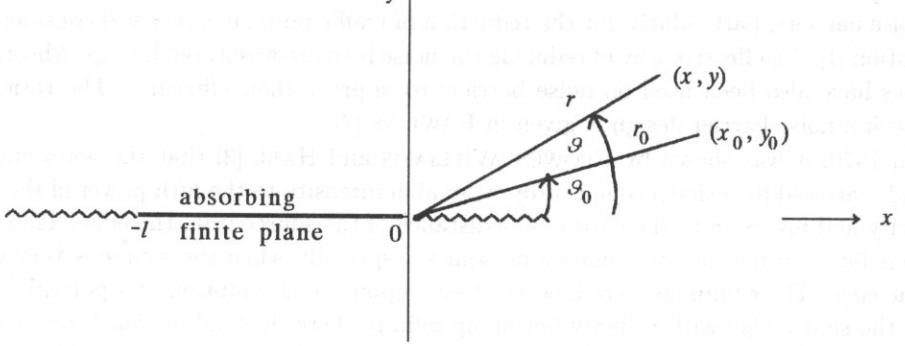

Fig. 1.

The perturbation velocity u of the irrotational sound waves can be expressed in terms of the total velocity potential $\phi_t(x, y)$ by $u = \operatorname{grad} \phi_t$. The resulting pressure in the sound field is given by $p = i\omega\varrho_0\phi_t(x, y)$, where ϱ_0 is the density of the initially undisturbed ambient medium. The primary source is taken to be a line source which is located at the

position (x_0, y_0), $y_0 > 0$. Thus, the wave equation satisfied by the total velocity potential ϕ_t in the presence of the line source is

$$\left(\frac{\partial^2}{\partial x^2} + \frac{\partial^2}{\partial y^2} + k^2\right)\phi_t = \delta(x - x_0)\delta(y - y_0), \tag{2.2}$$

where $k(= \omega/c)$ is the free space wave number and c is the speed of sound. For analytic convenience k is assumed to be complex and has a small positive imaginary part.

The effect of the strip is described by the boundary conditions

$$\left(\frac{\partial}{\partial y} \pm ik\beta\right)\phi_t(x, 0^{\pm}) \qquad (-l < x < 0), \tag{2.3}$$

where $\beta(= \varrho_0 c/z)$ is the small absorbing parameter and for acoustic absorption $\mathrm{Re}\,(\beta) > 0$. We remark that $\beta = 0$ corresponds to the rigid barier and $\beta = \infty$ corresponds to the pressure release barrier.

In order to satisfy the Kutta–Joukowski condition at the edge, JONES [5] introduced a discontinuity in the field at $0 < x < \infty$ and postulated the existence of a wake condition. According to him, ϕ_t is discontinuous, while $\partial\phi_t/\partial y$ remains continuous for $y = 0$, $x > 0$. With the same analysis as used by JONES [5], the boundary conditions can thus be expressed as

$$\frac{\partial}{\partial y}\phi_t(x, y^+) = \frac{\partial}{\partial y}\phi_t(x, y^-) \qquad (x < -l, \quad x > 0, \quad y = 0), \tag{2.4}$$

and

$$\begin{aligned} \phi_t(x, y^+) - \phi_t(x, y^-) &= \alpha e^{i\mu x} \qquad (x > 0, \quad y = 0), \\ \phi_t(x, y^+) - \phi_t(x, y^-) &= \alpha e^{-i\mu x} \qquad (x < -l, \quad y = 0). \end{aligned} \tag{2.5}$$

In Eq. (2.5), α and μ are constants. The constant μ is regarded as known and we shall write

$$\mu = k\cos\vartheta_1, \tag{2.6}$$

where $0 \leq \mathrm{Re}\,\vartheta_1 < \pi$, $\mathrm{Im}\,\vartheta_1 \geq 0$. While k has a positive imaginary part we shall take $0 < \mathrm{Re}\,\vartheta_1 < \pi$ and $\mathrm{Im}\,\vartheta_1 > 0$; eventually we shall be concerned primarily with the case $\mathrm{Re}\,\vartheta_1 = 0$, $\mathrm{Im}\,\vartheta_1 > 0$. In Eq. (2.5), α can be determined by means of a Kutta–Joukowski condition. We note that $\alpha = 0$ corresponds to a no wake situation. It is appropriate to split ϕ_t as

$$\phi_t(x, y) = \phi_0(x, y) + \phi(x, y), \tag{2.7}$$

where ϕ_0 is the incident wave which accounts for the inhomogeneous source term and ϕ is the solution of the homogeneous wave Eq. (2.2) that corresponds to the diffracted field. Thus ϕ_0 and ϕ satisfy the following equations

$$\left(\frac{\partial^2}{\partial x^2} + \frac{\partial^2}{\partial y^2} + k^2\right)\phi_0(x, y) = \delta(x - x_0)\delta(y - y_0), \tag{2.8}$$

$$\left(\frac{\partial^2}{\partial x^2} + \frac{\partial^2}{\partial y^2} + k^2\right)\phi(x, y) = 0. \tag{2.9}$$

In addition we insist that ϕ represents an outward travelling wave as $r = \sqrt{x^2 + y^2} \to \infty$ and satisfies the normal edge condition at the boundary discontinuity [8].

3. Solution of the problem

We define the Fourier transform pair by

$$\begin{aligned} \overline{\phi}(\nu,y) &= \frac{1}{\sqrt{2\pi}}\int_{-\infty}^{\infty}\phi(x,y)e^{i\nu x}dx, \\ \phi(x,y) &= \frac{1}{\sqrt{2\pi}}\int_{-\infty}^{\infty}\overline{\phi}(\nu,y)e^{-i\nu x}d\nu, \end{aligned} \tag{3.1}_1$$

where ν is a complex variable. In order to accomodate three part boundary conditions on $y=0$, we split $\overline{\phi}(\nu,y)$ as

$$\overline{\phi}(\nu,y) = \overline{\phi}_+(\nu,y) + e^{-i\nu l}\overline{\phi}_-(\nu,y) + \overline{\phi}_1(\nu,y), \tag{3.1}_2$$

where

$$\begin{aligned} \overline{\phi}_+(\nu,y) &= \frac{1}{\sqrt{2\pi}}\int_{0}^{\infty}\phi(x,y)e^{i\nu x}dx, \\ \overline{\phi}_-(\nu,y) &= \frac{1}{\sqrt{2\pi}}\int_{-\infty}^{-l}\phi(x,y)e^{i\nu(x+l)}dx, \end{aligned}$$

and

$$\overline{\phi}_1(\nu,y) = \frac{1}{\sqrt{2\pi}}\int_{-l}^{0}\phi(x,y)e^{i\nu x}dx.$$

In Eq. $(3.1)_2$, $\overline{\phi}_+$ is regular for $\operatorname{Im}\nu > -\operatorname{Im}k$, $\overline{\phi}_-$ is regular for $\operatorname{Im}\nu < \operatorname{Im}k$ and $\overline{\phi}_1(\nu,y)$ is an integral function and is therefore analytic in $-\operatorname{Im}k < \operatorname{Im}\nu < \operatorname{Im}k$. For this we recall that k is complex and ϕ represents an outward travelling wave. The solution of Eq. (2.8) can be written in a straight forward manner as

$$\begin{aligned} \phi_0(x,y) &= \frac{-1}{4i}H_0^{(1)}\left(k\left[(x-x_0)^2+(y-y_0)^2\right]^{1/2}\right), \\ &= \frac{1}{4\pi i}\int_{-\infty}^{\infty}\frac{e^{-i\nu(x-x_0)+i(k^2-\nu^2)^{1/2}|y-y_0|}}{\sqrt{k^2-\nu^2}}d\nu. \end{aligned} \tag{3.2}$$

Making change of variables

$$x_0 = r_0\cos\vartheta_0, \qquad y_0 = r_0\sin\vartheta_0 \qquad (0\le\vartheta_0\le\pi),$$

in Eq. (3.2) and letting $r_0\to\infty$, we obtain using the asymptotic form for the Hankel function

$$\phi_0 = be^{-ik(x\cos\vartheta_0+y\sin\vartheta_0)}, \tag{3.3}$$

where

$$b = \frac{-1}{4i}\sqrt{\frac{2}{\pi kr_0}}e^{i(kr_0-\pi/4)}, \tag{3.4}$$

and ϑ_0 is the angle measured from the x-axis. Now taking the Fourier transform of Eq. (2.9), we obtain

$$\left(\frac{d^2}{dy^2} + \gamma^2\right)\overline{\phi}(\nu, y) = 0, \tag{3.5}$$

where $\gamma = \sqrt{k^2 - \nu^2}$ and the ν-plane is cut such that $\operatorname{Im}\gamma > 0$. The solution of Eq. (3.5) which satisfies the radiation condition is

$$\overline{\phi}(\nu, y) = \begin{cases} A_1(\nu)e^{i\gamma y} & (y > 0), \\ A_2(\nu)e^{-i\gamma y} & (y < 0). \end{cases} \tag{3.6}$$

Transforming the boundary conditions (2.3) to (2.5), we have

$$\overline{\phi}_1'(\nu, 0^{\pm}) = \mp ik\beta\overline{\phi}_1(\nu, 0^{\pm}) \mp ik\beta\overline{\phi}_0(\nu, 0) - \overline{\phi}_0'(\nu, 0), \tag{3.7}$$

$$\overline{\phi}_{\pm}'(\nu, 0^+) = \overline{\phi}_{\pm}'(\nu, 0^-) = \overline{\phi}_{\pm}'(\nu, 0), \tag{3.8}$$

$$\begin{aligned} \overline{\phi}_+(\nu, 0^+) - \overline{\phi}_+(\nu, 0^-) &= \frac{i\alpha}{\sqrt{2\pi}(\nu + \mu)}, \\ \overline{\phi}_-(\nu, 0^+) - \overline{\phi}_-(\nu, 0^-) &= \frac{-i\alpha e^{i\mu l}}{\sqrt{2\pi}(\nu - \mu)}, \end{aligned} \tag{3.9}$$

where $'$ denotes differentiation with respect to y. From Eqs. $(3.1)_2$, (3.6) and (3.8), we can write

$$\begin{aligned} &\overline{\phi}_+'(\nu, 0) + \overline{\phi}_-'(\nu, 0)e^{-i\nu l} + \overline{\phi}_1'(\nu, 0^+) \\ &\qquad = i\gamma\left[\overline{\phi}_+(\nu, 0^+) + \overline{\phi}_-(\nu, 0^+)e^{-i\nu l} + \overline{\phi}_1(\nu, 0^+)\right], \\ &\overline{\phi}_+'(\nu, 0) + \overline{\phi}_-'(\nu, 0)e^{-i\nu l} + \overline{\phi}_1'(\nu, 0^-) \\ &\qquad = -i\gamma\left[\overline{\phi}_+(\nu, 0^-) + \overline{\phi}_-(\nu, 0^-)e^{-i\nu l} + \overline{\phi}_1(\nu, 0^-)\right], \end{aligned} \tag{3.10}$$

After eliminating $\overline{\phi}_1'(\nu, 0^+)$ from $(3.7)_1$ and $(3.10)_1$, $\overline{\phi}_1'(\nu, 0^-)$ from Eqs. $(3.7)_2$ and $(3.10)_2$ and adding the resulting expressions, we arive at

$$\begin{aligned} &\overline{\phi}_+'(\nu, 0) + \overline{\phi}_-'(\nu, 0)e^{-i\nu l} - i\gamma N(\nu)J_1(\nu, 0) \\ &\qquad = \overline{\phi}_0(\nu, 0) - \frac{\alpha\gamma}{2\sqrt{2\pi}}\left(\frac{1}{(\nu + \mu)} - \frac{e^{-i(\nu-\mu)l}}{(\nu - \mu)}\right), \end{aligned} \tag{3.11}$$

where

$$N(\nu) = 1 + \frac{k\beta}{\gamma}, \qquad J_1(\nu, 0) = \frac{1}{2}\left[\overline{\phi}_1(\nu, 0^+) - \overline{\phi}_1(\nu, 0^-)\right].$$

In a similar way by eliminating $\overline{\phi}_1(\nu, 0^+)$ from Eqs. $(3.7)_1$ and $(3.10)_1$, $\overline{\phi}_1(\nu, 0^-)$ from $(3.7)_2$ and $(3.10)_2$, and subtracting the resulting equations, we obtain

$$\begin{aligned} &\overline{\phi}_+(\nu, 0^+) + \overline{\phi}_-(\nu, 0^+)e^{-i\nu l} - \frac{N(\nu)J_1'(\nu, 0)}{ik\beta} \\ &\qquad = \overline{\phi}_0(\nu, 0) + \frac{i\alpha}{2\sqrt{2\pi}}\left[\frac{1}{\nu + \mu} - \frac{e^{-i(\nu-\mu)l}}{\nu - \mu}\right], \end{aligned} \tag{3.12}$$

where

$$J_1'(\nu,0)=\frac{1}{2}\left[\overline{\phi}_1'(\nu,0^+)-\overline{\phi}_1'(\nu,0^-)\right].$$

From Eqs. (3.3) and (3.11), we have

$$\begin{aligned}\overline{\phi}_+'(\nu,0)+\overline{\phi}_-'(\nu,0)e^{-i\nu l}-i\gamma N(\nu)J_1(\nu,0)\\ +\frac{\alpha\gamma N(\nu)}{2\sqrt{2\pi}}\left[\frac{1}{\nu+\mu}-\frac{e^{-i(\nu-\mu)l}}{\nu-\mu}\right]-\frac{\alpha k\beta}{2\sqrt{2\pi}}\left[\frac{1}{\nu+\mu}-\frac{e^{-i(\nu-\mu)l}}{\nu-\mu}\right]\\ =\frac{-kb\sin\vartheta_0}{\sqrt{2\pi}(\nu-k\cos\vartheta_0)}\left[1-e^{-i(\nu-k\cos\vartheta_0)l}\right].\end{aligned}\tag{3.13}$$

For the solution of Eq. (3.13), we make the following factorizations

$$\gamma=(k+\nu)^{1/2}(k-\nu)^{1/2}=K_+(\nu)K_-(\nu),\tag{3.14}$$

and

$$N(\nu)=N_+(\nu)N_-(\nu),\tag{3.15}$$

where $N_+(\nu)$ and $K_+(\nu)$ are regular for $\operatorname{Im}\nu>-\operatorname{Im}k$ and $N_-(\nu)$, and $K_-(\nu)$ are regular for $\operatorname{Im}\nu<\operatorname{Im}k$. The factorization (3.15) has been discussed by NOBLE [9, p. 164] and is directly quoted here as

$$N_\pm(\nu)=1-\frac{i\beta}{\pi}\left((\nu/k)^2-1\right)^{1/2}\cos^{-1}(\pm\nu/k).\tag{3.16}$$

Thus, substitution of Eqs. (3.14) and (3.15) in Eq. (3.13) yields

$$\begin{aligned}\overline{\phi}_+'(\nu,0)+\overline{\phi}_-'(\nu,0)e^{-i\nu l}+S_+(\nu)S_-(\nu)J_1(\nu,0)\\ +\frac{i\alpha S_+(\nu)S_-(\nu)}{2\sqrt{2\pi}}\left[\frac{1}{\nu+\mu}-\frac{e^{-i(\nu-\mu)l}}{\nu-\mu}\right]-\frac{\alpha k\beta}{2\sqrt{2\pi}}\left[\frac{1}{\nu+\mu}-\frac{e^{-i(\nu-\mu)l}}{\nu-\mu}\right]\\ =\frac{-kb\sin\vartheta_0}{\sqrt{2\pi}(\nu-k\sin\vartheta_0)}\left[1-e^{-i(\nu-k\cos\vartheta_0)l}\right].\end{aligned}\tag{3.17}$$

In Eq. (3.17), $S_+(\nu)$ $[=K_+(\nu)N_+(\nu)]$ is regular for $\operatorname{Im}\nu>-\operatorname{Im}k$ and $S_-(\nu)$ $[=K_-(\nu)$ $N_-(\nu)]$ is regular for $\operatorname{Im}\nu<\operatorname{Im}k$. The unknown functions $\overline{\phi}_+'(\nu,0)$ and $\overline{\phi}_-'(\nu,0)$ in Eq. (3.17) have been determined using the procedure discussed by NOBLE [9, p. 166] and are given by

$$\begin{aligned}\overline{\phi}_+'(\nu,0)&=\frac{-kb\sin\vartheta_0}{\sqrt{2\pi}}\left(S_+(\nu)G_1(\nu)+T(\nu)S_+(\nu)C_1\right)\\ &\quad+\frac{\alpha}{2\sqrt{2\pi}}\left(\frac{k\beta}{(\nu+\mu)}-\frac{iS_+(\mu)S_+(\nu)}{(\nu+\mu)}+\frac{T(\nu)S_+(\nu)}{(k+\mu)}C_3\right),\\ \overline{\phi}_-'(\nu,0)&=\frac{-kb\sin\vartheta_0}{\sqrt{2\pi}}\left(S_-(\nu)G_2(-\nu)+T(-\nu)S_-(\nu)C_2\right)\\ &\quad+\frac{\alpha}{2\sqrt{2\pi}}\left(\frac{k\beta}{(\mu-\nu)}-\frac{iS_+(\mu)S_-(\mu)}{(\mu-\nu)}+\frac{T(-\nu)S_-(\nu)}{(k+\mu)}C_3\right).\end{aligned}\tag{3.18}$$

In Eqs. (3.18),

$$
\begin{aligned}
S_+(\nu) &= \sqrt{k+\nu}N_+(\nu), \qquad S_-(\nu) = e^{i\pi/2}\sqrt{\nu-k}N_-(\nu),\\
C_1 &= \frac{S_+(k)}{[1-T^2(k)S_+^2(k)]}\left[G_2(k)+G_1(k)T(k)S_+(k)\right],\\
C_2 &= \frac{S_+(k)}{[1-T^2(k)S_+^2(k)]}\left[G_1(k)+G_2(k)T(k)S_+(k)\right],\\
C_3 &= \frac{-iS_+(\mu)S_+(k)}{[1-T^2(k)S_+^2(k)]}\left[T(k)S_+(k)-e^{i\mu l}\right],
\end{aligned}
$$

$$
\begin{aligned}
G_1(\nu) &= \frac{1}{\nu-k\cos\vartheta_0}\left[\frac{1}{S_+(\nu)}-\frac{1}{S_+(k\cos\vartheta_0}\right]-R_1(\nu)e^{ikl\cos\vartheta_0},\\
G_2(\nu) &= \frac{1}{\nu+k\cos\vartheta_0}\left[\frac{1}{S_+(\nu)}-\frac{1}{S_+(-k\cos\vartheta_0)}\right]e^{ikl\cos\vartheta_0}-R_2(\nu),
\end{aligned}
\tag{3.19}
$$

$$
\begin{aligned}
R_{1,2}(\nu) &= \frac{E_{-1}[W_{-1}\{-i(k\pm k\cos\vartheta_0)l\}-W_{-1}\{-i(k+\nu)l\}]}{2\pi i(\nu\mp k\cos\vartheta_0)}\\
T(\nu) &= \frac{1}{2\pi i}E_{-1}W_{-1}\{-i(k+\nu)l\},\\
E_{-1} &= 2\sqrt{l}e^{ikl-3i\pi/4},\\
W_{-1}(m) &= \Gamma\left(\frac{1}{2}\right)e^{m/2}(m)^{-3/4}W_{-1/4,-1/4}(m),
\end{aligned}
$$

[$m=-i(k+\nu)l$ and $W_{i,j}$ is a Whittaker function].

Now from Eqs. (3.1) and (3.6), we obtain

$$
\begin{aligned}
A_1(\nu)-A_2(\nu) &= e^{-i\nu l}\left[\overline{\phi}_-(\nu,0^+)-\overline{\phi}_-(\nu,0^-)\right]\\
&\quad+\left[\overline{\phi}_1(\nu,0^+)-\overline{\phi}_1(\nu,0^-)\right]+\left[\overline{\phi}_+(\nu,0^+)-\overline{\phi}_+(\nu,0^-)\right],\\
A_1(\nu)+A_2(\nu) &= \frac{1}{i\gamma}\Big\{\left[\overline{\phi}_1'(\nu,0^+)-\overline{\phi}_1'(\nu,0^-)\right]\\
&\quad+\left[\overline{\phi}_+'(\nu,0^+)-\overline{\phi}_+'(\nu,0^-)\right]+\left[\overline{\phi}_-'(\nu,0^+)-\overline{\phi}_-'(\nu,0^-)\right]e^{-i\nu l}\Big\}.
\end{aligned}
\tag{3.20}
$$

Using Eqs. (3.8) and (3.9) in Eqs. (3.20) and then adding and subtracting the resulting expressions we get

$$
A_1(\nu) = \frac{i\alpha}{2\sqrt{2\pi}}\left[\frac{1}{\nu+\mu}-\frac{e^{-i(\nu-\mu)l}}{\nu-\mu}\right]+J_1(\nu,0)+\frac{J_1'(\nu,0)}{i\gamma}, \tag{3.21}
$$

$$
A_2(\nu) = \frac{-i\alpha}{2\sqrt{2\pi}}\left[\frac{1}{\nu+\mu}-\frac{e^{-i(\nu-\mu)l}}{\nu-\mu}\right]-J_1(\nu,0)+\frac{J_1'(\nu,0)}{i\gamma}. \tag{3.22}
$$

Substituting the values of $J_1(\nu,0)$ and $J_1'(\nu,0)$ from Eqs. (3.11) and (3.12) into Eqs. (3.21) and (3.22), we obtain

$$A_1(\nu) = \frac{i\alpha}{2\sqrt{2\pi}}\left[\frac{1}{\nu+\mu} - \frac{e^{-i(\nu-\mu)l}}{\nu-\mu}\right] + \frac{1}{i\gamma N(\nu)}\left[\overline{\phi}_+'(\nu,0) + \overline{\phi}_-'(\nu,0)e^{-i\nu l} - \overline{\phi}_0'(\nu,0) + \frac{\alpha\gamma}{2\sqrt{2\pi}}\left\{\frac{1}{\nu+\mu} - \frac{e^{-i(\nu-\mu)l}}{\nu-\mu}\right\}\right] + \frac{ik\beta}{i\gamma N(\nu)}\left[\overline{\phi}_+(\nu,0^+) + \overline{\phi}_-(\nu,0^+)e^{-i\nu l} - \overline{\phi}_0(\nu,0) - \frac{i\alpha}{2\sqrt{2\pi}}\left\{\frac{1}{\nu+\mu} - \frac{e^{-i(\nu-\mu)l}}{\nu-\mu}\right\}\right], \tag{3.23}$$

$$A_2(\nu) = \frac{-i\alpha}{2\sqrt{2\pi}}\left[\frac{1}{\nu+\mu} - \frac{e^{-i(\nu-\mu)l}}{\nu-\mu}\right] - \frac{1}{i\gamma N(\nu)}\left[\overline{\phi}_+'(\nu,0) + \overline{\phi}_-'(\nu,0)e^{-i\nu l} - \overline{\phi}_0'(\nu,0) + \frac{\alpha\gamma}{2\sqrt{2\pi}}\left\{\frac{1}{\nu+\mu} - \frac{e^{-i(\nu-\mu)l}}{\nu-\mu}\right\}\right] + \frac{ik\beta}{i\gamma N(\nu)}\left[\overline{\phi}_+(\nu,0^+) + \overline{\phi}_-(\nu,0^+)e^{-i\nu l} - \overline{\phi}_0(\nu,0) - \frac{i\alpha}{2\sqrt{2\pi}}\left\{\frac{1}{\nu+\mu} - \frac{e^{-i(\nu-\mu)l}}{\nu-\mu}\right\}\right]. \tag{3.24}$$

We note that

$$N(\nu) \approx 1 + O(\beta), \qquad ik\beta/N(\nu) \approx O(\beta),$$

and assert that $(k\beta/\gamma)$ is very small provided that $|\nu/k|$ is not too near 1. This can be justified under small absorbing parameters β and low frequency of the acoustic wave. Thus using this Eqs. (3.16), (3.23) and (3.24) gives

$$\begin{aligned} N_\pm(\nu) &\approx 1 \mp \frac{\nu\beta}{\pi\gamma}, \\ A_1(\nu) &= -A_2(\nu) = \frac{1}{i\gamma}\left(\overline{\phi}_+'(\nu,0) + \overline{\phi}_-'(\nu,0)e^{-i\nu l} - \overline{\phi}_0'(\nu,0)\right). \end{aligned} \tag{3.25}$$

Note that in writing Eqs. (3.25), we have retained the terms of order $O(\beta/\gamma)$ and neglected the terms of $O(k\beta/\gamma)$.

Substitution of Eqs. (3.3) and (3.18) in Eq. $(3.25)_2$ yields

$$A_1\nu = -A_2(\nu) = \frac{kb\sin\vartheta_0}{\sqrt{2\pi}i\gamma(\nu - k\cos\vartheta_0)}\left\{\frac{S_+(\nu)}{S_+(k\cos\vartheta_0)} - \frac{S_+(-\nu)e^{-i(\nu-k\cos\vartheta_0)l}}{S_+(-k\cos\vartheta_0)}\right\} - \frac{kb\sin\vartheta_0}{\sqrt{2\pi}i\gamma}\left\{S_+(\nu)T(\nu)C_1 - S_+(\nu)R_1(\nu)e^{ikl\cos\vartheta_0} + S_+(-\nu)R_2(-\nu)e^{-i\nu l} + C_2T(-\nu)S_+(-\nu)e^{-i\nu l}\right\} + \frac{\alpha}{2\sqrt{2\pi}i\gamma}\left\{k\beta\left[\frac{1}{\nu+\mu} + \frac{e^{-i\nu l}}{\mu-\nu}\right] - iS_+(\mu)\left[\frac{S_+(\nu)}{(\nu+\mu)} + \frac{e^{-i\nu l}S_+(-\nu)}{\mu-\nu}\right] + \frac{C_3}{(k+\mu)}\left[T(\nu)S_+(\nu) + e^{-i\nu l}T(-\nu)S_+(-\nu)\right]\right\}. \tag{3.26}$$

Now putting the values of $A_1(\nu)$ in Eq. (3.6) and taking inverse Fourier transform the field $\phi(x,y)$ can be written as

$$\phi(x,y) = \phi^{\text{sep}}(x,y) + \phi^{\text{int}}(x,y), \tag{3.27}$$

where

$$\begin{aligned}\phi^{\text{sep}}(x,y) = {} & \frac{kb\sin\vartheta_0}{2\pi}\int_{-\infty}^{\infty}\frac{S_+(\nu)e^{i\gamma y-i\nu x}}{i\gamma(\nu-k\cos\vartheta_0)S_+(k\cos\vartheta_0)}d\nu \\ & - \frac{kb\sin\vartheta_0}{2\pi}\int_{-\infty}^{\infty}\frac{e^{-i(\nu-k\cos\vartheta_0)l}S_+(-\nu)e^{i\gamma y-i\nu x}}{i\gamma(\nu-k\cos\vartheta_0)S_+(-k\cos\vartheta_0)}d\nu \\ & + \frac{\alpha}{4\pi}\left[k\beta\int_{-\infty}^{\infty}\frac{1}{i\gamma}\left\{\frac{1}{\nu+\mu}+\frac{e^{-i\nu l}}{\mu-\nu}\right\} - iS_+(\mu)\int_{-\infty}^{\infty}\frac{1}{i\gamma}\left\{\frac{S_+(\nu)}{\nu+\mu}\right.\right. \\ & \left.\left. + \frac{e^{-i\nu l}S_+(-\nu)}{\mu-\nu}\right\}\right]e^{i\gamma y-i\nu x}d\nu, \end{aligned} \tag{3.28}$$

$$\begin{aligned}\phi^{\text{int}}(x,y) = {} & \frac{kb\sin\vartheta_0}{2\pi}\int_{-\infty}^{\infty}\frac{1}{i\gamma}\left[S_+(\nu)R_1(\nu)e^{ikl\cos\vartheta_0}\right. \\ & \left. - S_+(-\nu)R_2(-\nu)e^{-i\nu l} - S_+(\nu)T(\nu)C_1 - T(-\nu)S_+(-\nu)e^{-i\nu l}C_2\right]e^{i\gamma y-i\nu x}d\nu \\ & + \frac{\alpha C_3}{4\pi(k+\mu)}\int_{-\infty}^{\infty}\frac{1}{i\gamma}\left[T(\nu)S_+(\nu)+e^{-i\nu l}T(-\nu)S_+(-\nu)\right]e^{i\gamma y-i\nu x}d\nu. \end{aligned} \tag{3.29}$$

In order to solve the integrals appearing in Eqs. (3.28) and (3.29), we put $x = r\cos\vartheta$, $y = r\sin\vartheta$ and deform the contour by the transformation $\nu = -k\cos(\vartheta+i\xi)$, $(0<\vartheta<\pi$, $-\infty<\xi<\infty)$. Hence after using Eqs. (2.6) and (3.4), we have for large kr

$$\begin{aligned}\phi^{\text{sep}}(x,y) = {} & \frac{ie^{ik(r+r_0)}}{4\pi k(\cos\vartheta+\cos\vartheta_0)(rr_0)^{1/2}}f_1(-k\cos\vartheta) \\ & + \frac{\alpha}{2(2\pi kr)^{1/2}}\left[\beta e^{i\pi/4}\left\{\frac{1}{(\cos\vartheta_1-\cos\vartheta)}+\frac{e^{ikl\cos\vartheta}}{(\cos\vartheta_1+\cos\vartheta)}\right\}\right. \\ & \left. + \frac{e^{-i\pi/4}S_+(k\cos\vartheta_1)}{k}\left\{\frac{S_+(-k\cos\vartheta)}{(\cos\vartheta_1-\cos\vartheta)}+\frac{e^{ikl\cos\vartheta}S_+(k\cos\vartheta)}{(\cos\vartheta_1+\cos\vartheta)}\right\}\right]e^{ikr}, \end{aligned} \tag{3.30}$$

$$\phi^{\text{int}}(x,y) = \frac{ie^{ik(r+r_0)}}{4\pi(rr_0)^{1/2}}f_2(-k\cos\vartheta) + \frac{\alpha e^{i(kr+\pi/4)}}{2(2\pi kr)^{1/2}}f_3(-k\cos\vartheta). \tag{3.31}$$

In Eqs. (3.30) and (3.31)

$$f_1(-k\cos\vartheta) = -\sin\vartheta_0\left[\frac{S_+(-k\cos\vartheta)}{S_+(k\cos\vartheta_0)} - \frac{S_+(k\cos\vartheta)e^{ikl(\cos\vartheta+\cos\vartheta_0)}}{S_+(-k\cos\vartheta_0)}\right],$$

$$f_2(-k\cos\vartheta) = \sin\vartheta\Big[S_+(-k\cos\vartheta)R_1(-k\cos\vartheta)e^{ikl\cos\vartheta_0} - S_+(k\cos\vartheta)R_2(k\cos\vartheta)e^{ikl\cos\vartheta} - S_+(-k\cos\vartheta)T(-k\cos\vartheta)C_1 - S_+(k\cos\vartheta)T(k\cos\vartheta)C_2e^{ikl\cos\vartheta}\Big],$$

$$f_3(-k\cos\vartheta) = \frac{C_3}{(k+k\cos\vartheta_1)}\Big[T(-k\cos\vartheta)S_+(-k\cos\vartheta) + e^{ikl\cos\vartheta}T(k\cos\vartheta)S_+(k\cos\vartheta)\Big].$$

From Eqs. (3.27), (3.30) and (3.31), we obtain

$$\phi(x,y) = \frac{ie^{ik(r+r_0)}}{4\pi(rr_0)^{1/2}k}\left[\frac{f_1(-k\cos\vartheta)}{(\cos\vartheta+\cos\vartheta_0)} + kf_2(-k\cos\vartheta)\right] + \frac{\alpha e^{i(kr+\pi/4)}}{2(2\pi kr)^{1/2}}\left[\beta\left\{\frac{1}{(\cos\vartheta_1-\cos\vartheta)} + \frac{e^{ikl\cos\vartheta}}{(\cos\vartheta_1+\cos\vartheta)}\right\} + f_3(-k\cos\vartheta) - \frac{iS_+(k\cos\vartheta_1)}{k}\left\{\frac{S_+(-k\cos\vartheta)}{(\cos\vartheta_1-\cos\vartheta)} + \frac{e^{ikl\cos\vartheta}S_+(k\cos\vartheta)}{(\cos\vartheta_1+\cos\vartheta)}\right\}\right]. \tag{3.32}$$

In the limit $r \to 0$, Eq. (3.32) shows that

$$\phi(x,y) \approx 2r^{1/2}\left[-\frac{e^{ikr_0}}{4\pi(r_0)^{1/2}}\left\{f_1(-k\cos\vartheta) + \frac{k}{2}f_2(-k\cos\vartheta)\right\} + \frac{i\alpha e^{i\pi/4}k}{(2\pi k)^{1/2}}\left\{\beta\left(1+e^{ikl\cos\vartheta}\right) - \frac{iS_+(k\cos\vartheta_1)}{k}\left(S_+(-k\cos\vartheta) + e^{ikl\cos\vartheta}S_+(k\cos\vartheta)\right) + \frac{f_3(-k\cos\vartheta)}{2}\right\}\right],$$

where we have neglected the terms which are constant and $O(r)$. Therefore, the velocity will remain bounded at the edge if and only if the co-efficient of $r^{1/2}$ vanishes. Hence the Kutta–Joukowski condition requires that

$$\alpha = \frac{e^{ikr_0-3i\pi/4}}{(2\pi kr_0)^{1/2}}\mathcal{G}_1(-k\cos\vartheta), \tag{3.33}$$

where

$$\mathcal{G}_1(-k\cos\vartheta) = \left\{f_1(-k\cos\vartheta) + \frac{k}{2}f_2(-k\cos\vartheta)\right\}\left\{\beta\left(1+e^{ikl\cos\vartheta}\right) - \frac{iS_+(k\cos\vartheta_1)}{k}\left(S_+(-k\cos\vartheta) + e^{ikl\cos\vartheta}S_+(k\cos\vartheta)\right) + \frac{f_3(-k\cos\vartheta)}{2}\right\}^{-1}.$$

Using Eq. (3.33) in Eq. (3.32) the far field is given by

$$\phi = \phi_A + \phi_W, \tag{3.34}$$

where ϕ_A denotes that part of ϕ that arises when there is no wake and ϕ_W the part that arises when there is a wake. They are explicitly given by

$$\phi_A = \frac{ie^{ik(r+r_0)}}{4\pi(rr_0)^{1/2}k}\mathcal{G}_2(-k\cos\vartheta), \tag{3.35}$$

$$\phi_W = \frac{ie^{ik(r+r_0)}}{4\pi(rr_0)^{1/2}k}\mathcal{G}_3(-k\cos\vartheta). \tag{3.36}$$

In Eqs. (3.35) and (3.36)

$$\mathcal{G}_2(-k\cos\vartheta) = \left[\frac{f_1(-k\cos\vartheta)}{(\cos\vartheta+\cos\vartheta_0)} + kf_2(-k\cos\vartheta)\right],$$

$$\mathcal{G}_3(-k\cos\vartheta) = -\mathcal{G}_1(-k\cos\vartheta)\left[f_3(-k\cos\vartheta) + \beta\left\{\frac{1}{(\cos\vartheta_1-\cos\vartheta)} + \frac{e^{ikl\cos\vartheta}}{(\cos\vartheta_1+\cos\vartheta)}\right\} - \frac{iS_+(k\cos\vartheta_1)}{k}\left\{\frac{S_+(-k\cos\vartheta)}{(\cos\vartheta_1-\cos\vartheta)} + \frac{e^{ikl\cos\vartheta}S_+(k\cos\vartheta)}{(\cos\vartheta_1+\cos\vartheta)}\right\}\right].$$

4. Conclusion

We have solved a new diffraction problem using a method invented by Jones. As far as we know, this is the first new problem to be solved by this method. We also note from Eqs. (3.30) and (3.31) that ϕ^{sep} consists of two parts each representing the diffracted field produced by the edges at $x = 0$ and $x = -l$ respectively, as though the other edges were absent while ϕ^{int} gives the interaction of one edge upon the other. Further, from Eq. (3.34), it is observed that the field caused by the Kutta–Joukowski condition will be substantially in excess of that in its absence when the source is near the edge. The results for no wake situation can be obtained by taking $\alpha = 0$. Finally, the results correspond to the rigid barrier if we put $\beta = 0$ in Eq. (3.34). Thus the consideration of absorbing strip with wake presents a more generalized model in the theory of diffraction.

References

[1] U.J. KURZE, J. Acoust. Soc. Amer., **55**, 504 (1974).

[2] A.D. RAWLINS, Proc. Roy. Soc. London, **A346**, 469 (1975).

[3] J.E. FFOWCS-WILLIAMS and L.H. HALL, J. Fluid Mech., **40**, 657 (1970).

[4] J.B. ALBLAS, Appl. Sci. Res., **A6**, 237 (1957).

[5] D.S. JONES, J. Inst. Maths. Applic., **9**, 114 (1972).

[6] R. BALASUBRAMANYAM, IMA J. Appl. Maths., **33**, 1, 71 (1984).

[7] P.M. MORSE and K.U. INGARD, *Encyclopedia of Phys. Acoustic I*, Springer Verlag, Berlin 1961.

[8] D.S. JONES, *The theory of electromagnetism*, Pergamon, Oxford 1964.

[9] B. NOBLE, *Methods based on the Wiener–Hopf technique*, Pergamon Press, London 1958.

ARCHIVES OF ACOUSTICS
23, 3, 403–410 (1998)

ACOUSTIC PROPERTIES OF BIOLOGICAL SUSPENSIONS WITH NON-SPHERICAL SUSPENDED DROPLETS

J. LEWANDOWSKI

Institute of Fundamental Technological Research,
Polish Academy of Sciences
(00-049 Warsaw, Świętokrzyska 21, Poland)

A theoretical study is made of the propagation properties of a suspension of viscous liquid droplets in a fluid medium with low viscosity. The droplets are of the form of oblate ellipsoids; the values of the material, structure and compositions parameters of the suspension are that of human blood. From the presented results of the analysis it can be seen that the propagation velocity and attenuation of ultrasound strongly depend on the blood composition, mechanical properties of the blood components as well as the ultrasonic frequency.

1. Introduction

In many areas of research and in engineering application are of interest the effective dynamic properties of some types of suspensions and emulsions. These properties are related to the acoustic (ultrasonic) wave velocities and attenuation (propagation parameters) in the materials being of interest and their structure. Therefore, some dynamic properties and structure parameters of suspensions and emulsions can be estimated on the basis of ultrasonic measurements. For ultrasonic waves to be used for this purpose, it is necessary to establish the factors which influence ultrasonic propagation in these inhomogeneous media and to relate the measurable ultrasonic propagation parameters as well as effective dynamic elastic constants of the media to the physical properties of medium components, their concentrations, size and shape. There are a variety of theoretical formulations that describe ultrasonic propagation in heterogeneous media. These differ from one another by the mathematical approaches used in their derivation and their underlying physical assumptions. However, analytical studies on the wave propagation through such composite materials, if they are closely related to the wave scattering theory, do not achieve formulae explicitly expressing the propagation properties in terms of physical properties of the constituents of the medium considered and its structure. Even in the best situation such analytical studies often lead to more or less complicated systems of algebraic equations for complex quantities which, although they have perfectly clear physical meanings, can not in general be calculated analytically from these equations. Consequently, results obtained in the form of the equation systems are

not as satisfactory as could be hoped for; nevertheless they are of value because they can be thought of as supplying an algorithm for a numerical estimate of the propagation properties of the inhomogeneous material. Such a situation is presented in this paper where ultrasonic scattering was considered in the long-wavelength approximation and the BERRYMAN'S [1] self-consistent method of estimating effective dynamic elastic constants was used to identify the factors which influence ultrasonic propagation properties of blood.

2. Theoretical preliminaries

In the mathematical development which follows, it has been assumed:

1. That the effective propagation properties of blood can be deduced, in the long-wavelength approximation, from the Navier–Stokes equation of motion for a homogeneous isotropic viscous liquid called the equivalent homogeneous liquid.

2. That the dynamic properties of the equivalent liquid can be characterized by the effective dynamic material parameters: the density ϱ^*, and viscosities η^* (the dynamic viscosity) and ξ^* (the "second viscosity").

According to the two-phase model, blood may be regarded as an isotropic suspension consisting of the plasma liquid with low viscosity, in which are dispersed inclusions in the form of oblate ellipsoids (red cells) with random orientation made of a liquid with high viscosity. Throughout the paper, the effective material parameters of the suspension (blood) as a whole are labelled by the asteriks. Similarly, all the abbreviations with the sub- or superscripts f and p denote quantities referred to the isotropic suspending and suspended material, respectively. Finally, the sub- or superscripts s denote quantities referred to an isotropic solid material.

Due to the presence of acoustic field in the blood there exists a displacement field, which can be expressed as

$$\mathbf{u}^* = \frac{1}{i\omega}\mathbf{v}_0^* e^{i\omega t}, \tag{2.1}$$

where ω is the angular ultrasonic frequency and $\mathbf{v}_0^*$ is a complex quantity.

Then the velocity $\mathbf{v}^*$ and the acoustic pressure, Δp^*, is given by

$$\mathbf{v}^* = \mathbf{v}_0^* e^{i\omega t}, \qquad \Delta p^* = \frac{i}{\omega} K^* \operatorname{div} \mathbf{v}^*, \tag{2.2}$$

where K^* is the effective bulk modulus (adiabatic compressibility). If the above relations are applied to the description of the ultrasonic wave propagation in blood being represented by the homogeneous equivalent liquid, the equation of motion for blood (Navier–Stokes equation) will then become

$$-\mathbf{v}^* = (k_l^*)^{-2} \operatorname{grad} \operatorname{div} \mathbf{v}^* + (k_t^*)^{-2} (\Delta \mathbf{v}^* - \operatorname{grad} \operatorname{div} \mathbf{v}^*), \tag{2.3}$$

where

$$(k_l^*)^2 = \frac{\omega^2 \varrho^*}{K^* + i\omega\varrho^* \left(\xi^* + \frac{4}{3}\eta^*\right)}, \qquad (k_t^*)^2 = \frac{\omega^2 \varrho^*}{i\omega\eta^*}. \tag{2.4}$$

The second viscosity ξ occurs as an effect of the internal degrees of freedom which are absent in the case under consideration. Thus, we put

$$\xi = 0. \tag{2.5}$$

At this point we turn our attention to the similarity of the equations of motion which describe the wave propagation in a homogeneous viscous Newtonian liquid (f, p) and isotropic solid (s). All these equations are subtantially identical in appearance, being obtained from Eqs. (2.1)–(2.4) after inserting $\xi = 0$ and replacing each of the asterisks by the superscripts f, p and s, respectively.

On taking into account the known relation

$$K^s = \lambda^s + \frac{2}{3}\mu^s \tag{2.6}$$

and after extending it formally to the phases $*$, f and p, Eqs. (2.4) arrive us at the following relations:

$$\lambda^j = K^j - \frac{2}{3}i\omega\eta^j, \qquad \mu^j = i\omega\eta^j, \qquad j = *, f, p, s, \tag{2.7}$$

where K^s, λ^s and μ^s are the bulk modulus (adiabatic compressibility) and Lamé constants, respectively, μ^s being the shear modulus.

The material parameters ϱ^*, K^* and μ^* determine the propagation properties of the suspension (blood) for the plane ultrasonic waves propagating and being polarized along the directions of the reference axes Ox_j, $j = 1, 2, 3$ of the macroscopic Cartesian coordinate system. In this case

$$v_{ij}^* = \frac{1}{Z^{*(a)}}, \qquad \alpha_{ij}^* = -\omega Z^{*(b)}, \tag{2.8}$$

$$Z^* = \left(\frac{\varrho^*}{\Gamma_{ij}^*}\right)^{1/2}, \tag{2.9}$$

where

$$\Gamma_{ij}^* = \Gamma_l^* = K^* + \frac{4}{3}\mu^* \qquad \text{for} \quad i = j, \tag{2.10}$$

$$\Gamma_{ij}^* = \Gamma_t^* = \mu^* \qquad \text{for} \quad i \neq j. \tag{2.11}$$

v_{ij}^* and α_{ij}^* denote the propagation velocity and amplitude attenuation coefficient, respectively, of the plane wave propagating in the direction of the axis Ox_i and being polarized in the direction of the axis Ox_j. Throughout the paper, the real and imaginary parts of complex quantities are denoted by the subscripts (a) and (b), respectively. Therefore, the problem considered in the paper consists in establishing the dependence of the quantities ϱ^*, K^* and μ^* on ϱ^f, K^f, μ^f, ϱ^p, K^p, μ^p, ω and some structure parameters. In other words, this problem consists in predicting the propagation parameters of the suspension on the base of knowledge of the dynamic properties of the suspension components and some parameters of its structure.

Evidently, if the hyphothesis of the possibility of finding the homogeneous equivalent medium is reasonable and the effective response of the medium is a plane attenuated wave with propagation parameters v_{ij}^* and α_{ij}^*, then

$$\Gamma_{ij}^{*(a)} = B(1-z^2), \qquad \Gamma_{ij}^{*(b)} = 2Bz, \tag{2.12}$$

$$B = (v_{ij}^*)^2 \varrho^* (1+z^2)^{-2}, \qquad z = \left(\frac{\alpha_{ij}^*}{\omega}\right) v_{ij}^*. \tag{2.13}$$

Formulae (2.12) and (2.13) enable the effective complex moduli Γ_{ij}^* of the suspension to be determined from the measurements of the macroscopic parameters of the ultrasonic wave propagation, v_{ij}^* and α_{ij}^*, in the medium under examination.

In contrast to the simplicity of the above macroscopic relationships, which suggest the experimental assessment of the structure and frequency dependences of the propagation and material parameters of two-phase media, theoretical attempts of finding these dependences always involve problems of great complexity. The dynamics of the multi-phase media with non-spherical inclusions is so complicated that, for a wide range of the volume concentrations c of the inclusions, we would be content with performing a computational analysis of the problem of the propagation of ultrasonic waves in such media. The computational investigations, some results of which are presented in the next section of this paper, enable us to establish the desired dependences. To perform such numerical analysis we make use of the self-consistent approach proposed by BERRYMAN [1]. It should perhaps be noticed here that in Ref. [1] the self-consistent approach is presented in a generalized form to be applicable also for materials with complex material parameters.

BERRYMAN [1] arrived at an algorithm for computational investigation of N-phase media with ellipsoidal inclusions, with all the phase materials being characterized, in general, by complex Hooke's (stiffness) tensors. Of course, N is a natural number. Adopting Berryman's concept to the two-phase media in the form of suspensions with ellipsoidal inclusions, will achieve the below given algorithm, which is employed in our computational analysis. The adopting is possible due to the above mentioned similarity of the equations of motion which describe the wave propagation in the homogeneous viscous Newtonian liquid (f,p) and any isotropic solid (s). As it was stressed, all these equations are subtantially identical in appearance.

The numerical results of these calculations are presented in the next section. For making clear the physical meaning of the numerical results, it seems to be reasonable to point out shortly the adopting of the BERRYMAN'S [1] concept to the two-phase suspensions under considerations. For this purpose, consider a sphere of the volume V occupied by the suspending fluid f in which are dispersed numerous ellipsoidal inclusions made of the liquid p with very high viscosity as compared with that of fluid f. The ellipsoids are assumed to be randomly oriented. The volume concentrations of the both phases are n_f and n_p, respectively. The sphere, in turn, is imbedded in a homogeneous liquid whose acoustic properties may be varied freely in a controlled manner. The imbedding liquid and the liquids n_f, and n_p are assumed to be immiscible in each other. If the elastic and propagation constants of the suspension are identical to those of the imbedding liquid,

there is no scattering from the composite sphere. Then we can say that the imbedding liquid is identical to the effective (homogeneous equivalent) liquid, say, the liquid of type $*$, which is to be determined. Now, continuing the thought experiment, replace the true composite sphere with a sphere composed of the matrix (suspending) liquid of type $*$ and of ellipsoidal inclusions of both type-f and type-p material in the same relative proportion as in the original suspension. Then, if the frequency is sufficiently small enabling the multiple scattering to be neglected to the lowest order of approximation, the equations for the effective material parameters ϱ^*, K^* and μ^* can be derived from the condition:

$$< u(\mathbf{x})_i^s >^* = 0. \tag{2.14}$$

$< u(\mathbf{x})_i^s >^*$ denotes the ensemble average of the of the displacement field fluctuation, $u(\mathbf{x})_i^s$, given by

$$u(\mathbf{x})_i^s = u(\mathbf{x})_i - u(\mathbf{x})_0^s. \tag{2.15}$$

$u(\mathbf{x})_i^s$ denotes displacement field scattered by a single scatterer, $u(\mathbf{x})_0^s$ denote the incident field. The left-hand side of Eq. (2.14) denotes the net scattered displacement field due to the scattering in the above described suspension with the self-consistently determined matrix liquid of type-$*$. Relation (2.14) states that the self-consistent effective medium is determined by requiring the net scattered, long-wavelength displacement field to vanish on the average. To calculate $u(\mathbf{x})_i$ in the single scattering approximation we must first perform the summation of the scattering effects over all the single scatterers which are present in the bulk sample of the composite. This summation and averaging lead to the following relations, enabling us to calculate numerically the effective material and propapagation parameters of the two-phase composite under study:

$$K^* = \frac{n_p K^p P^{*p} + n_f K^f P^{*f}}{n_p P^{*p} + n_f P^{*f}}, \tag{2.16}$$

$$\mu^* = \frac{n_p \mu^p Q^{*p} + n_f \mu^f Q^{*f}}{n_p Q^{*p} + n_f Q^{*f}}. \tag{2.17}$$

The formulae for P^* and Q^* are listed in the Appendix of [1]. These formulae are not rewritten here.

3. Numerical results

Numerical calculations were performed for frequencies $f = 4$, 8, 12 and 16 Mc/sec. The following values were taken for the material parameters of the emulsion under analysis:

$$\varrho^f = 1.021 \frac{\text{g}}{\text{cm}^3}, \qquad \varrho^p = 1.021 \frac{\text{g}}{\text{cm}^3}, \qquad n_p = 0.4, \tag{3.1}$$

$$K^f = \frac{1}{40.9} 10^{11} \text{ Pa}, \qquad K^p = \frac{1}{34.1} 10^{11} \text{ Pa}, \qquad \eta^f = 1.8\ 10^{-2} \text{ Poise}. \tag{3.2}$$

Some results of the numerical calculations are presented in Figs. 1–3. These results visualize how the propagation velocities and attenuation coefficients of the ultrasonic

dilatation and shear modes depend on the dynamic viscosity of the ellipsoidal inclusions and the frequency of an ultrasonic mode. The calculalations were carried out for oblate ($a = b > c$) spheroids under the assumption that the shape of each inclusion in the suspension under examination is to be characterized by the same value of the shape factor $Z = a/c = 3.2$, independently of the inclusion size and orientation. a, b and c denote the principal axes of a spheroid. The shape factor is here a measure of the oblateness of an oblate pore.

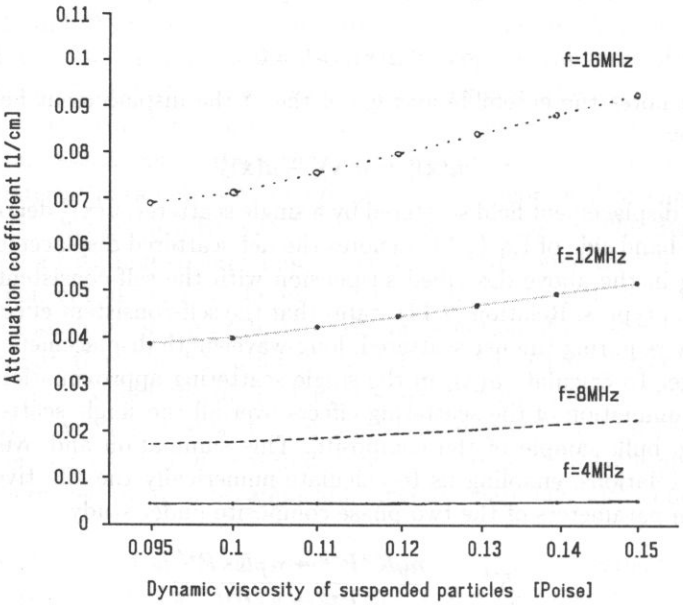

Fig. 1.

Figure 1 presents the dependency of the amplitude attenuation of the dilatation mode on the frequency and η^p. In Fig. 2, the propagation velocities of dilatation and shear modes are denoted by Cd and Cs, respectively. Similarly, in Fig. 3 the amplitude attenuation of dilatation and shear modes are denoted by ATs and ATd. The general tendency of the attenuation is to increase as frequency and η^p increase.

Although all the results presented above have been obtained under the assumption that the long-wavelength condition enables the single-scattering approximation to be used and that the non-spherical inclusions are randomly oriented in a macroscopic volume occupied by the suspension, it can be stated that the results show that the BERRYMAN'S [1] self-consistent method of estimating the effective dynamic elastic constants, if is applied to estimating the overall dynamical properties of the suspension, leads to rather strong dependence of the overall dynamic properties of the two-phase liquid on its composition, mechanical properties of the components as well as on the ultrasonic frequency.

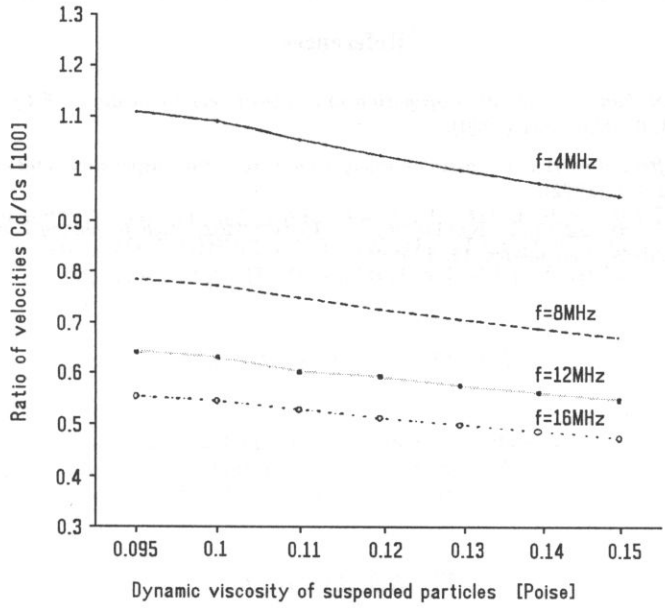
Ratio of velocities Cd/Cs [100]
1.3
1.2
1.1
1
0.9
0.8
0.7
0.6
0.5
0.4
0.3
f=4MHz
f=8MHz
f=12MHz
f=16MHz
0.095
0.1
0.11
0.12
0.13
0.14
0.15
Dynamic viscosity of suspended particles [Poise]

Fig. 2.

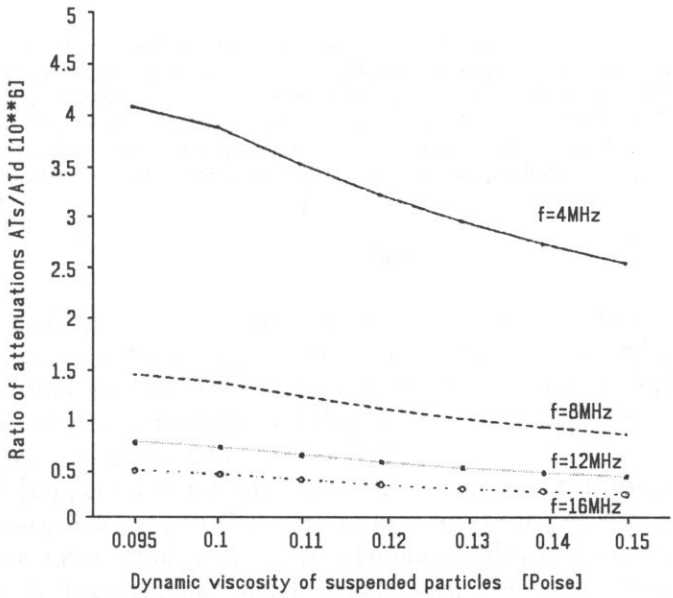
Ratio of attenuations ATs/ATd [10**6]
5
4.5
4
3.5
3
2.5
2
1.5
1
0.5
0
f=4MHz
f=8MHz
f=12MHz
f=16MHz
0.095
0.1
0.11
0.12
0.13
0.14
0.15
Dynamic viscosity of suspended particles [Poise]

Fig. 3.

References

[1] J.G. BERRYMAN, *Long-wavelength propagation in composite elastic media II. Ellipsoidal inclusions*, J. Soc. Am., **68**, 6, 1820–1831 (1980).

[2] A.S. AHUJA, *Effect of particle viscosity on ropagation of sound in suspensions and emulsions*, J. Soc. Am., **51**, 1, 182–191 (1972).

[3] A. NOWICKI, W. SECOMSKI, P. KARŁOWICZ, G. ŁYPACEWICZ, *High frequency Doppler ultrasound flowmeter*, Archives of Acoustics, **19**, 4 (1994).

ARCHIVES OF ACOUSTICS
23, 3, 411–428 (1998)

ABSORPTION OF ULTRASONIC WAVES IN AQUEOUS SOLUTIONS OF α-CYCLODEXTRIN WITH ALKYLPYRIDINIUM OR ALKYLTRIMETHYLAMMONIUM BROMIDES

A. BALCERZAK, R. PŁOWIEC

Institute of Fundamental Technological Research
Polish Academy of Sciences
(00-049 Warszawa, ul. Świętokrzyska 21)

A. JUSZKIEWICZ

Department of Chemistry
Jagiellonian University
(30-060 Kraków, ul. Ingardena 3)

Measurements of the absorption coefficient, α/f^2, of aqueous solutions of α-cyclodextrin with alkylpyridinium bromides $C_nH_{2n+1}C_5H_4NBr$ or alkyltrimethylammonium bromides $C_nH_{2n+1}N(CH_3)_3Br$ ($n = 8$, 10, 12), were carried out at 15, 25, 35 and 45°C in the concentration range 0.01 M to 0.04 M and frequency range 1 MHz to 150 MHz. The occurrence of two ultrasonic relaxation processes has been noted. The obtained results have been compared with data published previously for sodium alkyl sulfates.

1. Introduction

Different molecules or their moieties can penetrate a cavity of the cyclodextrin molecule forming an inclusion complex [1, 2]. This process is caused by driving forces of several kinds, among which the hydrophobic interaction plays an important role [2–6]. Many aqueous systems containing cyclodextrins and surfactants were investigated from the hydrophobic interaction point of view [7–25].

In a work [25] published formerly, the results of ultrasonic investigations of aqueous solutions of α-cyclodextrin (α-CD) with sodium alkyl sulfates were presented. In this work the presentation of ultrasonic investigations of other surfactants, alkylpyridinium and alkyltrimethyl-ammonium bromides is continued. The surfactants have anionic polar heads (in comparison to the cationic ones of sodium alkyl sulfates) of different dimensions.

The manner of making measurements and calculations is similar to that presented formerly [25].

2. Experimental part

Measurements of the absorption coefficient, α/f^2, in aqueous solutions of α-CD with alkylpyridinium bromides $C_nH_{2n+1}C_5H_4NBr$ or alkyltrimethylammonium bromides $C_nH_{2n+1}N(CH_3)_3Br$ (n = 8, 10, 12) were performed in the frequency range 1 MHz to 150 MHz at 15, 25, 35 and 45°C and at the concentration of 0.04 M of each of the components. At 25°C the measurements were also made for 0.01, 0.02 and 0.03 M equimolar solutions.

As previously the resonator and pulse methods were applied for the measurements [25].

The additional measurements of the speed of sound and the density for these solutions were also made. They are needed for further calculations [25]. The speed of sound was measured applying the resonator method [26–28]. The measurements of the density were performed by means of a MG-2 densimeter (Ecolab, Poland) which works on the principle of a U-shaped tube oscillator.

The parameters of the theoretical equations

$$\frac{\alpha}{f^2} = B + \sum_{i=1}^{l} \frac{A_i}{1 + (f/f_{ri})}, \tag{1}$$

$$\mu = 2\sum_{i=1}^{l} \mu_{mi} \frac{f/f_{ri}}{1 + (f/f_{ri})^2}, \tag{2}$$

were adjusted to the measured values of absorption by means of nonlinear regression. The adjusted parameters are: the relaxation frequency, f_{ri}, the relaxation amplitude, A_i, the contribution to the sound absorption from any other processes that may occur at higher frequencies beyond the frequency range measured, B, and the maximum of the excess absorption per wavelength, μ_{mi}. f is the measured frequency, α is the ultrasonic absorption, $\mu = (\alpha - Bf^2)\lambda$ is the excess absorption per wavelength λ ($\lambda = c/f$, c is the speed of sound), l is the number of relaxation processes (l = 1 or 2 in our case). The relation between A_i and μ_{mi} is as follows: $\mu_{mi} = f_{ri}A_i(c/2)$.

3. Results and discussion

The results of the measurements are presented in Tables 1–6.

Representative plots of the dependence of the excess sound absorption per wavelength, μ, on frequency, f, for several investigated systems are shown in Figs. 1–6.

The values of the parameters of Eqs. (1) and (2) are shown in Tables 7 and 8.

The occurrence of two relaxation processes for the surfactants with the decyl and dodecyl hydrocarbon chains should be noticed, while one relaxation process has been found for the octyl chain. This result is similar to that for aqueous systems of α-CD with the sodium alkyl sulfate [25]. The values of the B parameter are slightly greater then the absorption coefficient α/f^2 for pure water at corresponding temperatures. This can be caused by a greater viscosity of the liquid systems under test than that of water. This

Table 1. Ultrasound absorption, speed of sound and density for aqueous solutions of α-cyclodextrin with octylpyridinium bromide.

	temperature				concentration		
	15°C	25°C	35°C	45°C	0.01 M	0.02 M	0.03 M
	concentration 0.04 M				temperature 25°C		
f [MHz]	absorption α/f^2 [10^{-15} s^{2}m^{-1}]						
1.00	44.4	37.3	24.8	20.1	24.4	26.5	30.9
1.55	40.7	34.5	26.1	20.5	24.8	27.7	30.5
2.04	41.6	35.6	26.9	20.0	24.6	27.1	32.3
3.08	41.2	33.7	25.1	21.2	25.1	27.2	31.2
3.57	42.1	34.2	25.8	20.5	24.8	26.8	31.2
4.60	41.0	35.0	24.8	20.5	24.6	27.4	30.7
5.58	41.1	33.9	25.2	20.2	24.6	26.8	31.6
6.32	41.2	34.9	25.5	20.5	25.0	27.0	30.9
7.06	39.9	34.6	25.2	20.3	24.7	27.0	31.2
8.50	40.7	33.8	25.7	20.2	24.8	26.6	30.4
9.35	40.3	33.5	25.0	19.9	24.7	27.1	30.7
10.00	40.4	33.4	24.7	19.7	24.7	26.5	30.5
15.00	38.7	32.5	23.9	19.0	24.3	26.2	29.3
20.00	37.4	31.2	23.4	18.9	24.3	25.8	28.8
30.00	35.3	29.4	21.6	17.4	23.9	25.0	27.3
40.00	33.4	28.1	20.7	16.5	23.5	24.5	26.2
50.00	32.5	27.3	19.7	15.8	23.5	24.1	25.7
60.00	32.0	26.6	19.4	15.4	23.3	23.9	25.2
70.00	31.6	26.3	19.0	15.1	23.2	23.7	24.9
80.00	31.3	26.0	18.7	14.9	23.2	23.6	24.8
90.00	31.1	26.0	18.7	14.7	23.2	23.5	24.6
100.00	30.9	25.7	18.5	14.6	23.1	23.5	24.5
110.00	30.8	25.6	18.4	14.5	23.1	23.4	24.4
120.00	30.7	25.6	18.3	14.4	23.1	23.4	24.4
130.00	30.6	25.5	18.3	14.3	23.1	23.4	24.3
140.00	30.6	25.5	18.2	14.3	23.1	23.3	24.3
150.00	30.5	25.4	18.2	14.3	23.1	23.3	24.2
	speed of sound [m/s]						
	1481.3	1511.8	1531.8	1550.6	1500.5	1504.3	1508.0
	density [kg/m^3]						
	1010.0	1006.1	1002.3	998.2	999.3	1001.6	1003.9

Table 2. Ultrasound absorption, speed of sound and density for aqueous solutions of α-cyclodextrin with decylpyridinium bromide.

	temperature				concentration		
	15°C	25°C	35°C	45°C	0.01 M	0.02 M	0.03 M
	concentration 0.04 M				temperature 25°C		
f [MHz]	absorption α/f^2 [10^{-15} s^{2}m^{-1}]						
1.00	59.6	52.1	35.7	39.3	29.6	37.9	42.4
1.55	63.6	52.6	45.0	34.2	28.2	35.4	44.2
2.05	63.9	50.1	41.2	35.6	29.6	37.3	43.0
3.08	54.7	49.6	38.9	35.0	28.3	36.9	40.8
3.55	55.7	48.3	39.7	33.4	28.6	35.5	41.2
4.36	53.4	46.4	37.8	32.6	27.6	34.0	39.2
5.61	50.0	44.1	35.8	31.3	27.1	33.3	37.4
6.31	49.1	42.6	35.2	30.8	26.5	32.8	36.4
7.09	47.2	41.0	33.6	29.2	26.7	31.8	36.0
8.50	45.4	39.5	31.8	28.1	26.2	30.6	34.0
9.25	44.4	38.8	31.4	27.3	26.0	30.2	33.3
10.00	44.1	38.2	30.7	26.4	25.9	29.9	33.1
15.00	40.3	34.4	27.1	23.2	25.2	28.4	30.5
20.00	38.9	32.6	25.1	21.1	24.6	27.3	29.2
30.00	36.2	30.2	22.8	18.9	24.2	26.2	27.4
40.00	34.6	28.6	21.2	17.5	23.8	25.2	26.4
50.00	33.5	27.7	20.4	16.6	23.5	24.8	25.8
60.00	32.7	26.9	19.7	16.0	23.4	24.4	25.3
70.00	32.3	26.5	19.2	15.6	23.3	24.2	24.9
80.00	31.9	26.1	18.9	15.3	23.2	24.0	24.7
90.00	31.6	25.9	18.7	15.1	23.1	23.9	24.5
100.00	31.5	25.7	18.5	14.9	23.1	23.8	24.4
110.00	31.2	25.6	18.3	14.8	23.1	23.7	24.3
120.00	31.2	25.4	18.2	14.7	23.0	23.6	24.2
130.00	31.1	25.4	18.1	14.6	23.0	23.6	24.2
140.00	31.0	25.3	18.1	14.6	23.0	23.6	24.1
150.00	30.9	25.2	18.0	14.5	23.0	23.5	24.1
	speed of sound [m/s]						
	1481.4	1511.9	1532.0	1550.8	1500.6	1504.4	1508.2
	density [kg/m^3]						
	1011.3	1007.6	1003.5	999.4	999.8	1002.3	1004.9

Table 3. Ultrasound absorption, speed of sound and density for aqueous solutions of α-cyclodextrin with dodecylpyridinium bromide.

	temperature				concentration		
	15°C	25°C	35°C	45°C	0.01 M	0.02 M	0.03 M
	concentration 0.04 M				temperature 25°C		
f [MHz]	absorption α/f^2 [10^{-15} s^{2}m^{-1}]						
1.00	66.2	78.8	56.9	54.1	29.9	42.8	54.0
1.55	76.0	69.2	53.6	50.5	34.0	42.5	55.7
2.05	73.4	66.3	58.8	52.0	32.5	45.0	56.7
3.08	69.6	65.5	55.4	50.3	31.5	42.0	52.2
3.55	69.4	63.2	54.5	48.8	31.6	41.4	52.4
4.36	65.4	61.3	51.4	48.3	31.5	39.7	50.2
5.61	61.1	55.8	48.2	45.1	30.3	38.5	47.6
6.31	58.3	54.7	46.3	43.5	29.9	37.5	45.6
7.09	57.2	52.2	44.9	42.1	29.4	36.4	44.4
8.50	53.1	48.8	41.1	38.7	28.5	34.9	41.6
9.25	51.6	47.1	39.6	37.6	28.4	34.3	40.5
10.00	50.5	45.5	38.4	35.9	28.0	33.5	39.6
15.00	44.2	39.1	31.8	29.6	26.6	30.5	34.5
20.00	41.3	35.7	28.1	25.4	25.9	29.1	31.9
30.00	37.8	31.9	24.5	21.2	25.0	27.2	29.1
40.00	35.7	30.0	22.5	19.1	24.5	26.2	27.7
50.00	34.4	28.7	21.2	17.9	24.1	25.5	26.7
60.00	33.4	27.8	20.4	17.0	23.9	25.0	26.1
70.00	32.9	27.2	19.8	16.5	23.7	24.7	25.6
80.00	32.4	26.8	19.4	16.0	23.6	24.5	25.3
90.00	32.0	26.4	19.1	15.7	23.5	24.3	25.1
100.00	31.9	26.2	18.9	15.5	23.4	24.2	24.9
110.00	31.6	26.0	18.7	15.3	23.4	24.0	24.7
120.00	31.5	25.9	18.6	15.1	23.3	24.0	24.6
130.00	31.4	25.7	18.4	15.0	23.3	23.9	24.5
140.00	31.3	25.7	18.3	14.9	23.3	23.8	24.5
150.00	31.2	25.5	18.3	14.8	23.3	23.8	24.4
	speed of sound [m/s]						
	1482.2	1512.3	1532.4	1551.6	1500.6	1504.5	1508.4
	density [kg/m^3]						
	1013.4	1009.6	1005.3	1001.4	1000.2	1003.3	1006.5

Table 4. Ultrasound absorption, speed of sound and density for aqueous solutions of α-cyclodextrin with octyltrimethylammonium bromide.

	temperature				concentration		
	15°C	25°C	35°C	45°C	0.01 M	0.02 M	0.03 M
	concentration 0.04 M				temperature 25°C		
f [MHz]	absorption α/f^2 [10^{-15} s^{2}m^{-1}]						
1.00	40.7	32.1	26.3	22.1	23.6	26.5	30.5
1.55	40.9	33.5	24.8	19.8	25.0	27.0	31.4
2.04	41.8	34.3	24.0	20.4	24.8	28.1	31.2
3.08	40.0	33.5	24.3	20.6	24.8	27.1	31.0
3.57	42.5	33.5	24.8	20.3	24.5	26.8	30.8
4.60	40.5	33.0	24.9	20.3	24.8	26.9	30.8
5.58	42.0	33.5	23.9	20.3	24.9	26.8	31.4
6.32	40.7	33.0	24.5	19.7	24.8	27.2	30.6
7.06	40.9	33.0	24.8	20.2	24.6	26.8	30.3
8.50	40.4	32.7	24.6	20.3	24.6	26.7	30.3
9.35	40.2	32.9	24.1	20.0	24.6	26.6	30.2
10.00	39.9	32.4	23.9	19.9	24.6	26.9	29.9
15.00	38.9	31.5	23.2	19.3	24.2	26.0	29.3
20.00	37.1	30.4	22.4	18.6	24.3	25.6	28.5
30.00	35.0	28.6	20.9	17.4	23.8	24.8	27.2
40.00	33.4	27.1	19.8	16.4	23.6	24.2	26.2
50.00	32.4	26.4	19.1	15.8	23.4	23.9	25.5
60.00	31.7	25.8	18.5	15.2	23.2	23.7	25.2
70.00	31.4	25.3	18.3	15.0	23.2	23.5	24.9
80.00	31.0	25.1	17.9	14.7	23.1	23.4	24.6
90.00	30.8	25.0	17.8	14.5	23.1	23.3	24.5
100.00	30.7	24.8	17.7	14.4	23.0	23.3	24.4
110.00	30.5	24.7	17.5	14.3	23.0	23.2	24.3
120.00	30.4	24.6	17.5	14.3	23.0	23.2	24.3
130.00	30.4	24.5	17.4	14.1	23.0	23.2	24.2
140.00	30.3	24.5	17.3	14.1	23.0	23.1	24.2
150.00	30.2	24.4	17.3	14.1	23.0	23.1	24.1
	speed of sound [m/s]						
	1481.2	1511.7	1531.8	1531.6	1550.4	1504.3	1507.9
	density [kg/m^3]						
	1009.7	1005.8	1001.9	997.9	999.2	1001.4	1003.6

Table 5. Ultrasound absorption, speed of sound and density for aqueous solutions of α-cyclodextrin with decyltrimethylammonium bromide.

	temperature				concentration		
	15°C	25°C	35°C	45°C	0.01 M	0.02 M	0.03 M
	concentration 0.04 M				temperature 25°C		
f [MHz]	absorption α/f^2 [10^{-15} s^{2}m^{-1}]						
1.00	63.6	52.0	38.8	36.8	27.3	36.7	44.0
1.55	59.5	52.0	40.5	34.5	29.1	37.6	43.7
2.05	60.0	50.4	40.8	34.9	29.3	36.0	42.4
3.08	57.1	49.4	38.7	33.5	28.1	35.6	41.7
3.55	54.2	46.7	38.4	33.5	27.9	35.0	40.6
4.36	52.7	46.1	36.0	32.4	27.2	34.6	39.2
5.61	49.2	43.3	34.3	30.6	27.4	32.6	37.4
6.31	48.4	42.1	33.9	30.3	26.8	32.3	36.1
7.09	46.5	41.2	32.7	28.9	26.5	31.9	35.8
8.50	45.0	38.8	30.8	27.6	26.2	31.0	34.2
9.25	44.0	38.2	30.1	26.6	26.0	30.6	33.5
10.00	43.3	37.5	29.4	26.0	25.9	30.1	33.0
15.00	39.9	34.2	26.0	22.5	25.3	28.3	30.8
20.00	38.5	32.6	24.4	20.8	24.9	27.5	29.4
30.00	36.0	30.2	22.1	18.5	24.3	26.2	27.7
40.00	34.4	28.7	20.7	17.3	23.9	25.4	26.7
50.00	33.3	27.8	19.8	16.4	23.7	24.9	26.0
60.00	32.7	27.0	19.2	15.8	23.5	24.6	25.5
70.00	32.1	26.6	18.9	15.4	23.4	24.3	25.2
80.00	31.8	26.2	18.5	15.1	23.3	24.1	24.9
90.00	31.5	26.0	18.3	14.9	23.3	24.0	24.7
100.00	31.3	25.8	18.1	14.7	23.2	23.9	24.6
110.00	31.1	25.7	18.0	14.6	23.2	23.8	24.5
120.00	31.1	25.6	17.9	14.5	23.2	23.7	24.5
130.00	31.0	25.4	17.8	14.4	23.1	23.7	24.4
140.00	30.9	25.4	17.8	14.3	23.1	23.7	24.3
150.00	30.8	25.3	17.7	14.3	23.1	23.6	24.3
	speed of sound [m/s]						
	1481.2	1511.8	1532.0	1550.7	1500.5	1504.4	1508.1
	density [kg/m^3]						
	1011.1	1007.5	1003.3	999.2	999.7	1002.3	1004.9

Table 6. Ultrasound absorption, speed of sound and density for aqueous solutions of α-cyclodextrin with dodecyltrimethylammonium bromide.

	temperature				concentration		
	15°C	25°C	35°C	45°C	0.01 M	0.02 M	0.03 M
	concentration 0.04 M				temperature 25°C		
f [MHz]	absorption α/f^2 [10^{-15} s^{2}m^{-1}]						
1.00	73.8	71.6	60.6	52.4	33.6	41.5	59.4
1.55	77.8	65.7	60.4	50.4	35.0	45.0	55.8
2.05	76.3	66.6	57.7	53.6	35.1	43.7	56.1
3.08	70.4	64.7	55.2	50.4	33.7	43.6	53.0
3.55	68.8	62.3	55.2	48.5	33.4	42.0	52.0
4.36	64.9	59.4	52.6	47.0	32.6	40.5	49.0
5.61	60.8	54.6	48.3	43.0	31.1	38.5	46.1
6.31	58.0	53.5	46.8	42.5	30.8	37.8	44.7
7.09	55.8	50.8	44.7	40.3	30.2	36.3	42.7
8.50	52.4	47.2	41.1	37.3	29.3	34.5	40.3
9.25	50.6	46.0	40.0	35.5	28.8	33.9	39.0
10.00	49.8	44.5	38.2	34.4	28.4	33.3	38.0
15.00	44.2	38.2	31.9	27.8	26.9	30.3	33.8
20.00	41.3	35.1	28.3	24.1	26.0	28.7	31.6
30.00	38.1	31.6	24.6	20.6	25.1	27.1	29.2
40.00	36.1	29.9	22.6	18.7	24.5	26.1	27.8
50.00	34.9	28.6	21.4	17.4	24.1	25.4	26.9
60.00	34.0	27.8	20.6	16.8	23.9	25.1	26.3
70.00	33.4	27.2	20.1	16.2	23.7	24.7	25.8
80.00	33.0	26.8	19.6	15.8	23.6	24.5	25.5
90.00	32.7	26.4	19.3	15.5	23.5	24.4	25.3
100.00	32.4	26.2	19.1	15.3	23.4	24.3	25.1
110.00	32.2	26.0	18.9	15.1	23.3	24.1	25.0
120.00	32.1	25.9	18.7	15.0	23.3	24.0	24.8
130.00	31.9	25.7	18.6	14.9	23.2	24.0	24.8
140.00	31.8	25.6	18.5	14.8	23.2	23.9	24.7
150.00	31.8	25.6	18.4	14.7	23.2	23.9	24.6
	speed of sound [m/s]						
	1482.1	1512.3	1532.3	1551.5	1500.6	1504.5	1508.4
	density [kg/m^3]						
	1013.4	1009.5	1005.2	1001.3	1000.1	1003.3	1006.4

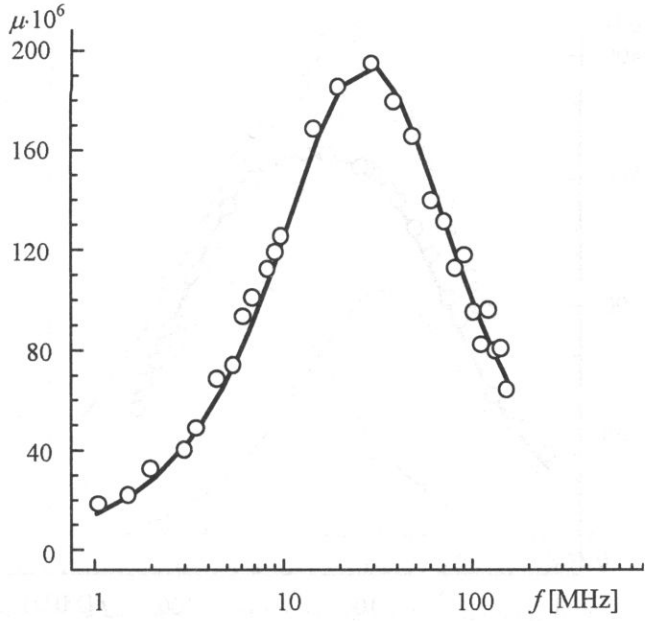

Fig. 1. Plot of the excess sound absorption per wavelength, μ, vs. frequency, f, for the aqueous solution of α-cyclodextrin and octylpyridinium bromide. Temperature: 25°C, concentration: 0.04 M.

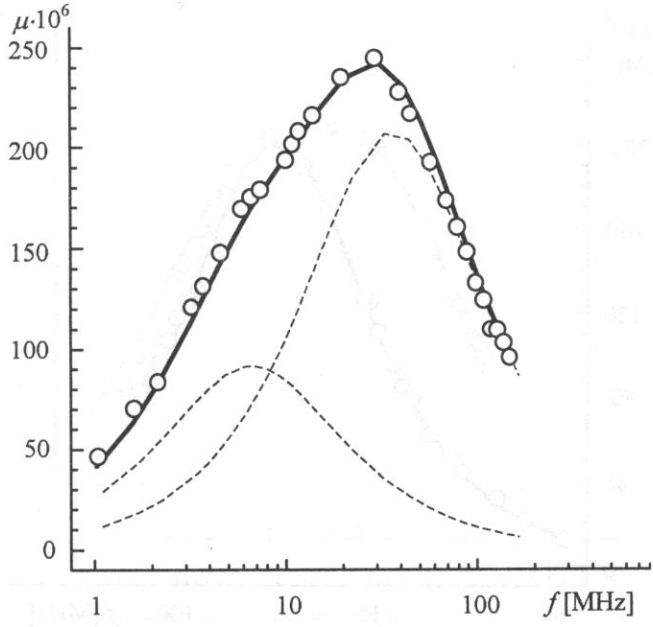

Fig. 2. Plot of the excess sound absorption per wavelength, μ, vs. frequency, f, for the aqueous solution of α-cyclodextrin and decylpyridinium bromide. Temperature: 25°C, concentration: 0.04 M.

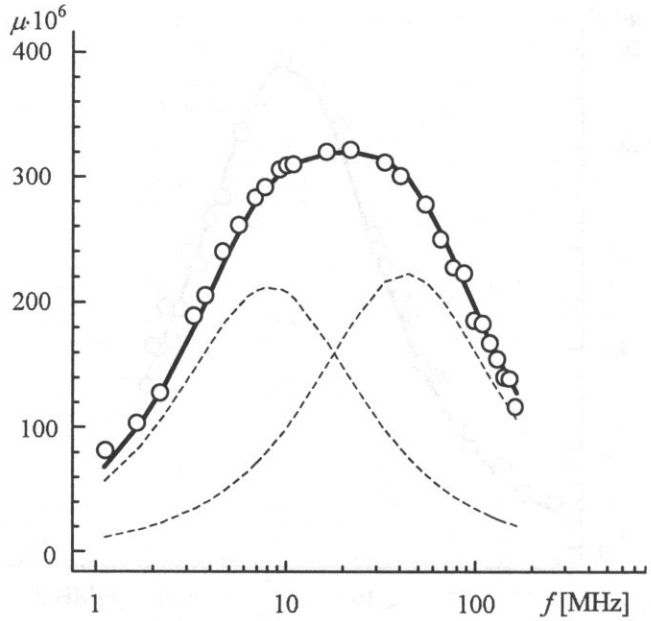

Fig. 3. Plot of the excess sound absorption per wavelength, μ, vs. frequency, f, for the aqueous solution of α-cyclodextrin and dodecylpyridinium bromide. Temperature: 25°C, concentration: 0.04 M.

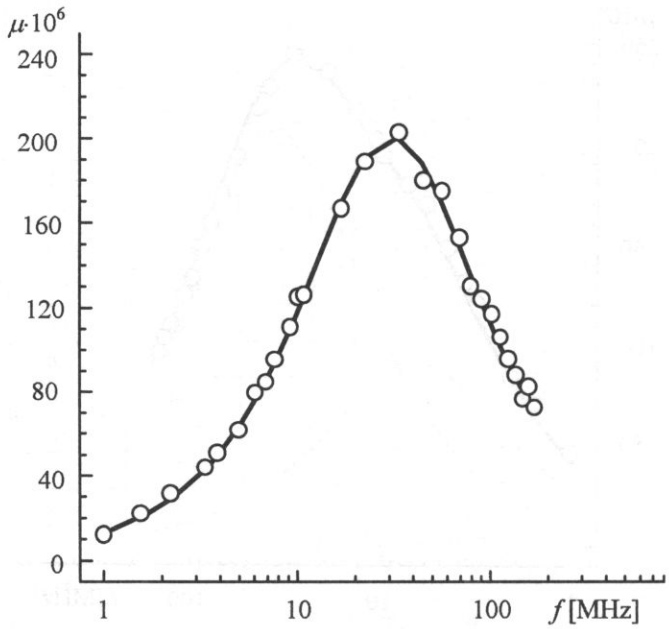

Fig. 4. Plot of the excess sound absorption per wavelength, μ, vs. frequency, f, for the aqueous solution of α-cyclodextrin and octyltrimethylammonium bromide. Temperature: 25°C, concentration: 0.04 M.

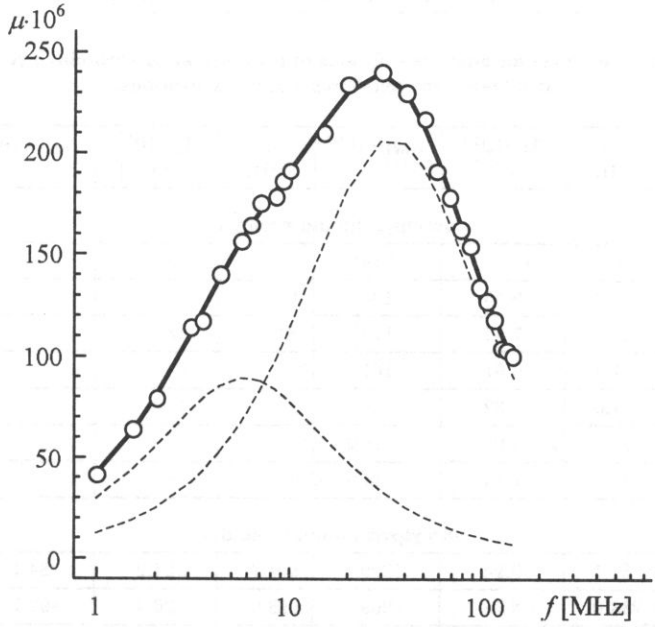

Fig. 5. Plot of the excess sound absorption per wavelength, μ, vs. frequency, f, for the aqueous solution of α-cyclodextrin and decyltrimethylammonium bromide. Temperature: 25°C, concentration: 0.04 M.

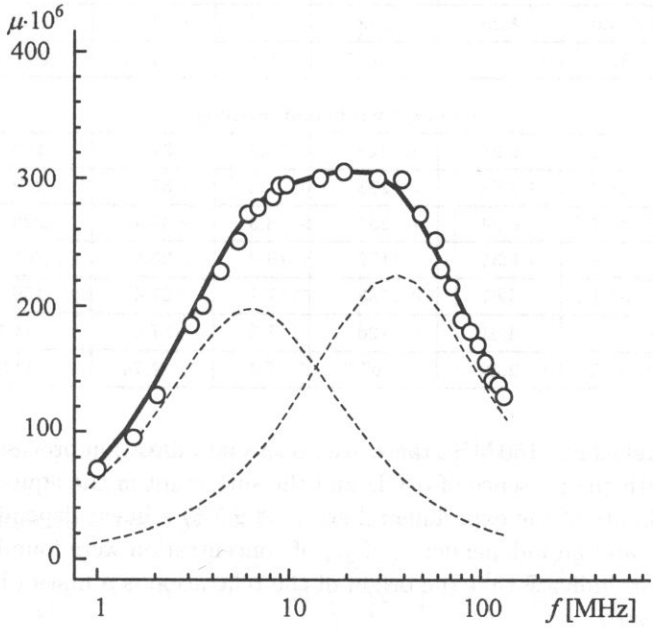

Fig. 6. Plot of the excess sound absorption per wavelength, μ, vs. frequency, f, for the aqueous solution of α-cyclodextrin and dodecyltrimethylammonium bromide. Temperature: 25°C, concentration: 0.04 M.

Table 7. Relaxation parameters for aqueous solutions of α-cyclodextrin with alkylpyridinium bromides at different temperatures and concentrations.

t [°C]	C [M]	f_{r1} [MHz]	$A_1 \cdot 10^{15}$ [s^2m^{-1}]	$\mu_{m1} \cdot 10^6$	f_{r2} [MHz]	$A_2 \cdot 10^{15}$ [s^2m^{-1}]	$\mu_{m2} \cdot 10^6$	$B \cdot 10^{15}$ [s^2m^{-1}]
octylpyridinium bromide								
15	0.04	25.7	11.5	219				30.2
25	0.04	27.0	9.55	195				25.1
35	0.04	28.9	7.82	173				17.9
45	0.04	31.4	6.61	161				14.0
25	0.03	27.0	7.32	149				24.0
25	0.02	26.8	4.03	81.2				23.2
25	0.01	27.9	1.84	38.6				23.0
decylpyridinium bromide								
15	0.04	31.1	9.94	229	4.7	24.2	84.1	30.5
25	0.04	33.0	8.38	209	6.0	20.4	92.7	24.8
35	0.04	35.3	7.06	191	7.6	17.5	102	17.6
45	0.04	37.2	5.72	165	8.8	16.3	111	14.1
25	0.03	32.8	5.66	140	6.0	15.2	68.9	23.8
25	0.02	34.0	4.26	109	5.9	10.7	47.4	23.3
25	0.01	32.6	1.95	47.7	5.8	4.62	20.1	22.9
dodecylpyridinium bromide								
15	0.04	36.2	9.28	249	6.5	37.4	180	30.6
25	0.04	38.4	7.68	223	7.4	37.9	212	25.0
35	0.04	40.7	6.54	204	8.3	35.4	225	17.7
45	0.04	42.8	5.33	177	10.0	33.6	261	14.3
25	0.03	38.1	5.67	163	7.7	27.4	159	24.0
25	0.02	37.1	4.51	126	7.3	17.0	93.4	23.5
25	0.01	37.3	2.40	67.2	7.4	7.74	43.0	23.1

fact indicates that above 150 MHz there are no special relaxation processes which could be connected with the presence of α-CD and the surfactant in the aqueous solution.

Within the limits of the experimental error ($\cong \pm 5\%$) a linear dependence of μ_{mi} on concentration C and an independence of f_{ri} of concentration were found.

These features indicate that the origin of the relaxation is a first-order or a pseudo-first-order processes

$$A_1 \underset{k_{21}}{\overset{k_{12}}{\rightleftarrows}} A_2\,, \tag{3}$$

where A_1 and A_2 denote two stages of the inclusion complex, k_{12} and k_{21} are the rate constants of the direct and opposite reactions, respectively.

Table 8. Relaxation parameters for aqueous solutions of α-cyclodextrin with alkyltrimethylammonium bromides at different temperatures and concentrations.

t [°C]	C [M]	f_{r1} [MHz]	$A_1 \cdot 10^{15}$ [s^2m^{-1}]	$\mu_{m1} \cdot 10^6$	f_{r2} [MHz]	$A_2 \cdot 10^{15}$ [s^2m^{-1}]	$\mu_{m2} \cdot 10^6$	$B \cdot 10^{15}$ [s^2m^{-1}]
octyltrimethylammonium bromide								
15	0.04	26.3	11.6	226				29.9
25	0.04	27.9	9.53	201				24.1
35	0.04	30.1	7.81	180				17.0
45	0.04	32.0	6.69	166				13.8
25	0.03	27.8	7.01	147				23.9
25	0.02	27.2	4.02	82.2				23.0
25	0.01	28.5	1.88	40.3				22.9
decyltrimethylammonium bromide								
15	0.04	31.8	9.43	222	4.6	24.2	82.4	30.4
25	0.04	34.0	8.09	208	5.9	20.0	89.4	24.9
35	0.04	35.7	6.47	177	7.3	17.5	98.0	17.3
45	0.04	38.4	5.51	164	8.6	16.3	109	13.9
25	0.03	32.8	5.86	145	5.7	15.2	65.3	24.0
25	0.02	34.4	4.29	111	6.1	9.89	45.4	23.4
25	0.01	33.0	2.07	51.2	5.7	4.23	18.1	23.0
dodecyltrimethylammonium bromide								
15	0.04	36.5	9.09	246	5.8	39.6	170	31.2
25	0.04	39.1	7.61	225	7.0	37.4	198	25.0
35	0.04	41.1	6.48	204	8.1	36.3	225	17.9
45	0.04	43.3	5.30	177	8.9	34.2	236	14.2
25	0.03	38.9	5.96	175	6.6	27.5	137	24.2
25	0.02	39.1	4.05	119	6.9	18.2	94.4	23.6
25	0.01	40.1	2.51	75.4	6.8	9.78	49.9	23.0

For this kind of relaxation processes, the following kinetic and thermodynamic formulas can be derived [29–31].

The relaxation frequency, f_r, can be expressed as

$$f_r = \frac{1}{2\pi} k_{21}(1+K) = \frac{kT}{2\pi h} \exp\left(\frac{\Delta S_{21}^{\neq}}{R}\right) \exp\left(\frac{-\Delta H_{21}^{\neq}}{RT}\right)(1+K), \tag{4}$$

where K is the equilibrium constant for reaction (3) ($K = k_{12}/k_{21}$), $\Delta S_{21}^{\neq}$ and $\Delta H_{21}^{\neq}$ are the activation entropy and activation enthaply for the opposite reaction, respectively. T is the absolute temperature. R, k and h are the gas, Boltzmann and Planck constants, respectively.

The function (4) is a linear one in the $\ln(f_r/T)$ and $(1/T)$ coordinates with the slope

$$a_f = -\frac{\Delta H_{21}^{\neq}}{R} - \frac{K}{1+K}\frac{\Delta H^0}{R} \tag{5}$$

and the intercept

$$b_f = \ln\left(\frac{k}{2\pi h}\right) + \frac{\Delta S_{21}^{\neq}}{R}, \tag{6}$$

when the relationship between the equilibrium constant K and the reaction enthalpy ΔH^0,

$$\frac{d\ln K}{d(1/T)} = -\frac{\Delta H^0}{R}, \tag{7}$$

is applied.

The maximum excess attenuation per wavelength, μ_m, is given by

$$\mu_m = \frac{\pi}{2\beta}\frac{\Delta V_S^2}{RT}\frac{K}{(1+K)^2}C, \tag{8}$$

where β is the adiabatic compressibility, ΔV_S is the isentropic change of volume which accompanies the transition from the state A_1 to the state A_2, C is the total molar concentration.

In the $\ln(\mu_m \beta T)$ and $(1/T)$ coordinates, the plot of equation (8) is a straight line with the slope

$$a_\mu = \frac{\Delta H^0}{R}\frac{K-1}{K+1} \tag{9}$$

and the intercept

$$b_\mu = \ln\left(\frac{\pi}{2}\frac{\Delta V_S^2}{R}C\right). \tag{10}$$

After combining equations (4), (5) and (9), one can get a formula from that K can be calculated:

$$\frac{f_r}{\frac{kT}{2\pi h}\exp\left(\frac{\Delta S_{21}^{\neq}}{R}\right)} = \exp\left[\frac{1}{T}\left(a_f + \frac{K}{K-1}a_\mu\right)\right](1+K), \tag{11}$$

where the values of a_f, a_μ and $\Delta S_{21}^{\neq}$ can be determined from the ultrasonic measurements.

From the mentioned formulas, the values of $\Delta S_{21}^{\neq}$, K, ΔH^0, $\Delta H_{21}^{\neq}$ and k_{21} can be calculated. Subsequently, the values of other kinetic and thermodynamic parameters can be established according to the formulas:

the rate constant of direct reaction

$$k_{12} = K k_{21}, \tag{12}$$

the free enthalpy of activation of the opposite reaction

$$\Delta G_{21}^{\neq} = \Delta H_{21}^{\neq} - T\Delta S_{21}^{\neq}, \tag{13}$$

the free enthalpy of the reaction (3)

$$\Delta G^0 = -RT \ln K, \tag{14}$$

the entropy of this reaction

$$\Delta S^0 = \frac{\Delta H^0 - \Delta G^0}{T}, \tag{15}$$

the enthalpy of activation of the direct reaction

$$\Delta H_{12}^{\neq} = \Delta H^0 + \Delta H_{21}^{\neq}, \tag{16}$$

the entropy of activation of this reaction

$$\Delta S_{12}^{\neq} = \Delta S^0 + \Delta S_{21}^{\neq}, \tag{17}$$

the free enthalpy of activation of the direct reaction

$$\Delta G_{12}^{\neq} = \Delta G^0 + \Delta G_{21}^{\neq}. \tag{18}$$

The modulus of the molar volume change, which accompanies reaction (3), can be calculated from a transformation of equation (8)

$$|\Delta V_S| = \left[\frac{2RT\beta}{\pi} \frac{(1+K)^2}{K} \frac{\mu_m}{C}\right]^{1/2}. \tag{19}$$

The thermodynamic and kinetic parameters of the high- and low-frequency processes are presented in Tables 9–12.

Table 9. Kinetic and thermodynamic parameters of the high-frequency relaxation process for aqueous solutions of α-cyclodextrin with alkylpyridinium bromides $C_nH_{2n+1}C_5H_5NBr$ at 25°C.

n	a_f [K^{-1}]	b_f	a_μ [K^{-1}]	b_μ	$(\mu_m/C)\cdot10^6$ [m^3/mole]	$K\cdot10^3$	ΔG^0 [kJ/mole]	ΔH^0 [kJ/mole]	ΔS^0 [J/(mole·K)]	$k_{12}\cdot10^{-5}$ [s^{-1}]
8	−309.1	12.46	901.4	−27.42	4.76	5.87	12.7	−7.58	−68.2	9.90
10	−256.5	12.48	922.3	−27.43	5.07	3.68	13.9	−7.73	−72.5	7.60
12	−211.3	12.48	951.6	−27.46	5.67	3.57	14.0	−7.97	−73.6	8.58

$\Delta G_{12}^{\neq}$ [kJ/mole]	$\Delta H_{12}^{\neq}$ [kJ/mole]	$\Delta S_{12}^{\neq}$ [J/(mole·K)]	$k_{21}\cdot10^{-8}$ [s^{-1}]	$\Delta G_{21}^{\neq}$ [kJ/mole]	$\Delta H_{21}^{\neq}$ [kJ/mole]	$\Delta S_{21}^{\neq}$ [J/(mole·K)]	$\lvert\Delta V_S\rvert$ [cm^3/mole]
38.8	−4.97	−147	1.69	26.1	2.61	−78.7	23.7
39.4	−5.59	−151	2.07	25.5	2.13	−78.5	30.8
39.2	−6.18	−152	2.40	25.2	1.79	−78.5	33.0

The high-frequency relaxation process in the liquid systems under test is connected with the exchange of water molecules in the hydratation shell of the α-CD molecule [32, 33], just as for the α-CD + sodium alkyl sulfate aqueous solutions [25]. This conclusion results from the similarity of the ultrasonic, kinetic and thermodynamic parameters of this relaxation process for systems with and without surfactants [34].

Table 10. Kinetic and thermodynamic parameters of the high-frequency relaxation process for aqueous solutions of α-cyclodextrin with alkyltrimethylammonium bromides $C_nH_{2n+1}(CH_3)_3NBr$ at 25°C.

n	a_f [K^{-1}]	b_f	a_μ [K^{-1}]	b_μ	$(\mu_m/C)\cdot10^6$ [m^3/mole]	$K\cdot10^3$	ΔG^0 [kJ/mole]	ΔH^0 [kJ/mole]	ΔS^0 [J/(mole·K)]	$k_{12}\cdot10^{-5}$ [s^{-1}]
8	−311.5	12.50	891.7	−27.35	4.83	5.56	12.9	−7.50	−68.3	9.69
10	−265.1	12.54	907.5	−27.41	5.13	4.40	13.5	−7.61	−70.6	9.36
12	−212.3	12.50	932.1	−27.39	5.80	3.00	14.4	−7.80	−74.4	7.35

$\Delta G_{12}^{\neq}$ [kJ/mole]	$\Delta H_{12}^{\neq}$ [kJ/mole]	$\Delta S_{12}^{\neq}$ [J/(mole·K)]	$k_{21}\cdot10^{-8}$ [s^{-1}]	$\Delta G_{21}^{\neq}$ [kJ/mole]	$\Delta H_{21}^{\neq}$ [kJ/mole]	$\Delta S_{21}^{\neq}$ [J/(mole·K)]	$\lvert\Delta V_S\rvert$ [cm^3/mole]
38.9	−4.87	−147	1.74	26.0	2.63	−78.3	24.6
38.9	−5.38	−149	2.13	25.5	2.24	−78.0	28.4
39.5	−6.01	−153	2.45	25.1	1.79	−78.3	36.4

Table 11. Kinetic and thermodynamic parameters of the low-frequency relaxation process for aqueous solutions of α-cyclodextrin with alkylpyridinium bromides $C_nH_{2n+1}C_5H_5NBr$ at 25°C.

n	a_f [K^{-1}]	b_f	a_μ [K^{-1}]	b_μ	$(\mu_m/C)\cdot10^6$ [m^3/mole]	K	ΔG^0 [kJ/mole]	ΔH^0 [kJ/mole]	ΔS^0 [J/(mole·K)]	$k_{12}\cdot10^{-7}$ [s^{-1}]
10	−1617	15.33	−924.7	−22.04	2.31	24.4	−7.92	−8.35	−1.43	3.62
12	−1004	13.49	−1136	−20.53	5.18	47.7	−9.58	−9.85	−0.90	4.55

$\Delta G_{12}^{\neq}$ [kJ/mole]	$\Delta H_{12}^{\neq}$ [kJ/mole]	$\Delta S_{12}^{\neq}$ [J/(mole·K)]	$k_{21}\cdot10^{-5}$ [s^{-1}]	$\Delta G_{21}^{\neq}$ [kJ/mole]	$\Delta H_{21}^{\neq}$ [kJ/mole]	$\Delta S_{21}^{\neq}$ [J/(mole·K)]	$\lvert\Delta V_S\rvert$ [cm^3/mole]
29.9	13.1	−56.2	14.8	37.8	21.5	−54.8	6.5
29.3	8.15	−71.0	9.55	38.9	18.0	−70.1	13.3

Table 12. Kinetic and thermodynamic parameters of the low-frequency relaxation process for aqueous solutions of α-cyclodextrin with alkyltrimethylammonium bromides $C_nH_{2n+1}(CH_3)_3NBr$ at 25°C.

n	a_f [K^{-1}]	b_f	a_μ [K^{-1}]	b_μ	$(\mu_m/C)\cdot10^6$ [m^3/mole]	K	ΔG^0 [kJ/mole]	ΔH^0 [kJ/mole]	ΔS^0 [J/(mole·K)]	$k_{12}\cdot10^{-7}$ [s^{-1}]
10	−1626	15.33	−913.7	−22.10	2.21	23.8	−7.86	−8.62	−1.36	3.56
12	−1022	13.47	−1096	−20.72	4.81	42.9	−9.32	−9.55	−0.77	4.30

$\Delta G_{12}^{\neq}$ [kJ/mole]	$\Delta H_{12}^{\neq}$ [kJ/mole]	$\Delta S_{12}^{\neq}$ [J/(mole·K)]	$k_{21}\cdot10^{-5}$ [s^{-1}]	$\Delta G_{21}^{\neq}$ [kJ/mole]	$\Delta H_{21}^{\neq}$ [kJ/mole]	$\Delta S_{21}^{\neq}$ [J/(mole·K)]	$\lvert\Delta V_S\rvert$ [cm^3/mole]
29.9	13.2	−56.1	15.0	37.8	21.4	−54.8	6.3
29.5	8.28	−71.0	10.0	38.8	17.8	−70.3	12.1

The origin of the low-frequency relaxation process is the penetration of the hydrophobic alkyl chain of the surfactant into the cavity of α-CD [26]. The rate constant k_{12} and the equilibrium constant K increase when the alkyl chain becomes longer (i.e. when n

increases). These facts reflect a deeper penetration of the longer (and more hydrophobic) hydrocarbon chain into the hydrophobic cavity of α-CD. For the short octyl chains (having rather weak hydrophobicity), this kind of penetration does not take place, thus there is no low-frequency relaxation process in the aqueous solutions of α-CD with octylpyridinium bromide or octyltrimethylammonium bromide. These conclusions are similar to those for sodium alkyl sulfates [26].

Taking into account the results for sodium alkyl sulfates, and presented in this work, for alkylpyridinium bromides and alkyltrimethylammonium bromides, one can notice that the occurrence of the low-frequency relaxation process does not depend on the structure of the polar head of the surfactant and on its electric character (cationic or anionic). This can be the evidence of a diminutive influence of interactions between the polar head of the surfactant with the α-CD molecule on above described penetration. Nevertheless, this influence exists since ultrasonic, kinetic and thermodynamic parameters have slightly different values for those three groups of the surfactants.

References

[1] M.L. BENDER and M. KOMIYAMA, *Cyclodextrin chemistry*, Springer-Verlag, Berlin 1978.

[2] J. SZEJTLI, *Cyclodextrins and their inclusion complexes*, Akademiai Kiado, Budapest 1982.

[3] M.KOMIYAMA and M.L. BENDER, J. Am. Chem. Soc., **100**, 2259 (1978).

[4] W. SAENGER, Angew. Chem., **19**, 344 (1980).

[5] W. SAENGER, *Inclusion compounds*, Vol. 2, Academic Press, London 1984.

[6] C. TANFORD, *The hydrophobic effect. Formation of micelles and biological membranes*, 2-nd ed., John Wiley and Sons, New York 1980.

[7] N. FUNASAKI, H. YODO and S. NEYA, Bull. Chem. Soc. Jpn., **65**, 1323 (1992).

[8] V.T. LIVERI, G. CAVALLARO, G. GIAMMONA, G. PITTARRESI, G. PUGLISI and C. VENTUNA, Thermochim. Acta, **199**, 125 (1992).

[9] D.J. JOBE, R.E. VERRAL, R. PALEPU and V.C. REINSBOROUGH, J. Phys. Chem., **92**, 3582 (1988).

[10] R. PALEPU and V.C. REINSBOROUGH, Can. J. Chem., **67**, 1550 (1989).

[11] R. PALEPU, J.E. RICHARDSON and V.C. REINSBOROUGH, Langmuir, **5**, 218 (1989).

[12] J.W. PARK and K.H. PARK, J. Inclusion Phenom. Mol. Recognit. Chem., **17**, 277 (1994).

[13] T. TOMINAGA, D. HACHITSU and M. KAMADO, Langmuir, **10**, 4676 (1994).

[14] E. JUNQUERA, J.G. BENITO, L. PENA and E. AIRCART, J. Colloid. Interface Sci., **163**, 355 (1994).

[15] E. JUNQUERA, G. TARDAJOS and E. AIRCART, Langmuir, **9**, 1213 (1993).

[16] D.J. JOBE, R.E. VERRAL, E. JUNQUERA and E. AIRCART, J. Phys. Chem., **98**, 10814 (1994).

[17] K.J. SASAKI, S.D. CHRISTIAN and E.E. TUCKER, J. Colloid. Interface Sci., **134**, 412 (1990).

[18] W.M.Z. WAN JUNUS, J. TAYLOR, D.M. BLOOR, D.G. HALL and E.J. WYN-JONES, J. Phys. Chem., **96**, 899 (1992).

[19] Y.-B. JIANG and X.-J. WANG, Appl. Spectrosc., **48**, 1428 (1994).

[20] U.R. DHARMAWARDANA, S.D. CHRISTIAN, E.E. TUCKER, R.W. TAYLOR and J.F. SCAMEHORN, Langmuir, **9**, 2258 (1993).

[21] D. JEZEQUEL, A. MAYAFFRE and P. LETELLIERA, Can. J. Chem., **69**, 1865 (1991).

[22] A. HERSEY, B.H. ROBINSON and H.C. KELLY, J. Chem. Soc. Faraday Trans., **182**, 1271 (1986).

[23] B.M. FUNG, W. GUO and S.D. CHRISTIAN, Langmuir, **8**, 446 (1992).

[24] E.S. AMAN, D. SERVE, J. Colloid. Interface Sci., **183**, 365 (1990).

[25] A. JUSZKIEWICZ and A. BALCERZAK, Archives of Acoustics, **21**, 431 (1996).

[26] F. EGGERS and T. FUNCK, Rev. Sci. Instrum., **44**, 969 (1973).

[27] F. EGGERS, T. FUNCK and K.H. RICHMANN, Rev. Sci. Instrum., **47**, 361 (1976).

[28] A. LABHARDT and G. SCHWARZ, Berichte der Bunsen-Gesellschaft, **80**, 83 (1976).

[29] J. LAMB, *Physical acoustics*, W.P. MASON [Ed.], Academic Press, New York 1965, Vol. II, Part A, Chapter 4.

[30] C.C. CHEN and S. PETRUCCI, J. Phys. Chem., **86**, 2601 (1982).

[31] L.J. RODRIGUEZ, E.M. EYRING and S. PETRUCCI, J. Phys. Chem., **93**, 6356 (1989).

[32] D.J. JOBE, R.E. VERRALL, E. JUNQUERA and E. AIRCART, J. Phys. Chem., **97**, 1243 (1993).

[33] S. KATO, H. NOMURA and Y. MIYARA, J. Phys. Chem., **89**, 5417 (1985).

[34] A. JUSZKIEWICZ and A. BALCERZAK, Archives of Acoustics, **18**, 447 (1993).

ARCHIVES OF ACOUSTICS
23, 3, 429–442 (1998)

MATHEMATICAL MODELLING OF AN ULTRASONIC FLOWMETER PRIMARY DEVICE

S. WALUŚ

Institute of Automatic Control,
Technical University of Silesia
(44-100 Gliwice, ul. Akademicka 16)

The role of the primary device of an ultrasonic flowmeter is described. The author proposed a classification of the ultrasonic flowmeter primary devices based on: 1) the principle of operation of the flowmeter sensor, 2) the method of obtaining information about the measured quantity from the flow phenomenon, 3) the kind of heads (inserted in the pipe wall and clamped-on), 4) the number of ultrasonic paths and their configurations. Mathematical models of flowmeter primary devices with a point velocity measurement are calculated (for laminar and turbulent flow). Also the model for an average velocity measurement over the surface of the ultrasonic transducer inserted in flow area is given. The next models are derived for a primary device with average velocity measurements over a single segment (most frequently in pipe diameter) or over a few segments (in the multi-path ultrasonic flowmeter primary device).

1. Introduction

Ultrasounds are of great importance in flow measurements. Flow-rate measurements are employed in industry, in water supply systems, as well as in medicine [1, 3, 6, 10, 15, 16, 18, 20]. They are used to determine the blood flow-rate in blood vessels by means of a Doppler ultrasonic flowmeter [7] and the flow-rate of water in large rivers by means of a transit-time ultrasonic flowmeter [10, 18, 19]. There are many kinds of ultrasonic flowmeters in which different constructions of the primary devices are used [11, 22, 27]. They are used in measurements of liquid flow-rates (in most cases) and also in measurements of gas flow-rates [1, 4].

The main purpose of the mathematical modelling of a flowmeter primary device [12, 17] is to describe the flow phenomenon under various conditions in order to reproduce a measuring value (measurand), and to estimate the total error for a real flowmeter under rated operating conditions [22]. The primary device of an ultrasonic flowmeter consists of a meter tube and heads (with probes and transducers) as shown in Fig. 2. The most commonly used devices for the ultrasonic transducers (emitters and receivers) are piezoelectric sensing elements (ultrasonic sensors). The greatest influence on the mathematical model of the flowmeter has the primary device because the measured quantity is converted in it into a signal that can be detected by a secondary device

(measuring transmitter). The modelling of the ultrasonic flowmeter primary device under conditions which differ from the rated operating ones is more difficult [22]. It is possible to choose a kind of an ultrasonic flowmeter for concrete conditions [21] on the ground of a mathematical model of the flowmeter primary device. The mathematical model enables us to use some flowmeters without experimental calibration [9, 22]. The greatest influence on the model of the flowmeter primary device has the velocity distribution shape, although the shape of the ultrasonic beam [16, 20] influences the primary device model. The modelling of the velocity distribution changes (with flow changes and changes of the conditions of the measurement) enables a correction of the systematic error [24]. The volume flow-rate is estimated in many cases in virtue of the velocity measurement at a defined place (or places) of the stream. In this case, a place (places) must be found in that the measured value is representative for the whole cross-sectional area of the conduit (pipe or open channel).

2. Importance of the primary device in the flow-rate measurement with an ultrasonic flowmeter

The flow phenomenon is a space-time one and the measurement can be usually treated as a static measurement in the presence of fluctuations of the measured quantity (measurand). The velocity vector in a turbulent flow shows fluctuations of about 30% of the average value; the flowmeter measures the average velocity on the grounds of many single measurements. The scheme of the flow-rate measurement is shown in Fig. 1.

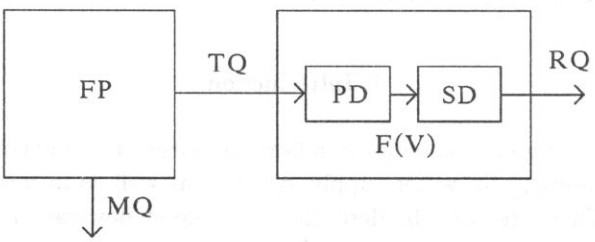

Fig. 1. Scheme of the flow-rate measurement: FP – flow phenomenon, PD – primary device, SD – secondary device (measuring transmitter), F(V) – flowmeter (velocitymeter), MQ – measured quantity (measurand), TQ – taken quantity, RQ – reproduced quantity (result of measurement).

The flow phenomenon induces the state of the fluid as well as the state of flow. The fluid can be transparent or nontransparent for ultrasonic beam, it can be homogenous or can contain gas bubbles (solid particles). This determines the kind of the ultrasonic flowmeter that has to be applied; transit-time ultrasonic flowmeters are used for clean liquids, the Doppler-type ultrasonic flowmeters are used for two-phase liquids [3, 6, 22]. The flow can be laminar, turbulent or of an intermediate regime.

Two main parts can be distinguished in the flowmeter [13]: a primary device and secondary one (measuring transmitter, transmitter [27], control unit [11]). Sometimes third part is distinguished: a data output unit; however, the last two parts are usually in a single device. A simplified diagram of ultrasonic flowmeter is shown in Fig. 2.

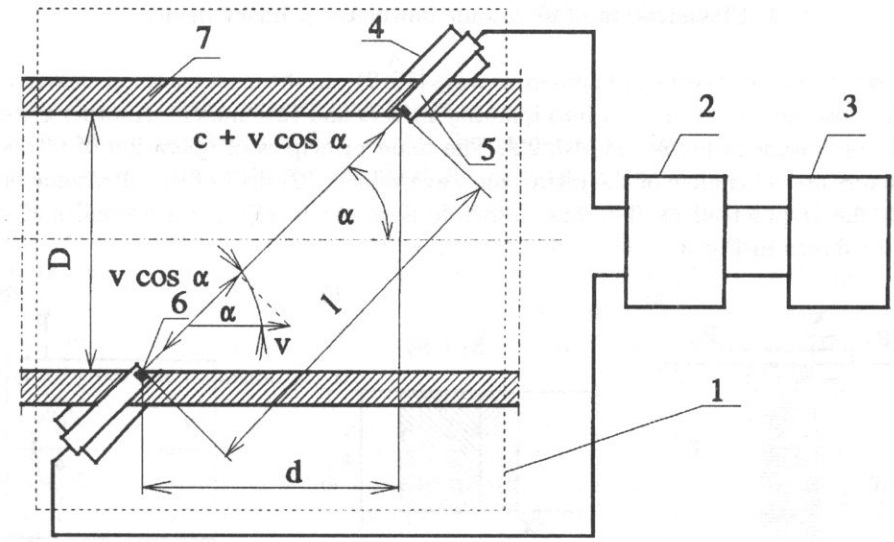

Fig. 2. Simplified diagram of the ultrasonic flowmeter: **1** – primary device, **2** – secondary device, **3** – output data unit, **4** – head, **5** – probe, **6** – ultrasonic transducer, **7** – meter tube, D – internal pipe diameter, l – distance between the centres of the ultrasonic wave emitting surfaces, d – projection of l on the pipe axis, α – angle between the ultrasonic beam direction l and the pipe axis, c – velocity of sound in the fluid at rest, v – velocity of the fluid.

The primary device takes a quantity (velocity, volume flow-rate) from some place of the flow. In the secondary device, the output value is calculated on virtue of the mathematical model of the flow phenomenon and the primary device construction. Modelling is a process of formulating a mathematical equation which gives an approximate description of the phenomenon in the measurement system [14].

The flowmeter is very often composed of many parts, and many factors must be taken into account: the nominal cross-sectional area of the conduit or the open channel, the methods and measuring procedures, the result of the measurement, the goal for which the results of the measurement are to be used, the measuring installation, influencing quantities, reference signals, standards and simulators.

The measured quantity (MQ in Fig. 1) can be the velocity v, the velocity profile $v(r)$, the velocity distribution $v(x, y)$, the volume flow-rate q_v or mass flow-rate q_m, the volume V or mass m. The taken quantity (TQ in Fig. 1) is sometimes only the representation of the measured one (for example, the velocity measured by means of two ultrasonic transducers at a given point of the cross-section (Fig. 5)), and is the basis for the calculation of the volume flow-rate. The reproduced quantity (RQ in Fig. 1) is calculated on the grounds of the taken quantity and of mathematical model of flow, as well as in virtue of the ultrasonic flowmeter primary device construction.

From the metrological point of view, the primary device is of greatest importance because it causes the main contribution to the total error of the results of the measurement [22]. Ultrasonic flowmeter transducers do not influence the measured quntity and do not disturb the flow phenomenon.

3. Classification of ultrasonic flowmeter primary devices

Flowmeters are classified in numerous ways [15, 21]; in the most common classification system, flowmeters are divided into quantity meters and rate meters. Another criterion is their operating principle [11, 16, 22]. The main principles of operation of ultrasonic flowmeters are: 1) change of the ultrasonic wave velocity, 2) drift of the ultrasonic beam, and 3) the Doppler effect. The first principle is shown in Fig. 2, the second and third ones are shown in Fig. 3.

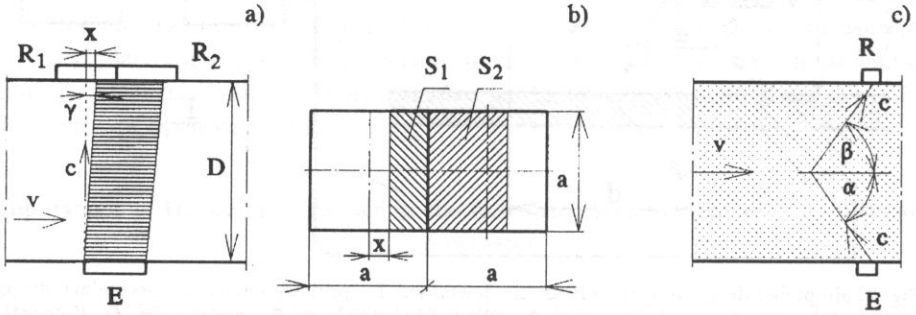

Fig. 3. Principles of the operation of the ultrasonic flowmeters: a) b) drift of the ultrasonic beam (beam deflection principle), c) Doppler effect, E – emitter (sender) of the ultrasound, R – receiver of the ultrasound, γ – angle between the drifted ultrasonic beam and the axis perpendicular to the pipe, x – drift of the incidence point of the ultrasonic beam, α – angle between the emitted ultrasonic beam and the pipe axis, β – angle between the received ultrasonic beam and the pipe axis.

For the ultrasonic flowmeters based on the first principle (change of the ultrasonic wave velocity) shown in Fig. 2, the downstream and upstream travel times are:

$$t_1 = \int_0^l \frac{dx}{c + v(x)\cos\alpha}, \tag{3.1}$$

$$t_2 = \int_0^l \frac{dx}{c - v(x)\cos\alpha}. \tag{3.2}$$

From (3.1) and (3.2), the average fluid velocity in the ultrasonic path (v_l) of velocity $v_l \ll c$ can be expressed by

$$v_l = \frac{c^2}{2l\cos\alpha}(t_2 - t_1) = \frac{c^2}{2l\cos\alpha}\Delta t, \tag{3.3}$$

where v_l is equal to the average velocity on the pipe diameter v_D,

$$v_l = v_D = \frac{1}{D}\int_0^D v(x)\,dx. \tag{3.4}$$

Volume flow-rate is the product of v_l, the velocity distribution shape coefficient K, and the cross-sectional area S:

$$q_v = S\,K\,v_l\,. \tag{3.5}$$

The velocity distribution shape coefficient K is defined as the ratio of v_S to v_D,

$$K = v_S/v_D\,, \tag{3.6}$$

where v_S is the average velocity over the pipe section.

In the sensor presented in Fig. 3 a, the beam deflection principle is used [2, 8, 14]. The sonic beam drift in the flowing fluid is a measure of the average velocity over the path of the ultrasonic beam. The emmiter sends a continuous ultrasonic wave; for a velocity of the liquid equal to zero, the amplitudes of the signals at the receivers R_1 and R_2 are the same. The signals from ultrasonic receivers go to the input of the differential amplifier and, for fluid velocity $v = 0$, the output signal is zero. For $v > 0$, the drift of the incidence ultrasonic beam will appear as shown in Fig. 3 a and the value of x can be calculated from the equation [2, 8]:

$$x = \sin\gamma D = \frac{v_D}{c} D. \tag{3.7}$$

When the pipe diameter is not large so that the ultrasonic beam is in the near field, the amplitudes of the received singnals can be calculated from the relations (see Fig. 3 a and Fig. 3 b):

$$A_1 = kS_1\,, \tag{3.8}$$

$$A_2 = kS_2\,, \tag{3.9}$$

where k is the factor of proportionality of the receiving ultrasonic transducer.

The sum of the surfaces S_1 and S_2, on which the ultrasonic beams falls, is equal to a^2

$$S_1 + S_2 = a^2. \tag{3.10}$$

The surfaces S_1 and S_2 can be calculated from

$$S_1 = a^2/2 - xa \tag{3.11}$$

and

$$S_2 = a^2/2 + xa. \tag{3.12}$$

From (3.8)–(3.12) we obtain

$$\Delta A = A_2 - A_1 = 2xak. \tag{3.13}$$

From (3.7) and (3.13) it follows that

$$v_D = \frac{c}{2akD}\Delta A. \tag{3.14}$$

The volume flow-rate can be calculated from (3.14) and (3.5) bacause $v_l = v_D$ (the ultrasonic beam is in the pipe axis).

The scheme of the principle of operation of a Doppler flowmeter primary device [2, 3, 15, 16] is given in Fig. 3 c. The frequency difference between the frequency of the received signal and that of the emitted one is equal to [16 p. 401]:

$$\Delta f = \left(\frac{c - v\cos\alpha}{c + v\cos\beta} - 1\right) f, \tag{3.15}$$

where f is the frequency of the emitted signal.

For $v \ll c$ and for $\beta = \alpha$ the fluid velocity can be calculated from:

$$v = \frac{c}{2f \cos \alpha} \Delta f. \tag{3.16}$$

In this paper, the author proposes a classification based on the method of taking information about measured value from the flow phenomenon; this classification is shown in Fig. 4 as an example of flow-rate measurements in open channels.

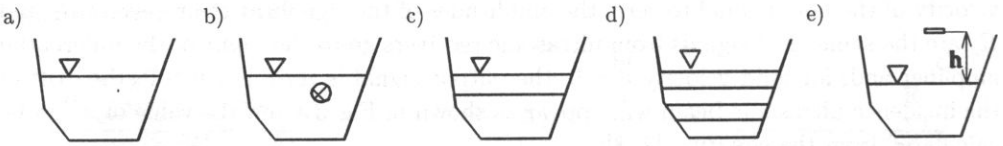

Fig. 4. Classification of flowmeter primary devices: a) the flow measurement is based on the point velocity measurement, b) the flow measurement is based on the average velocity measurement over some surface in the flow area, c) the flow measurement is based on the average velocity measurement along a segment in the flow area, d) the flow measurement is based on the average velocity measurements along some segments in the flow area, e) the flow measurement is based on the level measurement h and the model of the flow in the channel.

From the point of view of the measurement user (in automatic control or data processing), the operation principle and the construction of the flowmeter are less important, because the main metrological parameter is the measurement error, which depends mostly on the flowmeter sensor.

Ultrasonic flowmeter sensors with clamp-on heads are shown in Fig. 5.

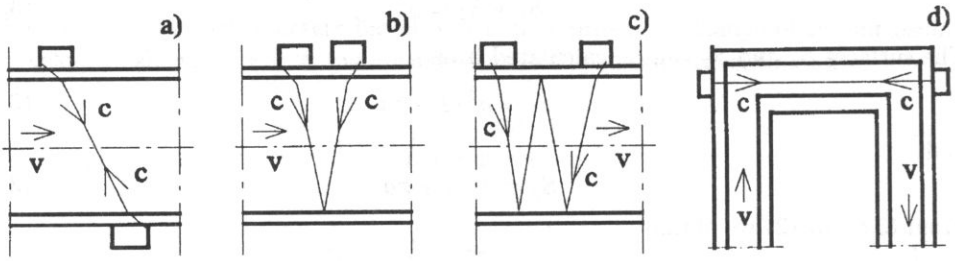

Fig. 5. Configurations of the ultrasonic flowmeter primary devices with clamp-on heads: a) with a single path in the pipe diameter, b) with a single path in the pipe diameter and a single reflection from the internal wall surface, c) with a single path in the pipe diameter and multiple internal reflections, d) with a path along the pipe axis.

4. A mathematical model of an ultrasonic flowmeter primary device with a point velocity measurement

The mathematical model of the primary device is based on the sensitivity factor which depends on the shape of the velocity distribution and on the construction of the primary device (the segment of the pipe, ultrasonic transducers and their layout). The point velocity is only a mathematical idea because each real sensor has some dimensions,

even a laser beam sensor. In every situation we must take into account the ratio of the sensor dimension to that which characterizes the flow phenomena. For example, in a large shallow river, an ultrasonic transducer with a diameter of a few centimetres can be accepted as a point velocity measurement device, but it could not be accepted for measurements in a pipe with a diameter 5 times greater than that of the ultrasonic transducer. The scheme of the primary device is shown in Fig. 6, but the diameters R_s of the ultrasonic emitter and receiver are negligible in comparison with the pipe radius R.

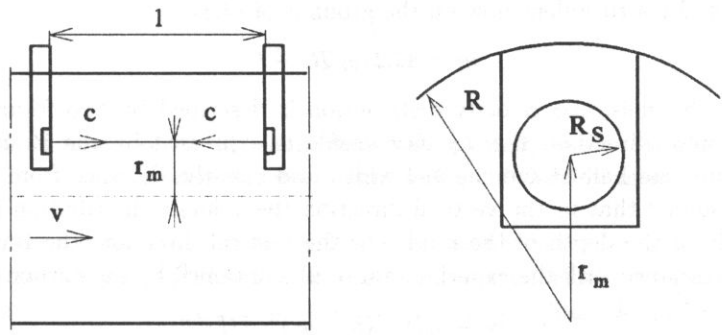

Fig. 6. Insertion meter: R_S – ultrasonic transducer radius, r_m – distance from the pipe axis.

In most practical cases, the goal of velocity measurements is to calculate the volume flow-rate in a conduit or in an open channel. There are two main solutions of this problem:

a) to measure the velocity at one point and calculate then the volume flow-rate on the grounds of the mathematical model of the primary device, or

b) to measure the velocities at many points of the flow area and obtaining the flow-rate by averaging single measurements or using some integration methods.

The first method needs a mathematical model of the velocity distribution in the conduit or in the open channel. The real velocity profiles are so different [5] that it is difficult to estimate the true value of the sensitivity factor.

The velocity distribution in laminar regime in a pipe with a circular cross-section is expressed by

$$v = v_0 \left[1 - (r/R)^2\right], \tag{4.1}$$

where: R – pipe radius, r – current radius, v_0 – velocity along the pipe axis.

For a turbulent flow, the Prandtl formula (power-low velocity profile) is most frequently used:

$$v = v_0(1 - r/R)^{1/n}, \tag{4.2}$$

where n depends on the Reynolds number and the roughness of the pipe wall.

MILLER [15] proposes that the value of n for smooth pipes can be calculated as a function of the Reynolds number,

$$n = 1.66 \log Re. \tag{4.3}$$

The author proposed [22] the following formula for the laminar ($m = 2$) and for the turbulent flow:

$$v = v_0 [1 - (r/R)^m] . \tag{4.4}$$

The last equation enables the description of the velocity distribution also for the intermediate regime (between a laminar and a turbulent flow). Assuming that the velocity distribution shape coefficients K, defined by (3.6) for the velocity distributions described by (4.2) and (4.3) and expressed by (6.2) and (6.3), are equal, it is possible to calculate the value of m for a turbulent flow on the grounds of (4.3):

$$m = 3.32 \log Re - 1. \tag{4.5}$$

For open channels, the velocity distribution is described by two formulae [5, 25]. In the horizontal direction, the velocity profile is expressed by the Prandtl formula (4.2); R means one half of the channel width and r is the distance from the channel axis. It is assumed that in the vertical direction the velocity distribution is the same, independently of the depth of the fluid. For the vertical direction, the Bazin formula, which is in acordance with the experimental results obtained by the author [22], is used:

$$v = v_0 - mH^{-2}(h - h_0)^2 (JH)^{0.5}, \tag{4.6}$$

where h – depth of the liquid, v_0 – maximum velocity for the depth h_0, H – liquid level, m – experimental coefficient which depends on the roughness of the channel, J – hydraulic gradient.

For these equations it is possible to calculate the sensitivity factor K_s as the ratio of the average velocity at the cross-section v_s to the measured velocity v_m:

$$K_s = v_s / v_m , \tag{4.7}$$

where v_m is the velocity for the radius r_m or, in an open channel, the velocity at a point of distance r_m from the channel axis and h_m from the liquid level.

For velocity distributions described by the Eqs. (4.1), (4.2) and (4.4) at a distance r_m from the pipe axis, the sensitivity factors will be as follows [22]:

$$K_s = \frac{0.5}{1 - (r_m/R)^2} , \tag{4.8}$$

$$K_s = \frac{2n^2}{(n+1)(2n+1)(1 - r_m/R)^{1/n}} , \tag{4.9}$$

$$K_s = \frac{m}{(m+2)[1 - (r_m/R)^m]} . \tag{4.10}$$

The mathematical model of the ultrasonic flowmeter primary device is a relation between the output value (time difference Δt) and the measured value (volume flow-rate q_v):

$$\Delta t = f(q_v). \tag{4.11}$$

The time difference for a sensor like that in Fig. 6, but for $R_s \ll R$, can be calculated from the following equation:

$$\Delta t = \frac{l}{c - v_m} - \frac{l}{c + v_m} . \tag{4.12}$$

For $v_m \ll c$,

$$\Delta t = \frac{2lv_m}{c^2}. \tag{4.13}$$

The measured value q_v is a product of the pipe cross-section and the average velocity v_S:

$$q_v = \frac{\pi D^2}{4} v_S. \tag{4.14}$$

From Eqs. (4.7), (4.13) and (4.14), the mathematical model of the primary device can be found,

$$\Delta t = \frac{8l}{\pi D^2 c^2 K_S} q_v. \tag{4.15}$$

5. Mathematical model of an ultrasonic flowmeter primary device for average velocity measurements over some surface of the flow area

In Fig. 6 the scheme of a flowmeter of the ultrasonic insertion type is shown. The output signal of this primary device depends on the average velocity on the surface of the ultrasonic transducer, and in virtue of this signal the total volume flow-rate is calculated.

For the velocity distribution described by the formula (3.1) (laminar flow), the measured average velocity can be calculated from

$$v_m = v_0 \left(1 - \frac{r_m^2}{R^2} - \frac{R_S^2}{2R^2}\right). \tag{5.1}$$

For a turbulent flow and the velocity distribution model (3.3) for $m = 6$,

$$v_m = v_0 \left(1 - \frac{r_m^6}{R^6} - \frac{9r_m^4 R_S^2}{2R^6} - \frac{3r_m^2 R_S^4}{R^6} - \frac{R_S^6}{4R^6}\right). \tag{5.2}$$

For a velocity distribution described by (4.4), the averaged velocity over the cross-sectional area is as follows:

$$v_S = v_0 \frac{m}{m+2}. \tag{5.3}$$

From (5.1) or (5.2), (4.14), (5.3) and (4.13) we obtain the model of the primary device. For example, for a laminar flow:

$$\Delta t = \frac{16l}{\pi D^2 c^2} \left(1 - \frac{r_m^2}{R^2} - \frac{R_s^2}{2R^2}\right) q_v. \tag{5.4}$$

6. Mathematical models of flowmeter primary devices for average velocity measurements over some segments of the flow area

In Fig. 7 typical primary devices of ultrasonic flowmeters are shown.

In the case of a time of flight ultrasonic flowmeter (which is most popular in practice [11, 27] and with primary devices like that shown in Fig. 7 a, the mathematical model of primary device is expressed from (3.3), (3.5) and (3.6) by the formula

$$\Delta t = \frac{8l \cos \alpha}{\pi D^2 c^2 K_S} q_v. \tag{6.1}$$

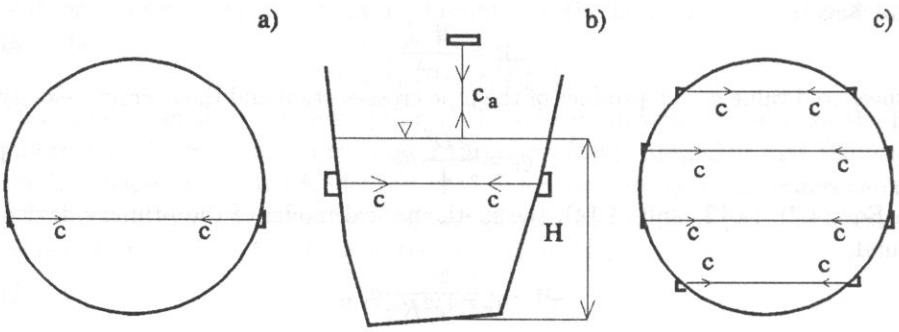

Fig. 7. Primary devices of ultrasonic flowmeters: a) one-path with heads mounted in the pipe wall, b) one-path for an open channel with level measurement, c) multi-path for a closed conduit, c_a – sound velocity in air being at rest.

When the ultrasonic beam is located at the pipe diameter, as in Fig. 2, the sensitivity factor value K_S is equal to that of the velocity distribution shape coefficient K. The value of K for a laminar flow is 0.75, and for a turbulent one we have, according to equations (4.2) and (4.4),

$$K = 2n/(2n+1), \tag{6.2}$$

$$K = (m+1)/(m+2). \tag{6.3}$$

On the grounds of the sensor model in secondary device, the measured value q_v is calculated. For example as shown in Fig. 7 b, the model of the primary device can be expressed in the following way:

$$\Delta t = \frac{2l\cos\alpha}{c^2 K_s(H) S(H)} q_v\,, \tag{6.4}$$

where $K_s(H)$ is the sensitivity factor, $S(H)$ is the flow area.

In [25] a one-path ultrasonic flowmeter was analysed. It is possible to decrease the measurement error in the multi-path primary device (which is recommended for a distorted velocity distribution). The mathematical model of the multi-path primary device is expressed by $N+1$ equations:

$$\Delta t_i = \frac{2l_i\cos\alpha_i}{c^2 K_{si} S_i} q_{vi}\,, \tag{6.5}$$

$$\sum_{i=1}^{N} q_{vi} = q_v\,, \tag{6.6}$$

where N is the number of ultrasonic paths (in Fig. 7 c $N = 4$), l_i is the length of the path i of the ultrasonic beam in the fluid, α_i is the angle between l_i and the pipe axis, K_{si} is the sensitivity factor in the part i of the cross-section, S_i is the surface of the part i of the cross-section, q_{vi} is the volume flow-rate through S_i.

In [11, 22, 27] recommendations for spacing of ultrasonic paths in the conduit with a circular section are given. Multi-path ultrasonic flowmeters are used in the case when

the velocity profile is distorted [13, 24] and the accuracy demands are high. There are two reasons for the primary device sensitivity changes:

1) velocity distribution shape coefficient changes with: a) Reynolds number changes accompanying the flow-rate and viscosity changes, b) roughness of the pipe wall changes;

2) velocity profiles distortion caused by disturbing flow elements before or behind the ultrasonic flowmeter primary device. In such situations multi-path primary devices shown in Fig. 8 are recommended.

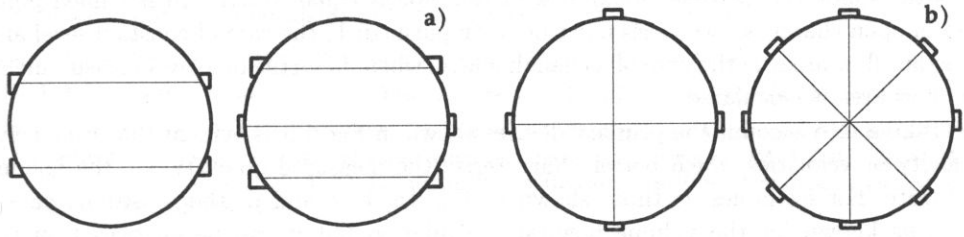

Fig. 8. Multi-path primary devices: a) with paraller paths, b) with crossed paths.

Reynolds number changes or wall roughness changes make the sensitivity of the primary devices shown in Fig. 8 b change as in the case of a one-path primary device. The primary devices presented in Fig. 8 b decrease the influence of the distorted flow profile, while those shown in Fig. 8 a decrease the sensitivity error in both situations.

For an ultrasonic flowmeter primary device with clamp-on heads (Fig. 5 a) [26], the model of the primary device is expressed as follows:

$$\Delta t = \frac{8l\cos\alpha}{\pi D^2 c^2 K} q_v + t_r \,, \tag{6.7}$$

where: l – length of the path of the ultrasonic beam in the fluid, t_r – time being the following sum:

$$t_r = \sum_{i=1}^{4} l_i / c_i \,. \tag{6.8}$$

Here l_i – paths of the ultrasonic beams in the pipe wall and in the heads, c_i – sound velocities in the pipe wall and in wedges of the heads.

7. Discussion of the results obtained

In the article, theoretical fundamentals of mathematical modelling of ultrasonic flowmeter primary devices are given. The classification of the principles of measurements used in ultrasonic flowmeters is commonly known. The mathematical descriptions of principles shown in Fig. 2 (change of the ultrasonic wave velocity) and in Fig. 3 c (Doppler effect) were taken from the literature. The author derived a simple model of the physical phenomena for the beam deflection principle (Fig. 3 a) on the grounds of equation (3.7) given in literature [2, 8] and made a sugestion concerning the construction of the primary device (Fig. 3 b). This model (Eq. (3.14)) combines the difference of the amplitudes of

the received electric signals with the average velocity over the pipe diameter. When the projection of the ultrasonic path on the cross-section of the pipe is on line with the pipe diameter, the velocity v_l is equal to v_D and the measured value can be calculated from (3.5) and (3.6). The methods of estimation of the velocity distribution shape coefficient K were given in [22].

The classification of the ultrasonic flowmeter primary devices proposed by the author in Fig. 4 covers all practical cases of pipes and open channels. In pipes (filled with gas or with liquid) the cross-sectional area of the pipe is equal to πR^2. In not filled pipes and in open channels, two cases must be distinguished: 1) the case of constant level and constant flow area, 2) the case of a changing level when, in virtue of a level measurement, the flow area is calculated.

Taking into account the primary devices shown in Fig. 4 it is evident that we receive velocity or velocities which better characterize the measured quantity, i.e. the volume flow-rate. For examples as those shown in Fig. 4a, b, c and d, the sensitivity factor must be known for the volume flow-rate calculation but it can be estimated on the grounds of the shape of the velocity distribution in the channel. The situation shown in Fig. 4e demands prior calibration in order to estimate the swelling curve, i.e. the function $q_v = f(h)$.

The classification of primary devices with clamp-on transducers shown in Fig. 5 is based on a review of the literature and on the author's papers (the first is mentioned in [26]). The author took part in the joint scientific work which resulted in models of ultrasonic flowmeters with primary devices introduced in Fig. 5a and 5b. The author worked out the primary device shown in Fig. 5d and the ultrasonic flowmeter with this primary device has worked in the student laboratory for several years.

The velocity distribution shape coefficient K defined by the equation (3.6) depends on the mathematical model of the velocity distribution (Eqs. (4.2) and (4.4) for turbulent flow), and the functions of K are given in (6.2) and (6.3). In literature many equations for n in the Prandtl formulae are reported (Eq. (4.3) is only an example) and the author derived the formulae for m in Eq. (4.4), i.e. Eq. (4.5).

8. Conclusions

1. The classification of the principles of measurements with ultrasonic flowmeters and the classification of the primary devices with clamp-on heads and with heads mounted in the pipe wall are presented.

2. An original equation for m (power in Eq. (4.4) for describing the velocity profile) is derived, and also an original model for primary device based on the beam deflection principle is presented.

3. For various (Fig. 2, 3, 4, 5) ways of taking a measured quantity, mathematical models are given; they enable the calculation of the relation between the volume flow-rate q_v and the quantity measured in the secondary device (Fig. 6, 7, 8).

4. The derived mathematical models enable the calculation of errors connected with the installation of the ultrasonic sensors in the primary device, with the fluid properties

and the flow conditions (Reynolds number which depends on the volume flow-rate and fluid viscosity).

References

[1] N. BIGNELL, A.F. COLLINGS, K.J. HEWS-TAYLOR, B.J. MARTIN, C.W. BRAATHEN, M. PETERSEN, C. WELSH, *An ultrasonic domestic gas meter*, Proceedings of the 6th International Conference on Flow Measurement FLOMEKO'93, Seoul 25-29 October 1993, S.D. PARK, F.C. KINGHORN, Korea Research Institute of Standards and Science, Taejon, 1993, pp. 403–409.

[2] K.W. BONFIG, *Technische Durchflussmessung*, Vulkan-Verlag, Essen 1977.

[3] P.J. DE CARLO, *Fundamentals of flow measurement*, ISA, Research Triangle Park, 1984.

[4] J.G. DRENTHEN, F.J.J. HUIJSMANS, Gassonic-400 & Q. *Sonic ultrasonic gas flow meters*, Proceedings of the 6th International Conference on Flow Measurement FLOMEKO'93 , Seoul 25-29 October 1993, S. D. Park, F. C. Kinghorn, Korea Research Institute of Standards and Science, Taejon 1993, pp. 285–298.

[5] R. GRYBOŚ, *Mechanika płynów z hydrauliką*, Politechnika Śląska, Skrypty Uczelniane, Nr 1901, Gliwice 1995.

[6] L. FILIPCZYŃSKI, R. HERCZYŃSKI, A. NOWICKI, T. POWAŁOWSKI, *Przepływy krwi. Hemodynamika i ultradźwiękowe dopplerowskie metody pomiarowe*, PWN, Warszawa – Poznań 1980.

[7] L. FILIPCZYŃSKI, *Ultradźwiękowe metody wizualizacji w medycynie*, Problemy Biocybernetyki i Inżynierii Biomedycznej, M. NAŁĘCZ [Ed.], Vol. 2. Biopomiary, L. FILIPCZYŃSKI, W. TORBICZ [Eds.], WKiŁ, Warszawa 1990, pp. 96–114.

[8] R.E. FISCHBACHER, *The ultrasonic flowmeter*, Transactions of the Society of Instrument. Technology, **11**, 2, pp. 114–119 (1959).

[9] S.G. FISCHER, P.G. SPINK, *Ultrasonics as a standard for volumetric flow measurement*, Modern developments in flow measurement, Peter Peregrinus, Harwell, 1972, pp. 139–159.

[10] ISO 6416: 1985, *Liquid flow measurement in open channels*, Measurement of discharge by the ultrasonic (acoustic) method, 1985.

[11] ISO/TR 12765: 1996 (E) *Measurement of fluid flow in closed conduits – Methods using transit time ultrasonic flowmeters*, 1996.

[12] J. JAWORSKI, *Pomiar jako identyfikacja parametryczna modelu matematycznego obiektu mierzonego*, Metrologia i Systemy Pomiarowe, Vol. II, 1, pp. 5–23 (1995).

[13] H. LECHNER, *Ultrasonic flow metering based on transit time differentials which are insensitive to flow profile*, J. Acoust. Soc. Am., **74**, 3, 955–959 (1983).

[14] R.S. MEDLOCK, *The techniques of flow measurement* (Part 2), Measurement and Control, **16**, 1, pp. 9–13.

[15] R.W. MILLER, *Flow measurement engineering handbook*, Mc Graw-Hill, Inc., 1989.

[16] J. OBRAZ, *Ultradźwięki w technice pomiarowej*, WNT, Warszawa 1983.

[17] J. PIOTROWSKI, *Theory of physical and technical measurement*, PWN, Elsevier, Warszawa 1992.

[18] K. RÓŻDŻYŃSKI, *Metody hydrometrii ultradźwiękowej*, Prace Instytutu Budownictwa Wodnego PAN, No. 14, PAN, Instytut Budownictwa Wodnego, Gdańsk 1984.

[19] D.PH. SCHMIDT, *Acoustic flow measurement in wide rivers, flow measurement of fluides*, Proceedings of FLOMEKO'1978, North-Holland Publ. Comp., Amsterdam, New York, Oxford, pp. 391–395.

[20] A. ŚLIWIŃSKI, *Ultradźwięki i ich zastosowanie*, Wydawnictwa Naukowo-Techniczne, Warszawa 1993.

[21] S. WALUŚ, *Pomiary wielkości nieelektrycznych*, Poradnik Inżyniera Elektryka (wydanie drugie częściowo zmienione), Vol. 1, WNT, Warszawa 1996, pp. 492–501.

[22] S. WALUŚ, *Ultradźwiękowe pomiary strumienia objętości wody w rurociągach i w kanałach otwartych*, Politechnika Śląska, Zeszyty Naukowe, No. 1075, Seria: Automatyka, z. 99, Gliwice 1990.

[23] S. WALUŚ, *Ultraschalldurchflußmessung bei gestörtem Strömungsprofil*, 36. Internationales Wissenschaftliches Kolloqium, 21-24.10.1991, TH Ilmenau, Germany, pp. 427–432.

[24] S. WALUŚ, *The mathematical modelling of the velocity distribution in closed conduits*, Proceedings of the 8th International Conference on Flow Measurement, FLOMEKO'96, October 20-24, 1996, Beijing, China, Edited by Zhang Baoyu, Han Lide, Zhao Xiaona, Standard Press of China, Beijing 1996, pp. 474–479.

[25] S. WALUŚ, *The mathematical model of one-path ultrasonic flowmeter for open channels*, Proceedings of the 11-th Triennial World Congress of the International Measurement Confederation, IMEKO XI, Houston, Texas, USA, 16-21 Oct. 1988, Vol. Metrology, pp. 301–307.

[26] S. WALUŚ, *The mathematical model of ultrasonic flowmeter with clamp-on transducers*, 30 Internationales Wissenschaftliches Kolloqium, 21-25 X 1985, Technische Hochschule Ilmenau, DDR. Heft 2, Vortragsreihe B, C, pp. 103–106.

[27] VDI/VDE 2642, *Ultraschall-Durchflußmessung von Fluiden in voll durchströmten Rohrleitungen*, 1994.

ARCHIVES OF ACOUSTICS
23, 3, 443–450 (1998)

THE INFLUENCE OF LIGHT ON FATIGUE IN PZT FILMS WITH PLANAR ELECTRODES

D. CZEKAJ, Z. SUROWIAK

University of Silesia,
Institute of Engineering Problems,
(41-200 Sosnowiec, ul. Śnieżna 2, Poland)

V.P. DUDKIEVICH, I.M. SEM and E.V. SVIRIDOV

Institute of Physics,
Department of Crystal Physics,
(SU-344101 Rostov-on-Don, Stachki Ave. 194, Russia)

Degradation properties, such as a low voltage breakdown, fatigue, and ageing of ferroelectrics are believed to be the major problems of ferroelectric films affecting their lifetime. Although these properties have been studied for a long time, the information is still insufficient for both a quality improvement of ferroelectric devices and their lifetime predictions. Degradation mechanisms should be studied for the lifetime prediction, as well as for material development.

Fatigue is the decrease in switchable polarization with increasing number of polarization reversals. In this paper, general features and the mechanisms of fatigue are briefly referred to and the light influence on fatigue in PZT films is discussed.

A set of fatigue measurements has been performed on RF-sputtered PZT films of about 2 μm in thickness. Polarization switching characteristics by applying sinusoidal a.c. electric fields were studied both with sandwich-type and planar electrodes. The planar structure has allowed for the study of the influence of the free charge carries induced by UV – illumination in the planar capacitor gap. The fatigue became noticeable after 10^6 switching cycles for a sandwich structure and after 10^9 those cycles for films with planar electrodes. The film illumination during the polarization switching accelerates significantly the fatigue process. The additional fatigue induced by the photoactive light was completely reversible.

Of special importance is the fact that the films on metal substrates (sandwich-capacitor) were fatigued more rapidly than those on dielectric substrates (planar capacitor), though they were prepared under the same conditions. This evidences the major contribution of transition layers to the development of the fatigue process that agrees well with the model of fatigue proposed in the literature.

1. Introduction

Due to the unique properties, such as a high value of dielectric permittivity ε, spontaneous polarization P_s, piezoelectric moduli d_{ij} and electromechanical coupling coefficient k_p, ferroelectric materials have gained widespread application in engineering. In parti-

cular, the perovskite-type ferroelectric thin films are very promising for application in microelectronics as high dielectric capacitors [1, 2], piezoelectric sensors [3, 4], electro-acoustic transducers [5], high frequency SAW devices [6, 7], ultrasonic sensors [8] and many others [e.g. 9–13]. It is common knowledge that the basic physical properties of those materials depend on the chemical constitution, atomic structure, domain structure and microstructure that, in turn, depend on technological conditions of the preparation process. However, their practical application depends on the degradation properties such as a low voltage breakdown, fatigue and ageing of ferroelectric that have been pointed out as major problems of ferroelectric films affecting their lifetime.

Fatigue is the decrease in the switchable polarization with the increasing number of polarization reversals. Several mechanisms for fatigue have been proposed for both the bulk and thin film ferroelectrics including dendrite formation of oxygen deficient filaments [14], domain pinning by defects [15, 16], space – charge accumulation at the film – electrode interface or domain boundaries under the repeated polarization switching, grain-boundaries compensating for the externally applied voltage, polarization screening by defects [17–20] and locking domains by electronic charge trapping centres (electron domain pinning) [18, 19]. There are far more approaches to the explanation of the fatigue phenomenon e.g. the formation of a-domain wedges and micro-cracks due to the piezoelectric deformation [21], the pinning of domains at grain boundaries triggered by the migration of pores [22]. A simple model for ferroelectric fatigue based on the Landau theory has been also developed [23–25]. The model suggests the formation of mesocopic domain/defect structures consisting of opposing domains stabilised by planes of charged defects.

Although the fatigue properties have been studied for a long time and they can be significantly diminished in PZT thin films by using appropriate electrode materials [16, 26–31], a fundamental understanding of the phenomenon is still lacking and the information is still insufficient for both a quality improvement of ferroelectric devices and their lifetime predictions. Therefore, degradation mechanisms should be studied for the lifetime prediction, as well as for the material development.

The influence of illumination on the polarization switching has been observed for a number of ferroelectrics with significant photosensitivity; it is known as the polarization switching or simply photoswitching [32]. An analysis of the published data [17–19, 21, 32, 33] shows that the nature of photoswitching in different ferroelectrics is basically the same: an increase in the density of free carriers by photogeneration of nonequilibrium carriers reduces the coercive field E_c and the switching time τ_s. The total number of the 180° domains participating in the polarization switching process increases and so does the mobility of the 180° domain walls.

It should be also noted that all of the known studies of the effect of fatigue of ferroelectric thin films were carried out on sandwich-type structures (conducting or covered with a conducting layer substrate – ferroelectric film – conducting upper electrode). In this case, the emphasis is laid, in our opinion, on the inhomogeneity of the object under study in the direction normal to its surface that makes it difficult to interpret the results.

In the present work the symmetrical planar electrodes were used to study the effect of the photoactive light on fatigue.

2. Samples and method of investigation

Polycrystalline $Pb(Zr_{0.53}Ti_{0.45}W_{0.01}Cd_{0.01})O_3$ films of about 2×10^{-6} m in thickness were obtained on the substrates made of stainless steel and dielectric radioceramics (Al_2O_3 with additives) [34, 35]. The measurements were performed using Al electrodes of a thickness of 0.3×10^{-6} m deposited by evaporation in vacuum (Fig. 1).

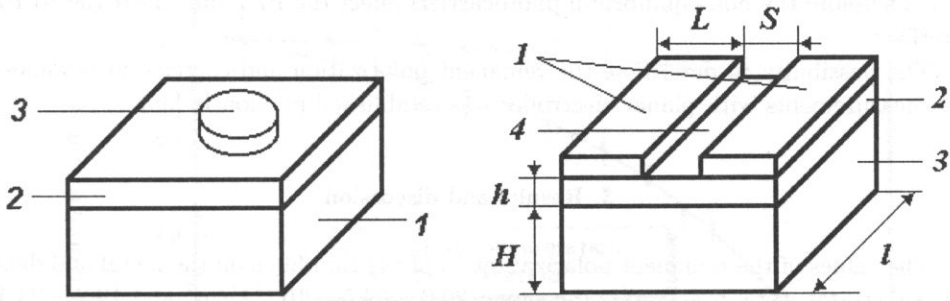

Fig. 1. a) The sandwich-type capacitor scheme: *1* – the stainless steel substrate of 100×10^{-6} m in thickness; *2* – the ferroelctric thin film; *3* – the disk-shaped Al electrode of 1.76×10^{-6} m^2 in area. b) The planar capacitor scheme: *1* – Al electrodes of 1×10^{-3} m in length (l) and 2×10^{-3} m in width (L); *2* – the thin ferroelectric film of 2×10^{-6} m in thickness (h); *3* – the Al_2O_3 polycrystalline substrate of 1×10^{-3} m in thickness (H); *4* – the dielectric gap of 8×10^{-6} m in thickness (S).

The dielectric hysteresis loops were recorded according to the Sawyer–Tower scheme "modified" by the application of an amplifier of small signals due to the small capacitance of planar capacitors $(1.5 - 5.0) \times 10^{-12}$ F.

To switch the polarization repeatedly the sinusoidal field of frequency ranging from 20 to 20×10^4 Hz was used. The relative error of the calculation $\Delta P_0/P_0$ was at 5%.

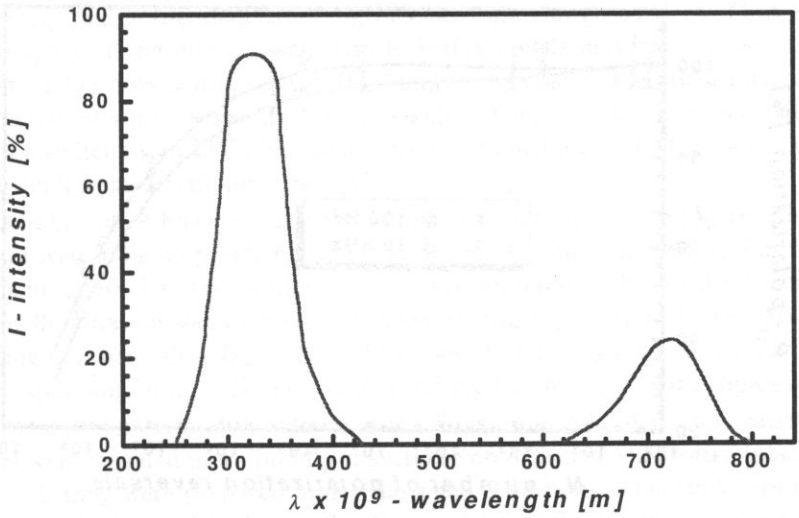

Fig. 2. The spectral characteristics of the filter used.

Since the band gap of the PZT materials is 3.6 eV [17], the quartz lamp and the filter that did not transmit the visible or almost all the infrared radiation ($\lambda = 250 - 420 \times 10^{-9}$ m; $E = 4.95 - 2.94$ eV) were used (Fig. 2) to induce non-equilibrium photocarriers to the conduction band in PZT films through the band-band transition [17]. According to the estimations of the absorption coefficient of the PZT films carried out for the wavelength of 325×10^{-9} m, the optical penetration depth is about 130×10^{-9} m [17]. Therefore the non-equilibrium photocarriers affect the PZT films near the Al-PZT interface.

The possibility to determine the remanent polarization and coercive field values in the measurements with planar electrodes was established previously [36].

3. Results and discussion

The values of the remanent polarization P_r of the thin films on the metal and dielectric substrates were, practically, the same ($20.0 - 24.5 \times 10^{-2}$ C/m^2 and $19.2 - 23.4 \times 10^{-2}$ C/m^2, respectively). However, the coercive field value E_c of the thin films deposited on the metal substrates was higher by c.a. an order of magnitude ($15 - 25 \times 10^6$ V/m and $3 - 5 \times 10^6$ V/m, respectively) than those of the thin films obtained on the dielectric substrates. Such a great difference in the E_c values seems to be due to the formation of a transition layer with pyrochlore structure on the boundary between the substrate and the thin film with the perovskite structure [37, 38].

Figure 3 shows the fatigue characteristics of the films on metal substrates (sandwich-type capacitors) at the frequencies of 10^2 Hz (down-triangles) and 10^4 Hz (circles). As can be seen, with increase of the frequency, the fatigue decreases as in the case of switching by bipolar rectangular pulses [15, 39–41] and triangular voltage pulses [31].

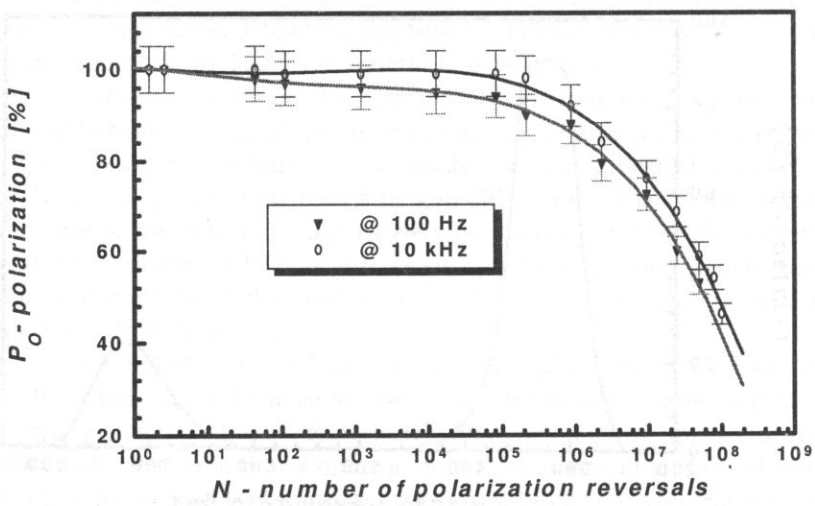

Fig. 3. The fatigue characteristics of the thin films deposited on the metal substrates at the frequencies of 10^2 Hz (triangles) and 10^4 Hz (circles). The field amplitude $E_a = 20 \times 10^6$ V/m.

Figure 4 shows the fatigue characteristics of the thin films grown on the dielectric substrates (planar capacitors) in the dark state (squares) and on continuous illumination with photoactive light (circles). Figure 5 represents the same curves for the higher frequency of the switching field. One can see that UV-illumination of the thin films accelerates the fatigue process.

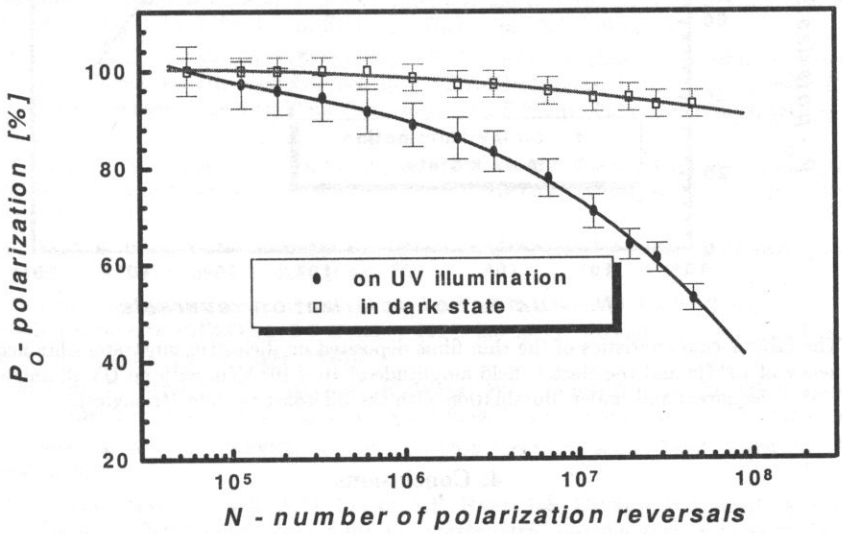

Fig. 4. The fatigue characteristics of the thin films deposited on dielectric substrates obtained at the frequency of 10^3 Hz and the electric field amplitude of 10×10^6 V/m with no UV-illumination (squares) and under illumination with the photoactive light (circles).

It has been argued by DIMOS *et al.* [19] that switchable polarization can be suppressed by generating and subsequent trapping of electronic charge carriers. That electronic charge trapping at the domain walls can lock those walls and lead to the suppression of the switchable polarization in the PZT films subjected to electrical fatigue [18, 19] what is consistent with our results. Similar results on suppressing the process of the 180° polarization switching by UV-illumination were obtained for $PbTiO_3$ single crystals [31] and other bulk ferroelectric materials [42].

It should be noted, however, that the "additional" fatigue induced by the photoactive light has proved to be, in practice, completely reversible. In other words, if in the course of a run similar to that the results of which are represented in Fig. 5 (the curve with stars), the illumination was stopped and the switching was continued after several cycles of switching n_o, then, after $D_n = 2.4 \times 10^6$ cycles of switching, the sample went into the state corresponding to $n_o + D_n$ cycles of switching for the curve with squares in Fig. 5.

Of special importance is the fact that the films on metal substrates (sandwich-type capacitor) were fatigued more rapidly than those on dielectric substrates (planar capacitor), though they were prepared under the same conditions. This evidences the major contribution of transition layers to the development of the fatigue process that agrees well with the model of fatigue proposed in [15, 16].

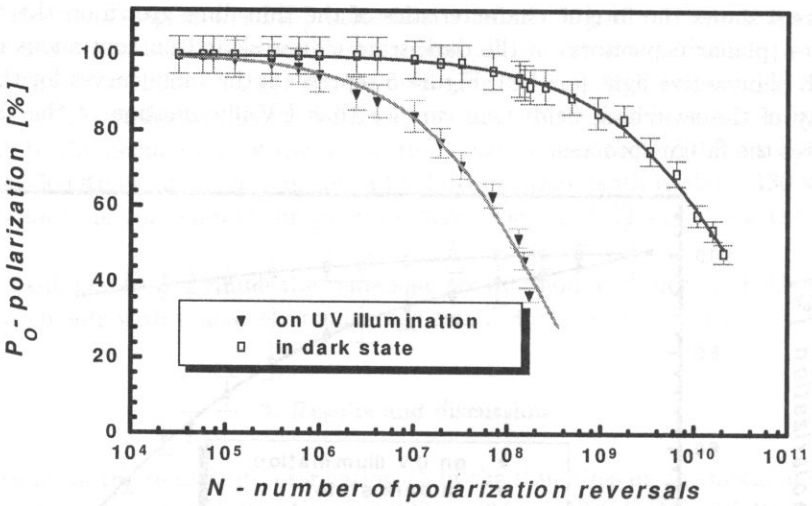

Fig. 5. The fatigue characteristics of the thin films deposited on dielectric substrates obtained at the frequency of 10^3 Hz and the electric field amplitude of 10×10^6 V/m with no UV-illumination (squares) and under illumination with the photoactive light (triangles).

4. Conclusions

In the present paper, the results of particular fatigue measurements performed on RF-sputtered PZT films of about 2×10^{-6} m in thickness are presented. Polarization switching characteristics obtained as a result of the application of sinusoidal a.c. electric fields were studied for both the sandwich-type thin film capacitors and the planar-type ones. The planar-type structure enables the study of the influence of the free charge carries induced by UV-illumination on the planar capacitor gap. It has been ascertained that (i) the fatigue of the thin PZT films became noticeable after 10^6 switching cycles for a sandwich-type structure and after 10^9 switching cycles for the thin film capacitors with planar electrodes, (ii) the film illumination during polarization switching accelerates significantly the fatigue process and (iii) the additional fatigue induced by the photoactive light was completely reversible.

Nevertheless, the authors realise that the results of the experiments presented in this paper are of tentative character: there is no experimental evidence available about the effect of the light intensity, temperature, field strength amplitude, etc. Therefore we can hardly make more general conclusions. However, even at this step of the investigations it is safe to say that the effect of fatigue is largely determined by the concentration of the free charge carriers as well as by the presence of transition layers.

5. Acknowledgements

The present work was supported by the State Committee for Scientific Research, Poland, within the framework of personal grant No 8 T11B 079 10.

References

[1] K. Okamoto, Y. Nasu, Y. Hamakawa, *Low-treshold-voltage thin-film electroluminescent devices*, IEEE Trans. Elec. Dev., **ED-28**, 6, pp. 698–702 (1981).

[2] R. Khamankar, J. Kim, B. Jiang, C. Sudhama, P. Maniar, R. Moazzami, R. Jones, J. Lee, *Impact of post processing damages on performance of high dielectric constant PLZT thin film capacitors for ULSI DRAM applications*, International Electron Devices Meeting, San Francisco, CA, December 11-14, 1994, IEDM Technical Digest, pp. 337–340 (1994).

[3] Z. Surowiak, D. Czekaj, A.A. Bakirov, V.P. Dudkevich, *Czujniki odkształceń dynamicznych na bazie cienkich warstw elektrycznych typu PZT*, Elektronika, **1**, pp. 12–19 (1994); Dynamical Deformation Sensors Based on Thin Ferroelectric PZT Films, Thin Solid Films, **256**, pp. 226–233 (1995).

[4] D. Czekaj, Z. Surowiak, A.A. Bakirov, V.P. Dudkevich, *Piezoelektryczne sensory odkształceń mechanicznych na bazie cienkich warstw* $LiNbO_3$ *i* $BaTiO_3$, Akustyka Molekularna i Kwantowa, **15**, pp. 43–57 (1994).

[5] N.F. Foster, *The deposition and piezoelectric characteristics of sputtered lithium niobate films*, J. Appl. Phys., **40**, 1, pp. 420–423 (1969).

[6] J. Dudek, *Piezoelectric acoustotransducers SAW on the basis of* $Pb(Zr,Ti)O_3$, The 8th Piezoelectric Conference PIEZO'94, 5-7 October 1994, Zakopane, Poland. Proceedings, Tele & Radio Research Institute, pp. 359–364 (1995).

[7] H. Adachi, T. Mitsuya, O. Yamazaki, K. Wasa, *Ferroelectric* $(Pb,La)(Zr,Ti)O_3$ *epitaxial thin films on sapphire grown by rf-magnetron sputtering*, J. Appl. Phys., **60**, pp. 736–741 (1986).

[8] Z. Surowiak, V.P. Dudkevich, *Cienkie warstwy ferroelektryczne*, Wyd. Uniw. Śl., Katowice, (1996) p. 331.

[9] K.R. Udayakumar, J. Chen, A.M. Flynn, S.F. Bart, L.S. Tavrov, D.J. Ehrlich, L.E. Cross, R.A. Brooks, *Ferroelectric thin films for piezoelectric micromotors*, Ferroelectrics, **160**, pp. 347–356 (1994).

[10] W.Y. Pan, S. Sun, B.A. Tuttle, *Electromechanical and dielectric instability induced by electric field cycling in ferroelectric ceramic actuators*, Smart Mater. Struct., **1**, pp. 286–293 (1992).

[11] D. Bondurant, F. Gnadinger, *Ferroelectrics for nonvolatile RAMs*, IEEE Spectrum, **7**, pp. 30–33 (1989).

[12] J.F. Scott, C.A. Paz de Araujo, *Ferroelectric memories*, Science, **246**, pp. 1400–1405 (1989).

[13] J.F. Scott, *Ferroelectric memories*, Physics World, **2**, pp. 46–50 (1995).

[14] H.M. Duiker, P.D. Bale, J.F. Scott, C.A. Paz de Araujo, B.M. Melnick, J.D. Cuchiaro, L.D. McMillan, *Fatigue and switching in ferroelectric memories: Theory and experiment*, J. Appl. Phys., **68**, pp. 5783 (1990).

[15] I.K. Yoo, S.B. Desu, *Mechanism of fatigue in ferroelectric thin films*, J. Phys. Stat. Sol. (a), **133**, pp. 565–573 (1992).

[16] S.B. Desu, I.K. Yoo, *Electrochemical models of failure in oxide perovskites*, Integrated Ferroelectrics, **3**, pp. 365–376 (1993).

[17] J. Lee, S. Esayan, A. Safari, R. Ramesh, *Fatigue and photoresponse of lead zirconate titanate thin film capacitors*, Integrated Ferroelectrics, **6**, pp. 289–300 (1995) and references cited therein.

[18] W.L. Warren, D. Dimos, B.A. Tuttle, R.D. Nashby, G.E. Pike, *Electronic domain pinning in* $Pb(Zr,Ti)O_3$ *thin films and its role in fatigue*, Appl. Phys. Lett., **65**, pp. 1018–1020 (1994).

[19] D. Dimos, W.L. Warren, B.A. Tuttle, *Photo-induced storage and imprinting in* $(Pb,La)(Zr,Ti)O_3$ *thin films*, In: Science and Technology of Electroceramic Thin Films, O. Auciello, R. Waser [Eds.], Kluwer Acad. Pub., Dordrecht (1995), pp. 291–300 and references quoted therein.

[20] Ch.K. Kwok, D.P. Vijay, S.B. Desu, N.R. Parikh, E.A. Hill, *Conducting oxide electrodes for ferroelectric films*, Integrated Ferroelectrics, **3**, pp. 121–130 (1993).

[21] E.G. Fesenko, V.G. Gavrilyatchenko, A.F. Sementchev, *Domain structure of multi-axis ferroelectric crystals* [in Russian], Rostov University Press, Rostov-on-Don, 1990, p. 185.

[22] S.A. MANSOUR, D.A. BINFORD, R.W. VEST, *The dependence of ferroelectric and fatigue behaviours of PZT films on annealing conditions*, Integrated Ferroelectrics, **1**, pp. 43–56 (1992).

[23] C. BRENNAN, *Model of ferroelectric fatigue due to defect/domain interactions*, Ferroelectrics, **150**, pp. 199–208 (1993).

[24] C. BRENNAN, R.D. PARELLA, D.E. LARSEN, *Temperature dependent fatigue rates in thin-film ferroelectric capacitors*, Ferroelectrics, **151**, pp. 33–38 (1994).

[25] C. BRENNAN, *Landau theory of thin ferroelectric films*, Integrated Ferroelectrics, **8**, pp. 335–346 (1995).

[26] J.M. BELL, P.C. KNIGHT, *Ferroelectric electrode interactions in* $BaTiO_3$ *and PZT thin films*, Integrated Ferroelectrics, **4**, pp. 325–332 (1994).

[27] S. MATSUBARA, S. MIYAZAKI, T. SAKUMA, Y. MIYASAKA, *Advances in ferroelectric thin film research at NEC and in Japan*, Mat. Res. Soc. Symp. Proc., **243**, pp. 281–290 (1992).

[28] T. NAKAMURA, Y. NAKAO, A. KAMISAWA, H. TAKASU, *Preparation of* $Pb(Zr,Ti)O_3$ *thin films on* Ir *and* IrO_2 *electrodes*, Jpn. J. Appl. Phys., **33**, pp. 5207–5210 (1994).

[29] T. NAKAMURA, Y. NAKAO, A. KAMISAWA, H. TAKASU, *Electrical properties of* $Pb(Zr,Ti)O_3$ *thin film capacitors on* Pt *and* Ir *electrodes*, Jpn. J. Appl. Phys., **34**, pp. 5184–5187 (1995).

[30] Y. NAKAO, T. NAKAMURA, A. KAMISAWA, H. TAKASU, N. SOYAMA, T. ATSUKI, K. OGI, *Study on* Pb*-based ferroelectric thin films prepared by sol-gel method for memory application*, Jpn. J. Appl. Phys., **33**, pp. 5265–5267 (1994).

[31] T. NAKAMURA, Y. NAKAO, A. KAMISAWA, H. TAKASU, *Preparation of* $Pb(Zr,Ti)O_3$ *thin films on electrodes including* IrO_2, Appl. Phys. Lett., **65**, 12. pp. 1522–1524 (1994).

[32] V.M. FRIDKIN, *Ferroelectric Semiconductiors*, Consultants Bureau, New York 1980.

[33] A.F. SEMENCHEV, V.G. GAVRILYACHENKO, E.G. FESENKO, *Influence of illumination on the process of* 180° *polarization switching in* $PbTiO_3$ *single crystals*, Phys. Solid State, **35**, 2, pp. 189–192 (1993).

[34] Z. SUROWIAK, D. CZEKAJ, A.M. MARGOLIN, E.G. SVIRIDOV, V.A. ALESHIN, V.P. DUDKEVICH, *The structure and the piezoelectric properties of thin* $Pb(Zr_{0.53}Ti_{0.45}W_{0.01}Cd_{0.01})O_3$ *solid films*, **214**, pp. 78–83 (1992).

[35] Z. SUROWIAK, D. CZEKAJ, V.P. DUDKEVICH, A.A. BAKIROV, I.M. SEM, E.V. SVIRIDOV, *Peculiarities of the switching process in polycrystalline thin ferroelectric films of PZT-type*, Thin Solid Films, **245**, pp. 157–163 (1994); *Osobliwości procesu przepolaryzowania w polikrystalicznych cienkich warstwach ferroelektrycznych typu PZT*, Kwartalnik Elektroniki i Telekomunikacji, **40**, 1, pp. 59–74 (1994).

[36] Z. SUROWIAK, D. CZEKAJ, J.S. NIKITIN, V.P. DUDKEVICH, *Badanie elektrycznych parametrów epitaksjalnych warstw ferroelektrycznych w układzie elektrod planarnych*, Elektronika, **9**, pp. 3–6 (1992).

[37] V.A. ALESHIN, E.V. SVIRIDOV, A.A. BAKIROV, A.M. MARGOLIN, I.A. ZAKHARCHENKO, I.M. SEM, V.P. DUDKEVICH, *The transition layer in polycrystalline PZT films*, Ferroelectrics, **128**, pp. 7–12 (1992).

[38] P.K. LARSEN, G.J.M. DORMANS, D.J. TAYLOR, P.J. VAN VELDHOVEN, *Ferroelectric properties and fatigue of* $PbZr_{0.51}Ti_{0.49}O_3$ *thin films of varying thickness: Blocking layer model*, J. Appl. Phys., **76**, 4, pp. 2405–2413 (1994).

[39] R.D. NASBY, J.R. SCHWANK, M.S. RODGARDS, S.L. MILLER, *Aspects of fatigue and rapid depolarization in thin film PZT capacitors*, Integrated Ferroelectrics, **2**, pp. 91–104 (1992).

[40] C.A. PAZ DE ARAUJO, L.D. MCMILLAN, B.M. MELNICK, J.D. CUCHIARO, J.F. SCOTT, *Ferroelectric memories*, Integrated Ferroelectrics, **104**, pp. 241–256 (1990).

[41] R. RAMESH, W.R. CHAN, B. WILKENS, T. SANDS, J.M. TARASCON, V.G. KERAMIDAS, *Fatigue and aging in ferroelectric* $PbZr_{0.2}Ti_{0.8}O_3/YBa_2Cu_3O_7$ *heterostructures*, Integrated Ferroelectrics, **1**, pp. 1–15 (1992).

[42] V.M. FRIDKIN, *Photoferroelectrics*, Springer, New York 1979.

ARCHIVES OF ACOUSTICS
23, 3, 451–456 (1998)

FREQUENCY CHARACTERISTIC OF THE ACOUSTIC EMISSION SIGNAL IN CONCRETE UNDER COMPRESSIVE LOADING

K. POGAN

(30-552 Kraków, 89 Wielicka Str., Poland)

Acoustic Emission measurements are very useful in the investigation of changes taking place in a composite during compressive tests. Among the AE intensity measurements (i.e. counts rate, root mean square, etc.) also the frequency analysis of the AE signal seems to be the useful method. In this paper the analysis of the AE signal characteristic for six different concrete compositions, also for those with silica fumes, is presented. Acoustic Emission signals were measured during quasi-axial compressive tests. The main aim of presented investigations was to demonstrate the spectral patterns of the AE waveforms generated by different concrete structures under compressive loading.

1. Introduction

Acoustic Emission signals are generated in materials as a result of local energy balance instabilities. External actions unsettle the primary state and cause energy radiation in the form of elastic waves called acoustic emission signals (AE). The acoustic emission phenomenon is very complex and depends many of internal and external factors, for instance, among other things: current stress level, load change speed, weighting history and also on the complex material's structure. Elastic waves generated by the source disperse inside or on the surface of the material and deflect are deflected many times. Those waves are received by a special sensor placed on the surface of the tested object. An electronic measurement apparatus makes it possible to observe the whole progress of acoustic emission signals versus time that are very similar in shape to those emitted directly by source. It is therefore vital to analyse the characteristic of these signals and especially their progress over a period of time [7]. The analysis of that progress in destructive tests has been the subject of several works by such authors as: J. HOŁA, A. MOCZKO, J. MIERZWA, K. POGAN and Z. RANACHOWSKI [3, 4, 6, 8, 10]. The obtained results show explicitly the dependence of the parameters of the Acoustic Emission on the concrete structure. It is of essential importance as well for theory as for practical purpose because a quantitative evaluation of the destructive changes appearing at different stress levels can be done using the Acoustic Emission signal parameters. A characteristic recognition of signals generated by the concrete under mechanic actions allows to locate the emission source and, furthermore, to estimate the destruction results, i.e. qualitative description of the progress of the destructive process. The frequency

spectrum characteristic of the Acoustic Emission signals would be also a criterion which allows to find the weakest link in the concrete microstructure and structure. BERTHELOT *et al.* [1] apply the frequency analysis of the AE signals related to the fracture mechanism induced during 3-point flexural tests.

This is the origin of research carried on by the author. From the wide investigation program, partly financed by the Polish Scientific Research Committee – Research Project No 7 TO7B 020 08 and referred to the analysis of the frequency characteristic of AE signals in different concrete structures submitted to compressive tests is presented.

Results of the Acoustic Emission signals frequency spectrum analysis in concrete under compressive loading have been presented so far in Poland. In 1996 some papers were published by A. JAROSZEWSKA, J. RANACHOWSKI and F. REJMUND [5] as well as by Z. RANACHOWSKI [9] but they referred to cement pastes and mortars. Those papers were the basis for the following analysis.

2. Experimental

For better a differentiation of the investigated concrete structures, three water-cement ratios (w/c = 0.60; 0.45 and 0.30 respectively) and two types of aggregate were selected, for the series 1, 3 and 5 – crushed aggregate and for the remaining ones (series 2, 4 and 6) – a natural aggregate. Concrete mixes number 3, 4, 5 and 6 were prepared by addition of the superplasticizer FM-6. To strengthen compositions number 5 and 6 micro-filler, silica fumes "Silimic" from Łaziska Ferro-Alloy Works, were added. It should be stressed that silica fume is a by-product of the reduction of high-purity quartz with coal in electric arc furnaces during manufacture of silicon and ferrosilicon alloys. The whole compositions were based on the Portland Cement "Małogoszcz" 45 N. The mix compositions were estimated by the iteration method and are shown in Table 1. Table 2 shows physical properties of the investigated concrete compositions.

Table 1. Concrete mix compositions.

No	W/C coefficient	Ingredents [kg/m^3]					
		Cement	Superplasticizer	Silica fumes	Water	Sand	Gravel
1	0.60	297	–	–	178	676	1248
2	0.60	288	–	–	174	440	1502
3	0.45	333	6	–	147	695	1281
4	0.45	359	7	–	162	433	1480
5	0.30	598	12	60	180	584	1078
6	0.30	645	13	64	194	359	1226

The specimens were 100 mm sided cubes. The hardening lasted for 28 days at the temperature of 18°C and at the relative humidity of 95%.

The hydraulic compressive machine EDU 400 "Fritz Heckert - Leipzig" was used to load the specimens. The surfaces of the specimen were polished to uniform the stress

Table 2. Physical properties of the investigated concrete compositions.

No	W/C coefficient	Compressive strength [MPa]	Density [kg/m^3]	Porosity [%]
1	0.60	24.8	2283	4.8
2	0.60	24.9	2284	5.0
3	0.45	37.0	2323	4.6
4	0.45	34.7	2328	4.6
5	0.30	62.4	2405	4.2
6	0.30	54.2	2400	4.0

distribution and improve the contact with the AE sensor. Additionally, the fibre plates were placed between the specimen and the test machine brackets to minimize the noise generated by the hydraulic drive.

The AE activity was measured by a 1000 kHz AE wideband transducer of WD type connected to a 40 dB/6 μV RMS noise preamplifier and a 43 dB main amplifier. The AE processor registered the AE signals in the "count" mode, i.e. the internal counter registered each excess above the specified rejection level set to 1 V. The AE measurements and the current level of the applied stress were transmitted to a PC compatible computer. Some of the investigated specimens were appropriated for recording the frequency spectrum of signals on two stress levels: between 30 and 60% and between 65 and 95% of the final strength. In this case, the waveform registration procedure was activated when the current Acoustic Emission Activity exceeded 50 counts per second.

A schematic diagram of the measuring set-up and the averaged results of the AE counts sum for the six sets of the examined specimens were shown in the paper [6].

3. Discussion of results

The Acoustic Emission signal analysis showed different time plots for the plain concrete (series 1, 2, 3 and 4) and for that with silica fumes (series 5 and 6) [6]. The concrete with the addition of silica fumes evidenced a σ_{II} critical stress displacement of the range of 70–80% of the compressive strength. For the plain concrete, the typical values of the σ_I and σ_{II} stresses are $(0.3 \div 0.4)$ in the range of σ/f_c and $(0.6 \div 0.7)$ in the range of σ/f_c, respectively [3, 4, 6, 8, 10]. This fact causes a smoothing the $\sigma - \varepsilon$ relationship and results from the modification of the cement paste – aggregate contact zone. The major structure damages, arising in σ_I to σ_{II} range of the stress level, are located just in this zone. The mentioned zone is compacted by the micro-filler and strengthened by the silica fumes reactivity which transforms the weak portlandite crystals into the strong C-S-H (calcium-silicate-hydrate) phase. The composite structure modifications described above change their physical and mechanical properties by increasing the density and compressive strength in comparison with those of the plain concrete (see Tab. 2), these results in brittleness increasing the high strength concrete.

The neural computation method was applied for the classification of the Acoustic Emission signals. The so called "generalized distance" was chosen as a discernment criterion. The generalized distance between two pattern vectors is the square root of the sum of the squares of all their components subtracted [2, 9].

From the six registered signals' groups, each of nearly 100 samples, the most characteristic and the most frequent frequency spectra were chosen by the computer. Then, for each investigated group an average frequency spectra were found. Within one group, the generalized distances between the particular spectra vary from 2.8 to 4.2, while between each series – from 5.4 to 9.5. This fact indicates that there are significant differences among the frequency spectra for the different concrete compositions. The type of the aggregate among other things influenced these differences. Crushed aggregate, applied in some of the investigated compositions, has a rougher texture which results in a greater adhesion or bond between the particles and the cement matrix. Likewise, the larger surface area of a more angular aggregate provides a greater bond. That is why those concretes have a stronger cement paste - aggregate contact zone. In the frequency spectra for the series with crushed aggregate (1, 3 and 5) a local maximum at the frequency of about 500 kHz can be seen (see Fig. 1).

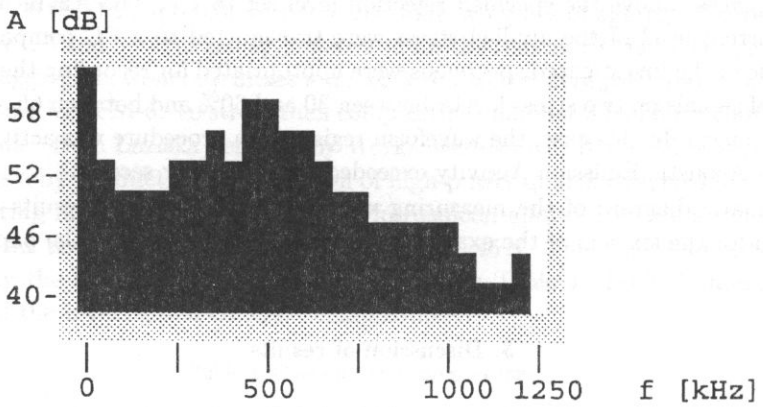

Fig. 1. Frequency spectrum for concrete series with crushed aggregate.

The concrete with silica fumes are also characterized by a strengthened contact zone. For these series the frequency spectra show a smaller participation of the lower frequency signals (see Fig. 2).

During the first loading stage (from 30 to 60% of strength) for the series 1 and 2 sounds characterized by low frequency dominate in frequency spectra. This fact shows that not only defects existing in structure develop but also new microcracks appear in the contact zones between the aggregate particles and the cement paste [5]. These zones are the weakest chains in the structure of compositions 1 and 2 (see Fig. 3). The stronger the composition (remaining series) the better visible becomes the participation of the higher frequency signals. This is connected with cement paste cracking. It can be also seen in the second loading stage (from 65 to 95% of strength) as shown in the Fig. 2.

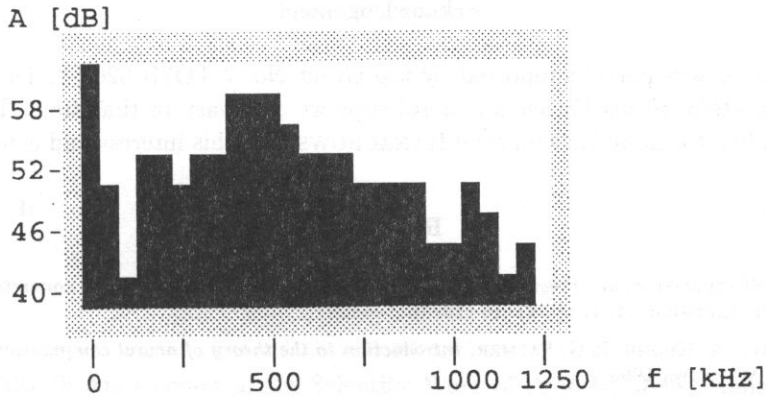

Fig. 2. Less participation of the lower frequency signals for concrete with silica fumes.

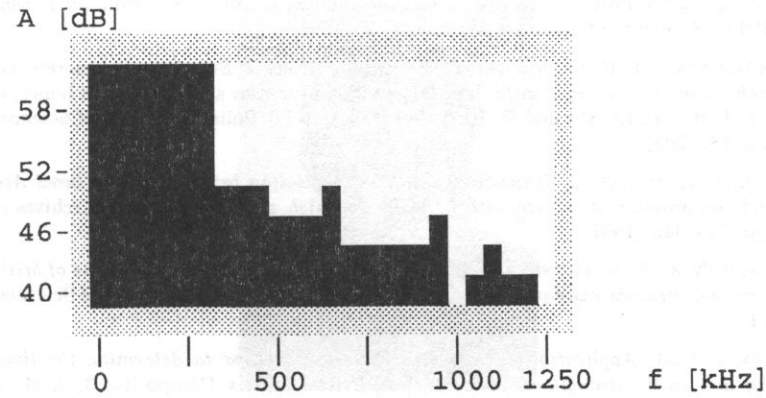

Fig. 3. Frequency spectrum for the weakest compositions.

4. Conclusions

The analysis of the obtained results allows to formulate the following conclusions:

1. The Acoustic Emission measurements made during compressive tests of the concrete compositions appear to be a useful tool providing information on the progress of the destruction processes. The time plots of the Acoustic Emission signal analysis gives only a quantitative image of those processes. The frequency spectra analysis of the Acoustic Emission signals is supplementary to the former one.

2. The frequency spectra analysis of the Acoustic Emission signals with application of the neural computation method gives a qualitative image of the destruction processes occurring during the structure loading. It can help to locate the emission source.

3. The emission source localization can be useful in material engineering, in modifications of existing materials and investigations of new compositions.

Acknowledgement

This paper was partly supported by the Grant No. 7 TO7B 020 08. The author is also very grateful to his Father for moral support necessary in that time. The author also would like to thank Dr Zbigniew RANACHOWSKI for his interest and essential help.

References

[1] J.-M. BERTHELOT *et al.*, *Frequency analysis of Acoustic Emission signals in concrete*, Journal of Acoustic Emission, **11**, 1, pp. 11–18 (1993).

[2] J. HERTZ, A. KROGH, R.G. PALMER, *Introduction to the theory of neural computation* [in Polish], WNT, Warszawa 1995.

[3] J. HOŁA, A. MOCZKO, *Analysis of destructive processes chosen concrete structures with an application of ultrasound and Acoustic Emission methods* [in Polish], PhD Thesis, Institute of Civil Engineering, Wrocław University of Technology, Wrocław 1984.

[4] J. HOŁA, Z. RANACHOWSKI, *Acoustic Emission method in concrete testing* [in Polish], IFTR Reports Polish Academy of Sciences, Warszawa, 26/1991.

[5] A. JAROSZEWSKA, J. RANACHOWSKI, F. REJMUND, *Acoustic Emission in concrete under thermal and mechanical stresses* [in Polish], [in:] Destructive processes and strength of bones, ceramics and concrete, J. RANACHOWSKI and F. REJMUND [Eds.], IFTR Polish Academy of Sciences, Warszawa 1996, pp. 183–208.

[6] J. MIERZWA, K. POGAN, Z. RANACHOWSKI, *The correlation between the fractured Acoustic Emission and compressive static strength in plain and high strength concrete*, Archives of Acoustics, **22**, 3, pp. 333–342 (1997).

[7] J. RANACHOWSKI, F. REJMUND, Z. LIBRANT, *Acoustic Emission investigations of brittle materials. Ceramics and concrete examples* [in Polish], IFTR Reports Polish Academy of Sciences, Warszawa, 28/1992.

[8] Z. RANACHOWSKI, *Application of Acoustic Emission method to determine the limit of proportionality nad static strength in concrete*, [in:] Brittle Matrix Composites 3, A.M. BRANDT and I.H. MARSHALL [Eds.], Elsevier Applied Science Publishers, London and New York, 1991, pp. 234–239.

[9] Z. RANACHOWSKI, *Neural network method in investigations on AE dependence on concrete strength* [in Polish], [in:] Destructive processes and strength of bones, ceramics and concrete, J. RANACHOWSKI and F. REJMUND [Eds.], IFTR Polish Academy of Sciences, Warszawa 1996, pp. 209–220.

[10] Z. RANACHOWSKI, *Measurement methods and analysis of Acoustic Emission* [in Polish], IFTR Reports Polish Academy of Sciences, Warszawa, 1/1997.

ARCHIVES OF ACOUSTICS
23, 3, 457–460 (1998)

C H R O N I C L E

The Fiftieth Anniversary of the Scientific Work of Prof. Dr. Jerzy Ranachowski

Prof. J. Ranachowski

The 3-rd International Symposium devoted to new trends in the technology and investigation of ceramic materials was held in Białowieża from the 8-th to 10-th of June this year. The participants of this meeting were scientists working in the field of materials technology and acoustics as well as representatives of the ceramic materials industry and electrical power engineering. The focus of attention was the presentation of the fifty years' scientific and technical output of Prof. J. Ranachowski and the research connected with his activity, especially the progress in the production and quality testing of high-voltage elements that has been achieved on the basis of Prof. Ranachowski's investigations. It should be emphasized that acoustic methods were the main tool in most of his research work. It seems therefore that *Archives of Acoustics* is the proper place to give a short profile of Prof. Ranachowski and a comprehensive presentation of his fifty years' scientific output.

Prof. Ranachowski was born in 1926; fifty years ago is assistant at the Electrical Faculty of the Technical University in Wrocław, he started his research by designing a High-Voltage Laboratory at this University. In the years 1951–1975 he worked as assistant, and later as senior lecturer and assistant professor, at the Institute of Electrical Engineering in Warsaw. At that time, it was a leading research institution that contributed to a large extent to the development and progress in the electrical engineering industries and electrical power systems in Poland. Over these years, Prof. Ranachowski was concerned mainly with technology of ceramic and materials elements, as well as with the investigation causes of breakdowns in electrical power systems. This was the subject of his Ph.D. Dissertation (1963) and, later on, of his thesis presented for professor title (1968). In connection with his research of that time, he was looking for the most effective methods of testing the electrical power systems. Prof. Ranachowski focused his attention on the application of acoustic techniques that have been considered then as the most innovatory ones. That is just why he start to cooperate in 1956 with the Institute of Fundamental Technological Research of The Polish Academy of Sciences. In 1975, Prof. Ranachowski started to full time work at this Institute holding for more than twenty years several responsible positions; among other things, he was active as laboratory chief and assistant director of this Institute. During the last years, before he retired, Prof. Ranachowski was the managinging director of the Acousto-Electronic Centre. He was nominated the full professor in 1976.

A complete profile of the scientific output of Prof. Ranachowski requires a more detailed study. Therefore, I would like to restrict myself only to the listing of Prof. Ranachowski's achievements that in my opinion are the most outstanding ones. They are connected mainly with the application of acoustic methods to the complex investigation of ceramic materials and elements. He found and determined quantitative relations between the velocity and absorption of ultrasonic waves and the structure and microstructure of ceramic materials, particularly the effect of porosity and the type of pores and texture defects in insulants. He made also a significant contribution to the study of the correlation between the acoustic properties of a material and its dynamic elasticity parameters.

Particularly profitable were the scientific and technical works concerning the application of the acoustic emission (AE) that were initiated by Prof. Ranachowski and have been continued by a scientific group working under his leading. Prof. Ranachowski has proved that the AE method is a unique tool for the investigation of dynamic processes occurring in ceramic materials, first and foremost of cracking and microcracking processes. Among other things, the research of Prof. Ranachowski resulted in a widespread application of the AE method in quality testing and in the evaluation of the current state of insulators and in the forecasting of their "life-time", particularly in the case of high-voltage insulators. His achievements concerning the study of thermal shock and dynamic load effects by the AE method are of special interest. This was connected with a new approach to the determination of the critical stress intensity vector $\mathbf{K}_{IC}$.

Prof. Ranachowski came up with significant improvements in the AE measuring equipment initiated the production of those equipments in Poland. This enabled the application of AE methods in many fields of technology and science. Beside the mentioned

above applications in the ceramic material industry and electrical power engineering, some other applications should be enumerated:

- investigation of transition states in superconductors,
- monitoring of hazards in engineering objects,
- evaluation of the state of electrical power systems,
- testing of concrete and concrete constructions,
- testing of technological process in the woodworking industry,
- monitoring the chemical reactions.

The above list of applications indicates that the scope of the effect of Prof. Ranachowski's research achievements extends far beyond his strict discipline.

I. Malecki

Polish and Hungarian co-ooperation in acoustics in the last forty years

The co-operation in acoustics was wide prosperous between the East Central European Countries in the second part of this century. Within the framework of this co-operation seems very fruitful and effective the collaboration typically between Hungarian and Polish acousticians and institutions. The personal companionships are originated in October of the year 1956 first, when Prof. Tarnóczy was unable to go home from Moscow, and during the days of Hungarian revolution he was a guest of Prof. Malecki in Warsaw.

The close contacts of the trade profession leaders of both countries, the historical well known friendly relationships of the Polish and Hungarian peoples, the contemporary very similar political and economic living space and the similar development of the acoustics at this time period of both partners, gave many many possibilities to prosper the contacts in acoustics. The official contacts were built in framework of the co-operation of both countries at the plane of Academics of Scientific first. These many decades long oficial contact made posible the change of researchers, the change of postdoctoral fellows, and the change of students. The systematic co-operation branches in the acoustics were in various decades with several intensities of the co-operation interest.

The common economic state teamwork in industry, in agriculture, in technics, in science, in university education, in the international standardisation gave many and many common platforms in our topic too. The regular acoustics seminars and conferences organised regularly in both countries to grow the personal relationships, the common mentality technics, and scientific co-operation. The colleagues in acoustics helped each other mutually in international committees and boards to achieve the job organise international conferences, congresses in the fraternal country (eg. INTER NOISE'79 in Warsaw, 7-th ICA Congress in Budapest 1971, OSA'85 in Kraków, INTER NOISE'97 in Budapest, FASE Conferences: in Warsaw 1978, Sopron 1986, Balatonfüred 1992).

The international managing of acoustics societies has very fruitful results in the Polish Hungarian co-operation. The idea of FASE, and the close co-operation in the board of FASE originated from common interesting in acoustics of both countries. The help to avoid EAA latter, the co-operation in ICA Board, and I-INCE gave many advantageous possibilities in the earlier and in the last decade too.

The co-operation in the field of scientific technics societies was such close, that the Acoustical Society of Poland was reward in 1993 with the Békésy Medal founded by the Hungarian society (OPAKFI) remembering 50-th anniversary of grounding the fraternal Polish Society, and the very effective contacts in acoustics and in scientific technics co-operation supported by this society.

András Illényi
G. Békésy Acoustics Research Laboratory TU. Budapest